A

5 mm

DEDICATED TO THE ADVANCEMENT OF SCIENCE, EDUCATION, EXPLORATION, AND CONSERVATION

The *Journal of Cave and Karst Studies* , ISSN 1090-6924, CPM Number #40065056, is a multi-disciplinary, refereed journal published four times a year by the National Speleological Society. The *Journal* is available by open access on its website, or check the website for current print subscription rates. Back issues are available from the NSS office.

POSTMASTER: send address changes to the National Speleological Society Office listed above.

The Journal of Cave and Karst Studies is covered by the following ISI Thomson Services Science Citation Index Expanded, ISI Alerting Services, and Current Contents/Physical, Chemical, and Earth Sciences.

Front cover: Cross Section of a square speleothem. See Forti and Springer in this issue.

GENESIS AND EVOLUTION OF THE SQUARE SODA STRAWS OF DRY CAVE, WEST VIRGINIA, USA

Paolo Forti[1] and Gregory S. Springer[2]

Abstract

A completely new (sub)type of calcite stalactite, similar to a soda straw but showing an external square shape, has been recently observed within Dry Cave, West Virginia, USA. Though rare speleothems with one or more planar sides (triangular to hexagonal cross sections) have been described in the past, this is the first reported example of a subaerial stalactite-like speleothem with a rhombic parallelepiped structure. More than a dozen examples were observed in the cave. The suggested genetic mechanisms allowing the atypical growth of a parallelepiped seem to be controlled by several boundary conditions that normally preclude their development. Constrained by the specifics of calcite crystallization in descending vadose waters and the morphology of collected (already broken) samples, we hypothesize that an initial very low supersaturation within the feeding tube, together with relatively fast dripping, causes the growth of a normal monocrystalline calcite soda straw with the C axis coincident with the tubular axis and circular cross sections. Calcite precipitation on the outside of the soda straw is possible only if there is a water film flowing on the straw's external surface. Normally, this external flow will cause the rapid transformation of a tubular straw into a typical, polycrystalline conical stalactite. But in this case, the external feeding film is minimally supersaturated or even absent, which slows epitaxial growth over the pre-existing monocrystalline structure of the soda straw and suppresses radial (polycrystalline) growth of calcite crystals. This induces, in stationary conditions, transformation of the straw into parallel, twinned calcite crystals stacked to form a pyramidal stalactite with rhombic cross sections and an overall tapering angle of <2°. In the most extreme cases, the soda straws are gradually transformed into a seemingly square monocrystalline parallelepiped. The necessary boundary conditions involve a non-stationary distribution of always scarce supersaturated/undersaturated flow over the soda straw, alternating with periods of simple saturation. The controlling factor for the development of conical, pyramidal, and parallelepiped stalactites seems to be the tapering angle. This just outlined genetic mechanism is speculative and should be experimentally tested. Finally, in the few collected samples of the square straws, this shape is often masked by another development step, which probably became active when they were already broken. This final stage was characterized by a sudden increase in supersaturation of epitaxial water, which induced the deposition of a thin layer of polycrystalline calcite that masks, at least partially, the monocrystalline structure of the speleothem.

Introduction

Speleothems are well-known features of caves that have received considerable scientific attention (see Hill and Forti 1997 and references therein). Nonetheless, as caves are explored and studied in greater detail, it is still possible to detect a completely new type of speleothem, or more often, to observe an unreported variant of an already known speleothem type. This is what occurred during a 2016 survey trip, led by Springer, in Dry Cave, West Virginia, USA. Strange, unusually shaped soda straws were observed for the first time in the world. These speleothems exhibit external square surfaces, whose cross sections are notable for their four sharp corners instead of normal round cross sections (Springer, 2019) that is common elsewhere in this cave and throughout the world. Monocrystalline speleothems (stalactites, stalagmites, columns, helictites etc.) with one or more planar sides are very rare, but do exist (Halliday, 1959; Basset and Basset, 1962; Hill and Forti, 1997), but square soda straws were previously unknown. A few fragments of these speleothems (already broken and laying on the floor) were collected in July 2019 for analysis to understand the mechanisms that allowed the evolution of these peculiar soda straws. In the present paper, possible genetic mechanisms for the evolution of these newly reported speleothems is presented on the basis of on-site observations and microscopy results, after a brief morphological description of the still growing square soda straws and naturally broken fragments.

Location

Dry Cave is in eastern Greenbrier County, West Virginia, USA (Fig. 1A) and developed under the eastern slopes of Beaver Lick Mountain, a NE-SW trending anticlinal ridge. The cave is developed in the Silurian-age Tonoloway Limestone, which has a thickness of 76 meters and is a generally thin-bedded, calcite-pure micrite containing a few minor shales (Price and Heck, 1939). Dry Cave continues to be explored and surveyed but has a surveyed length of 10.7 km as of October 2019. The cave is known in the local caving community for its spectacular and abundant speleothems, which include aragonite bushes, 10 cm scale cave popcorn bushes, helictites, and the full suite of more typical spele-

[1] NSS 46644, Italian Institute of Speleology, Via Zamboni 67, 40126 Bologna, Italy. paolo.forti@unibo.it
[2] NSS 29328FE, Department of Geological Sciences, Ohio University, Athens, OH, USA. springeg@ohio.edu

othems. Dry Cave is entirely vadose and consists of parallel abandoned stream passages offset along steeply dipping limestones and an active strike-oriented stream passage (Fig. 1B).

The square soda straws are located ~2.8 km upstream of the entrance near survey station DDF18 (Fig. 1C) in a short segment of a 2- to 4-meters wide and 0.5- to 2-meters high abandoned stream passage immediately overlying a larger relict 5 × 5-meter stream passage called the Mystery Trunk. The square straws are growing within and adjacent to dense groups of normal, still developing stalactites and soda straws hanging above a moderately dipping flowstone surface. Broken fragments of square soda straws lay on active calcite flowstone on which a few were slightly cemented. After this paper entered the review process, two additional examples were observed during a survey trip in a nearby passage in October 2019.

The longest still growing square soda straw (Fig. 2A) is over 24 cm long, 12.7 mm wide at its attachment (top), and 6.5 mm wide at its tip, while most of the attached and unbroken ones are between 8 cm and 12 cm long. Some of them are square from their attachments to near their tips, while others have their square structure interrupted close to their tips, which maintain the original rounded structure for the last few centimetres. Others behave in an opposite manner, enlarging and becoming squared only in the part close to the tip. Most of the square soda straws are wider at their top and progressively decrease in width towards the tip. A few maintain constant width for most, or even the totality, of their length.

The square soda straws described in greater detail below are euhedral, with monocrystalline forms having rhombic cross sections. The largest single crystals are many centimeters long, which is unusual for speleothems not growing subaqueously. For instance, the well-known giant gypsum crystals of Naica, Mexico grew in hydrothermal waters (García-Ruiz et al., 2007). This naturally raises the question of whether the square soda straws originally formed in a pool that has since drained. However, the host passage ends in 3-m drops into the underlying passage, which precludes pooling. Neither the host passage nor Mystery Trunk show signs of pooling or flooding other than small gour dams and rimstone. Square soda straws have water films or water droplets at their tips and are found within typical stalactites and soda straws, all of which appear to still be growing. The broken fragments of square soda straws lay on active flowstone, so overall evidence implies that the unusual straws are either actively forming or of very recent age.

Six fragments of square soda straws (samples S1 through S6 in Table 1) were taken from the cave floor to be analyzed at the Italian Institute of Speleology. In Table 1, sample S6 is subdivided into two different parts that we designate S6A and B; the upper one is square while the bottom portion still preserves the original rounded structure (Fig. 2B).

Morphologic characteristics of the square soda straws

The ends of samples S1–S6 are nearly perfectly flat, and inspection of their cross sections reveals that they are rhombic, not square (beside the tip of S6, which is still rounded). As such, the phrase square soda straw is a colloquialism derived from the local caving community, and we use the phrase synonymously with rhombic soda straw. Calcite commonly forms rhombic crystals because of its molecular structure, so it is perhaps not surprising that they have a rhombic structure instead of cubical cross sections.

Samples S1–S6 consist primarily of monocrystalline calcite with the C axis coincident with the soda straw growth axes (Fig. 3A, B). The monocrystalline calcite is overlain by a relatively thin pale yellowish calcite overgrowth (from 0.1 mm to over 2 mm thick), which partially masks straw shapes and consists of a layer of polycrystalline calcite with the C axis directed radially (Fig. 3C). Straw cross sections were measured along the natural breakage planes, and their long sides range between 8.1 mm and 13 mm in length and the short sides from 5.1 mm to 9.4 mm (Table 1). The diameters of their internal and still open feeding tubes are between 0.3 mm and 5.1 mm.

Optical microscope analyses were performed in the Biological, Geological and Environmental Department (BIGEA) of the University of Bologna and confirmed that the inner structure of all samples consist of monocrystalline calcite. In thin sections made parallel to soda straw axes, small voids are common and always developed along the main cleavage planes together with a few larger, partially rounded or lenticular voids (Fig. 4).

Genetic mechanisms and evolution of normal soda straws

It is useful to briefly recall the factors ruling the development of normal soda straws before discussing the possible mechanisms allowing the evolution of square soda straws. It is well known that the evolution of tubular soda straws is mainly controlled by drip frequency, which must be fast enough to allow slight supersaturation only in the outer part of the hanging drip; the drop must fall before the entire drop reaches greater supersaturation. In this manner, a thin (0.1mm or slightly greater) ring of calcite is deposited with a diameter of 5.1 mm, corresponding exactly to that of the equilibrium drop before its detachment (Fig. 5B) (Curl, 1973).

The supersaturation normally achieved during speleothem development is just high enough to allow selective competition among the embryonic crystals, so that the tubular structure consists of calcite crystals with all the C axes parallel to the growing speleothem (White, 1976; Fairchild and Baker, 2012). Moreover, in most occurrences, the supersaturation is low enough to avoid simultaneous development of several crystals; therefore, the structure of a soda straw is often
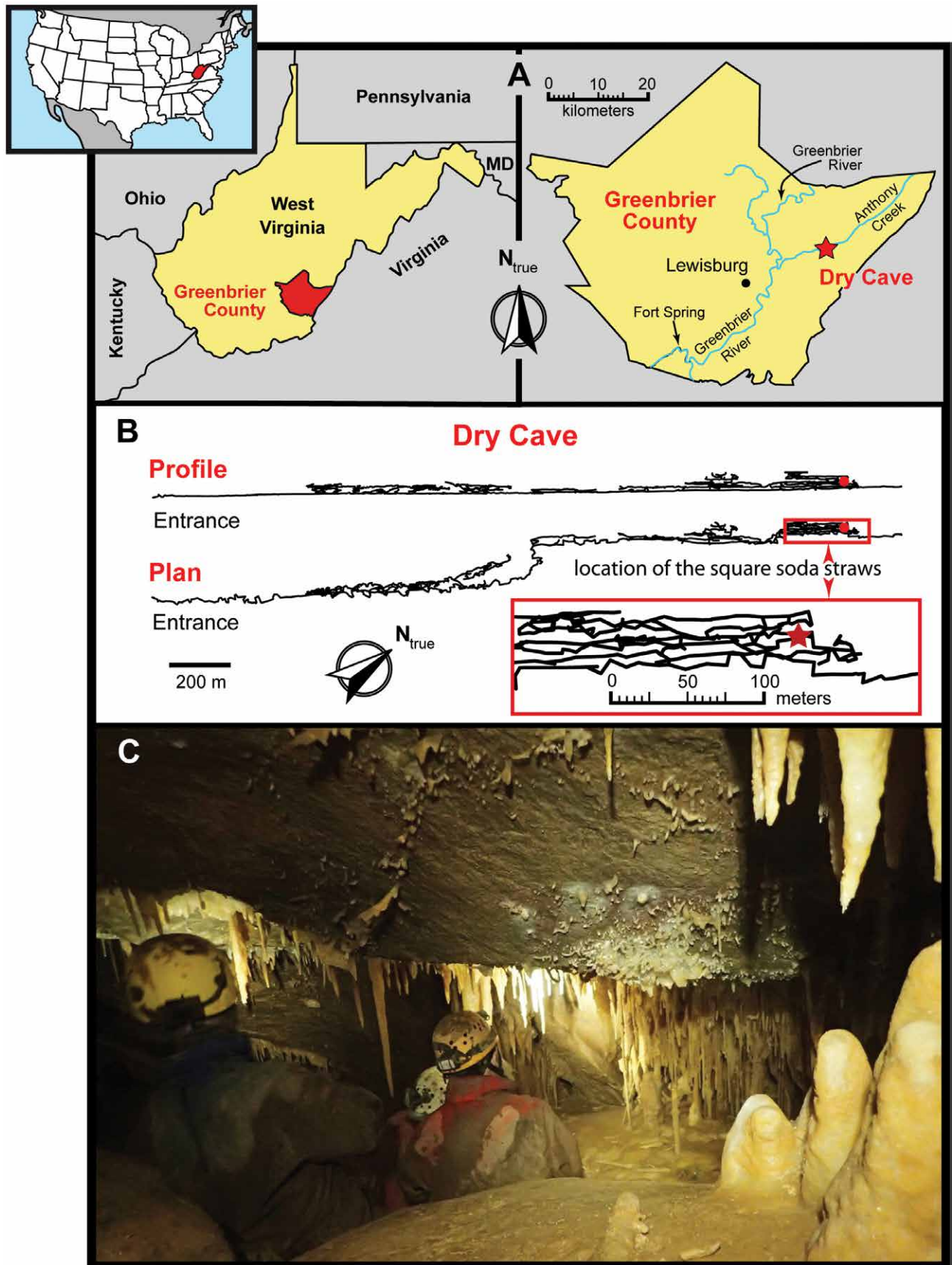
Figure 1. Dry Cave: A: Index map for Dry Cave; B: simplified profile and plan of the cave and location of the square soda straws (red dots and star indicate the survey station DDF18); C: general view of small area near survey station DDF18 in which the square soda straws are restricted.
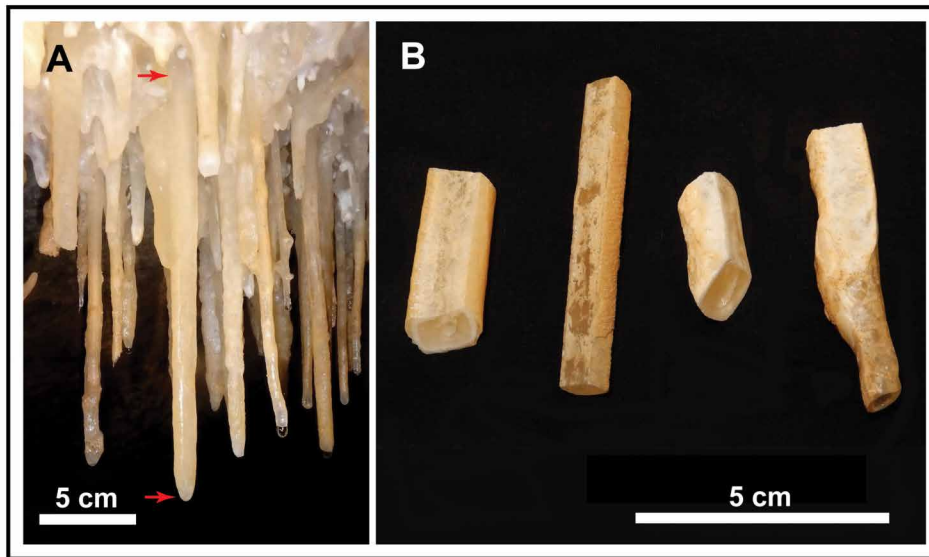
Figure 2. A: The longest still active square soda straw: red arrows point to the top and the tip of the speleothem; B: close-up view of some fragments of the analyzed square straws.

monocrystalline. A true tubular speleothem is expected to have an inner tube with a constant diameter, which is practically the same diameter as the equilibrium drop (Fig. 5B). As drip frequency decreases, supersaturation may increase and progressively extend into deeper portions of the drop. Consequently, calcite deposition occurs not only along the border of the equilibrium drop but also inside (Fig. 5C). This process progressively reduces the diameter of the inner tube, which can eventually become approximately the same size as the original feeding fracture (Fig. 5D).

While dripping ensures the elongation of a soda straw and the size of its internal tube, the increase of its overall diameter can be induced only by water films flowing over the outer surface (White, 1976; Fairchild and Baker, 2012). Several factors affect the evolution of the external shape and internal crystalline structure of a stalactite, including the original supersaturation of the feeding solution, velocity of downward flow, and evaporation and/or condensation processes. In most instances for which approximately constant environmental parameters prevail, the two most import-

Table 1. Dimensions of the cross sections measured on natural breakage surfaces corresponding to the main calcite cleavage planes of the sampled square soda straws. The sample S6 is characterized by a sudden narrowing about 2 cm from its natural tip with the last portion (S6B) having a quite normal tubular (rounded) form because the transformation into a square one was not yet begun. Long and short side measurements are affected by an experimental error of 0.05 mm and by the presence of variable but thin (from 0.5 mm to 1.5 mm thick) microcrystalline crust covering the calcite monocrystal structure. This uncertainty slightly affects the evaluation of tapering angles.

Sample No.	Length (mm)	Tapering Angle (°)	Long side (mm)	Short side (mm)	Inner tube diameter (mm)
S1	112	0.3	8.65−8.95	5.20−5.35	0.35
S2	93	<0.1	8.10−8.20	5.15−5.20	2.95−3.05
S3	85	0.3	9.15−9.40	5.25−5.40	5.15−3.80
S4	102	0.2	11.85−12.05	7.70−7.80	3.10−3.30
S5	57	0.1	12.95−13.00	8.15−8.20	4.25
S6A	64	0.9	12.35−12.75	8.80−9.40	4.40−4.50
S6B	24	0	6.45	6.24	4.90

ant factors are the original degree of supersaturation and the flow rate. The internal crystalline structure is a function of saturation state because it controls precipitation rates (Mullin, 1997) and locations, while flow rate rules the external shape through similar means (Short et al., 2005a, 2005b).

The degree of supersaturation is always the single parameter responsible for the development of a stalactite's crystal structure (Fig. 6). Initially, the stalactite is totally monocrystalline with the C axis coincident with that of the speleothem and the external structure being just an epitaxial growth of the original tubular straw (Fig. 6B). The stalactite subsequently evolves to a clearly banded structure characterized by concentric rings (Fig. 6C−D). Inside each band, the calcite crystals may be organized into palisade structures with the C axes directed radially (Fig. 6C). This occurs when the supersaturation degree is high enough to allow selective competition between crystals with different orientations. But when the supersaturation is very high (often thanks to concomitant evaporation), new nucleation is the ruling process; and therefore, the external rings are characterized by random orientations of C axes (Fig. 6D).

In steady-state conditions, the starting (super)saturation value is constant over time, and thus, cannot affect stalactite tapering because the supersaturated waters do not persist on the stalactite long enough to appreciably change their
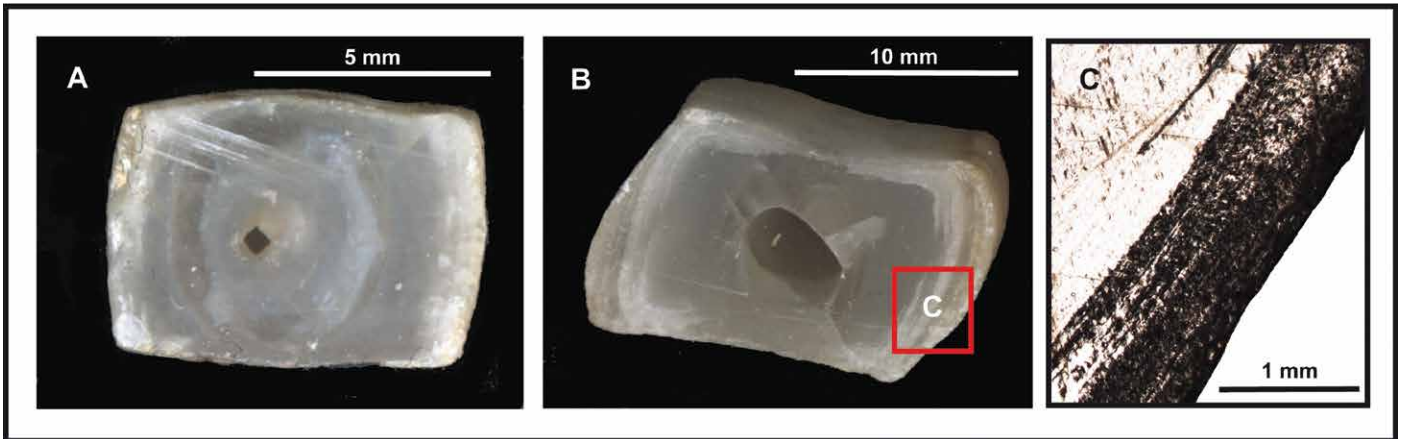
Figure 3. Cross sections of samples S1 (A) and S5 (B, C). A: The inner monocrystal structure of the square soda straws sometime preserve ghosts of the original rounded soda straw, which is particularly evident in S2, where it is also possible to see the effect of re-dissolution and subsequent re-deposition to the left of the inner hole. The central feeding tube has a diameter of 0.35 mm; B: Flat breakage of S5 with evident rhombic structure; C: Polarized microscope image of the thin section where the upper left part of the monocrystalline structure covered by the laminated structure of the polycrystalline layers is clearly visible.

Figure 4. Thin section of the soda straw axis of sample S3. The monocrystal lattice is very rich in voids aligned along the main cleavage planes. A few larger voids exhibit rounded lenticular shapes, suggesting re-dissolution.

Figure 5. Frequency of dripping and soda straw development. A: the frequency of dripping is too high to allow speleothem growth; B: a feeder tube drips above the limit frequency and therefore creates a normal soda straw with extremely thin external walls; C: a decrease in the drip rate induces a progressive narro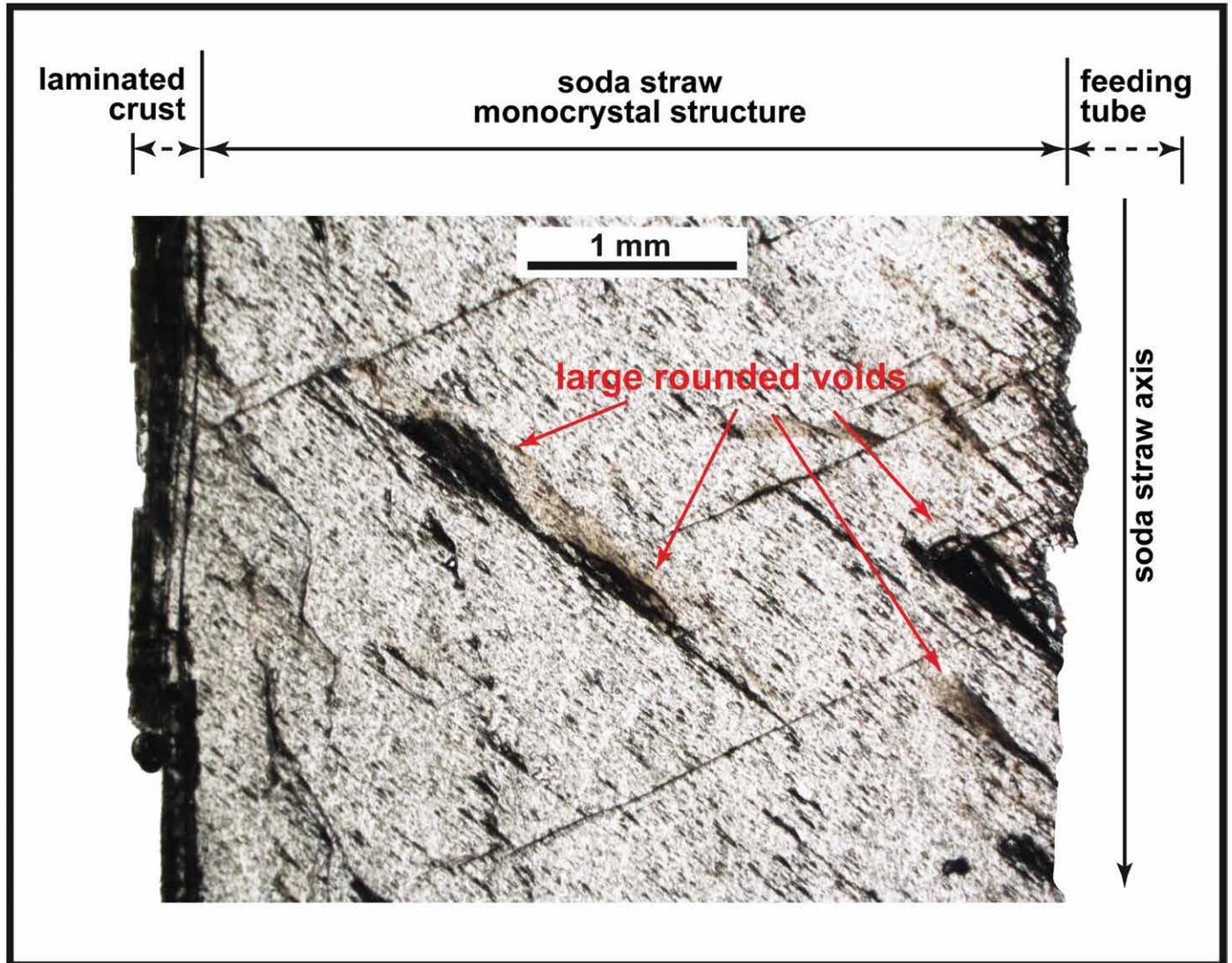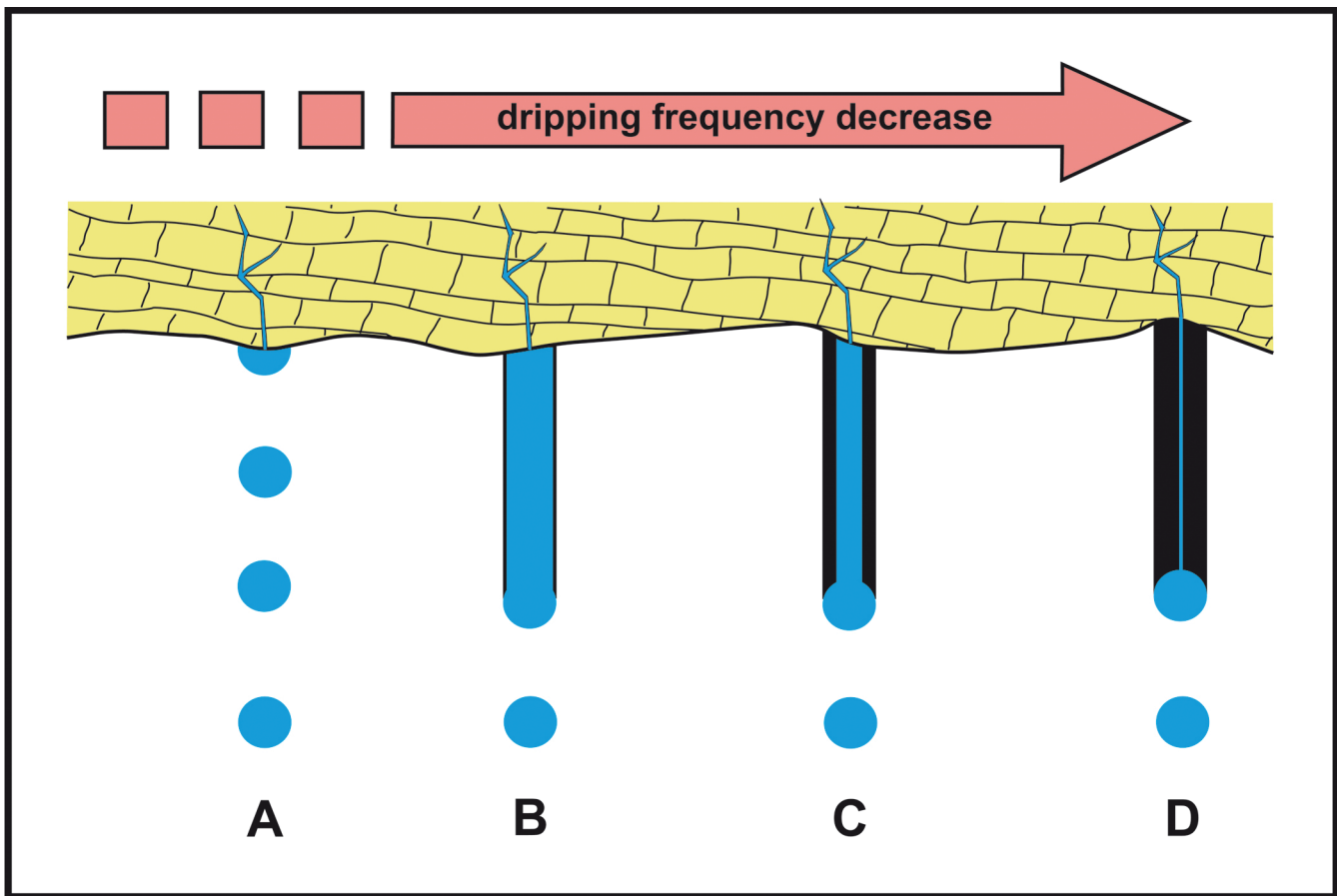wing of the internal tube; D: the internal tube evolves to become the same diameter of the feeding crack below the limit drip frequency.

saturation index via precipitation and degassing of CO_2. However, if the amount of water flowing over the speleothem surface is small, the correspondingly slow flow rate allows greater time for precipitation to occur and the saturation index decreases with distance from the attachment point. This enhances tapering because precipitation will be greatest where the saturation index is greatest (Fig. 7).

Thus, from a practical standpoint, in steady-state conditions and in absence of evaporation, the diameter at the top of a stalactite is inversely proportional to the amount of feeding water flowing over it. This is just the opposite of the well-known phenomenon responsible for stalagmite diameters (Franke, 1965). Normal values for the tapering angle (corresponding to the cone vertex angle) of stalactites range between 3° and 5°, but sometimes the angle can be significantly higher and very rarely it is smaller than 2.5° (Forti, unpublished experimental measurements). Finally, in steady-state conditions, the progressive decrease in supersaturation along the external surface negates any possibility of the development of perfectly cylindrical or even parallelepiped stalactites (i.e., without tapering).

The mechanism behind the evolution of square soda straws

The square soda straws are immediately adjacent to typical soda straws and stalactites with round exteriors. Therefore, development of the former cannot solely depend on the meteorology of the area; normal and square soda straws are forming side-by-side and share the same microclimate. Therefore, the controlling factor must be sought mainly in the hydrodynamics or the geochemistry of the feeding waters even if micro-meteorological variations may surely occur due to flow steering and turbulence associated with the many speleothems surrounding the square soda straws. This means condensation and evaporation will vary at multiple spatial and temporal scales, including at the scale of individual speleothems.

Ghosts of circular soda straws contained within the rhombic cross sections of some of the square soda straw fragments show that the first step in their development is the formation of a typical, cylindrical soda straw (Fig. 5). This implies an initial stage of more or less fast dripping of marginally supersaturated water. The measured feeder tubes of the antecedent tubular soda straws never exceed 5 mm, which is also consistent with initial development of a typical soda straw, although one of the observed feeder tubes is 0.35 mm in diameter. This small diameter may be primary, but
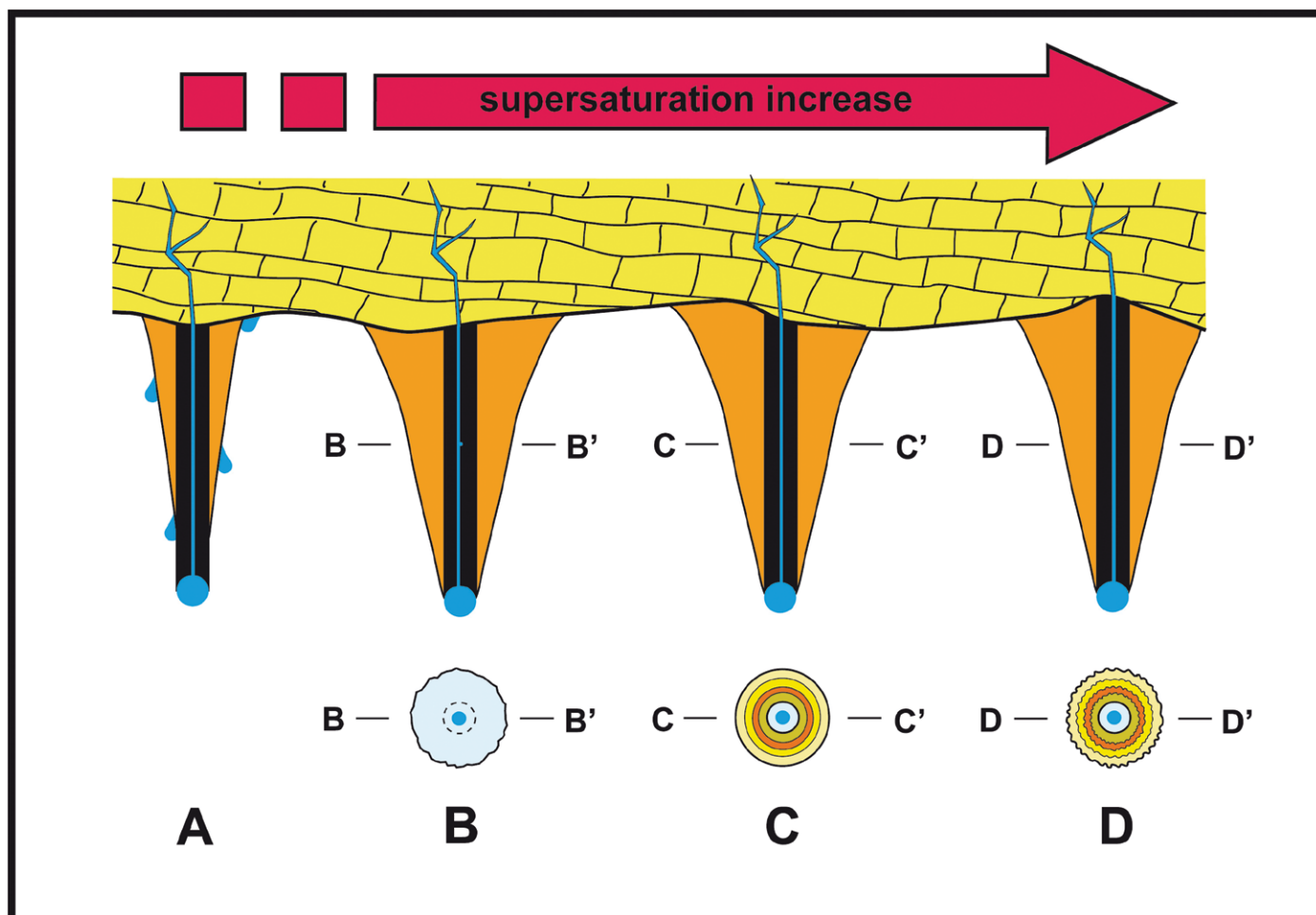
Figure 6. Supersaturation and stalactite crystal structure. A) a soda straw is progressively transformed into a more or less conical stalactite when water starts flowing over its external surface; B) monocrystalline stalactites with C axis coincident with that of the soda straw form which supersaturation is very low: concentric growth layers are entirely absent in their cross section; C) with higher supersaturation, normal stalactites characterized by smooth concentric growth layers and radial C axes are formed; D) when supersaturation is very high, stalactite growth layers exhibit botryoidal surfaces and completely random C axis orientations.

it is more likely that the feeder tube gradually became constricted through internal calcite precipitation. This may have occurred after or while the circular straw was forming because actively growing square soda straws were observed to have the same drop diameters as adjacent circular soda straws. Notably, the rhombic shape of active (still attached) square soda straws begins near their attachment points and the square straws taper toward their termini, which are round. For instance, the active 24 cm long square soda straw is 12.7 mm wide just below its attachment point and 6.5 mm wide at its tip (Fig. 8A). This square (pyramidal) stalactite has a tapering angle of about 1.6°.

A round soda straw can only increase in diameter if a water film flows on its external surfaces prior to being squared off. But, as briefly described in the previous paragraph, this is just the very commonly observed process responsible for the evolution of tapering polycrystalline (Fig. 5B) and more rarely, monocrystalline stalactites. Regardless of crystalline structure, such stalactites typically have a tapering angle between 3 and 5°. Therefore, the evolution of square soda straws is clearly an exception to the usual processes at work when soda straws transform into stalactites. But from a theoretical point of view, even if some of them are extremely similar to tubular straws, the square soda straws must be considered a new, peculiar sub-type of stalactite.

It is hard to say if the second, squaring stage was active when the soda straw first began to form or if it started later, when the round soda straw was already at least partially formed. In either case, water began to flow over the outer surface of some tubular straws, thus activating the process of transformation into square stalactites. But why in this occurrence did the soda straws gradually transform themselves into square pyramids (if tapering is present) or parallelepipeds (if tapering is absent) consisting of large rhombic, monocrystalline calcite crystals?

The pyramidal forms consist of a series of euhedral calcite crystals with parallel twinning along the C axis (Fig.8A), and in every case, the tapering angle (deviation of pyramid sides from orthogonality) is slight in comparison to normal cylindrical stalactites. And some of the analyzed fragments must be considered parallelepipeds because their tapering
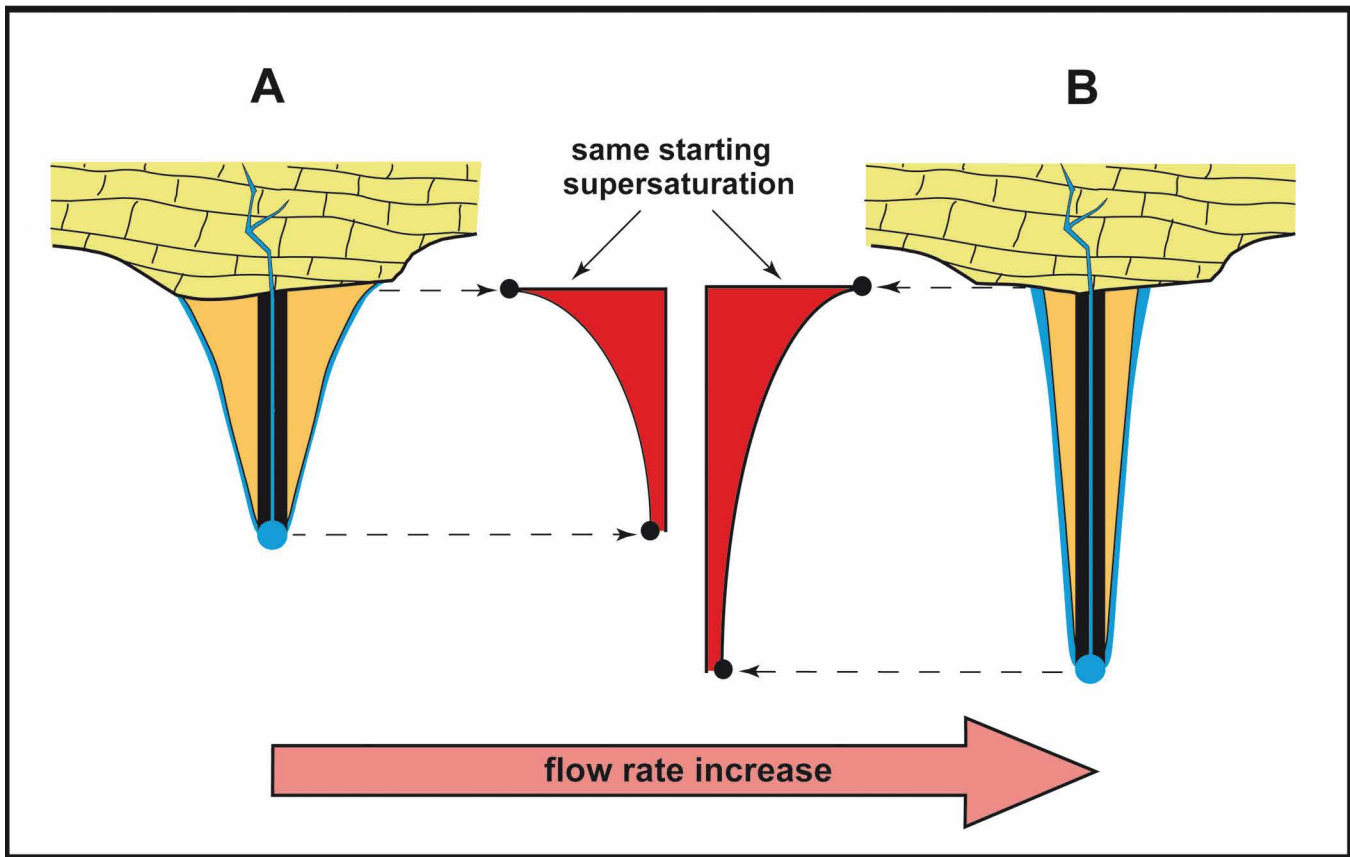
Figure 7. The flow rate on the outside of a stalactite is inversely proportional to the amount of water feeding the speleothem. A slow flow rate allows time for the degree of supersaturation to change because there is more time for precipitation near the attachment point. This favors greater tapering.

angle is less than 0.1−0.3°. Remarkably for a speleothem developing in the open air, these parallelepipeds consist of a single euhedral calcite crystal dramatically elongated along the C axis (Fig. 8B).

As stated previously, the external form of stalactites is generally a function of the saturation index, and in normal monocrystalline stalactites, the conical overgrowth is characterized by many small sub-euhedral crystals sharing a common crystal lattice structure. The many small crystals reflect sufficient saturation and flow as to allow comparatively rapid, competitive growth from many seeds. Such rapid growth would disrupt growth of large monocrystalline calcite crystals by introducing multiple C axis orientations. The formation of large euhedral crystals implies largely stable growth conditions such that any variation along the C axis is smoothed out by dissolution and re-precipitation. As discussed below, this would be possible if the water film was only slightly supersaturated because a highly-saturated solution would suppress re-dissolution and allow the misaligned crystals to grow before they could be eliminated to preserve the larger monocrystalline structure (Mullin, 1997).

Measurements of the intact (still attached) square speleothems and the sampled pieces (Table 1) demonstrate a dramatic change in their external shapes, but a relatively small variation in the dimensions of the original soda straws. As already stated, the always constant diameter of a normal soda straw is 5.1 mm (Curl, 1973), which corresponds to an area of about 26 mm^2, while the areas of the square soda straw fragments range between 42 (S2) and 106 mm^2 (S5). The longest square straw has an area of 161 mm^2 at its attachment point. We nonetheless refer to the square speleothems as straws rather than stalactites because, visually, they more closely resemble soda straws than conical stalactites, especially those that are still attached to the cave ceiling.

The area in which the square soda straws developed is relatively far from the cave entrance, and the local microclimate is presumably very stable with temperatures and humidity decoupled from the entrance region and surface. This would allow relatively long intervals characterized by rather steady water fully saturated with respect to calcite. Therefore, the transformation from rounded to square was mainly induced by the solution-redeposition and recrystallization of the already formed speleothem, while the precipitation of new calcite played a second-order role. The recrystallization responsible for the ghost straws in the broken samples is further evidence for transformation of a pre-existing soda straw.
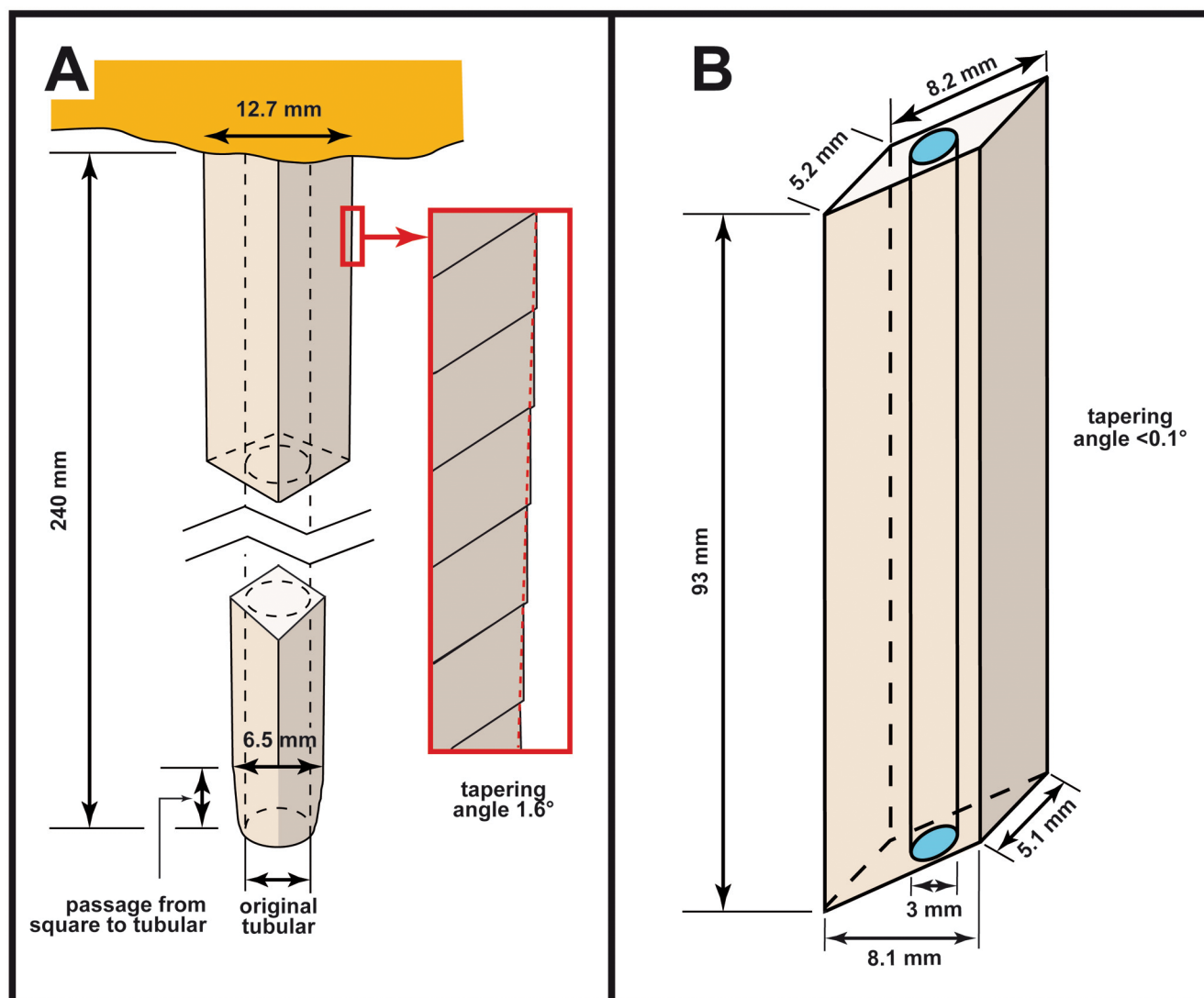
Figure 8. A: drawing of the longest attached square soda straw growing from the cave ceiling. The inset shows the displacement of the parallel twinned calcite crystals that creates tapering of the speleothem toward its tip. Both the dimension of the crystals and the degree of tapering are exaggerated to make the resulting structure evident; B: drawing of the S2 sample consisting of a single dramatically elongated calcite crystal.

Moreover, the relatively small volume increases suggest that for much of the time, the water flowed over the samples with an extremely low supersaturation with respect to calcite, allowing only a scarce epitaxial growth of a few, relatively large crystals. The extremely low tapering angle of the pyramidal stalactites is in perfect agreement with this hypothesis.

It is highly probable that the feeding solution also experienced several periods of simple saturation (no overall solution capacity with respect to $CaCO_3$), allowing only the simultaneous exchange of equivalent amounts of ions from solid to liquid and vice versa that caused the progressive enlargement (cannibalism) of a few crystals, while the smaller ones – being more easily dissolved – progressively disappeared. In this respect, the square pyramidal stalactites must be considered the limit crystal structure developing when the external feeding solutions are characterized by a $CaCO_3$ content swinging from extremely low supersaturation to neutral or even extremely low undersaturation.

At least theoretically, square pyramidal stalactites can develop in relatively stable conditions, but this is not the case for the parallelepiped ones: in fact, stationary conditions cannot explain a constant deposition rate from top to tip of the former soda straw. The observed constant sectional areas can be maintained only if the overall balance between periods of under-saturation and super-saturation is in approximate equilibrium (with a slight prevalence of supersaturation to justify the slight increase of volume observed in all the analyzed samples) and if for most of the time, only saturated (neutral) solutions are in contact with the soda straw surfaces.

Therefore, to transform a tubular soda straw into a square parallelepiped, it seems necessary that two strict boundary conditions are met simultaneously:

1. A film of water flowing very slowly, or even sometimes being stationary, over the whole external surface of the tubular soda straw must be maintained for a rather long interval of time. This is required to allow the slow process of progressively transforming the calcite crystal lattice of the tubular straw into a single, elongated euhedral rhombic crystal.

2. The concentration of calcium carbonate in this water must regularly fluctuate from slightly under-saturated to slightly super-saturated, never varying significantly in either direction. This is required to avoid fast dissolution that may severely damage the outer surface of the mono-crystal, or fast deposition that, in turn, may allow the evolution of several embryonic crystals with different orientation and disrupt the monocrystalline structure.

But these two boundary conditions alone cannot justify the resulting constant size of the square soda straw along its growing axis instead of the more common pyramidal shape, in which the size of the soda straw decreases as it nears the tip. Same size means that a constant supersaturation is maintained along the whole speleothem, but this seems to be in conflict with the fact that local deposition will necessarily deplete the solution in calcium carbonate and therefore the supersaturation must decrease from the top to the bottom of the speleothem (as normally occurs with the conical or even pyramidal stalactites). Condensation is the only water source that can allow such behavior (being at the beginning necessarily undersaturated with respect to calcite). Therefore, the third boundary condition is:

3. External feeding water mostly (if not totally) coming from condensation processes.

Most of the condensation will naturally occur on the ceiling of the cave passage; therefore the subsequent slow seepage toward the top of the squared soda straws will produce a solution of $CaCO_3$ that can sometimes also bring, if the condensing process is slow enough, the water to a complete saturation before reaching the top of the straws. In rare periods of extremely scarce condensation or enhanced evaporation, the seeping water may eventually become even more supersaturated before reaching a straw's top. Obviously, condensation will occur, with different intensities over the whole external surface of the straws, thus locally lowering the $CaCO_3$ concentration. The presence of several small voids along the mean cleavage planes within the monocrystalline structure of the square soda straws, as well as larger re-dissolution features, such as the lens-shaped cavities (Fig. 4), confirms that aggressive water must have been in contact with the external surfaces of at least some of the square soda straws during their development.

The A and B axes of the rhombic crystals forming the square speleothems are not of equal length; the rhombic cross sections show that the lateral increases in soda straw widths or diameters were not homogeneous, and one axis always grew faster than the other (Table 1 and Fig. 9).

This phenomenon is probably a consequence of air currents inverting their directions twice a year, thus causing selective alternations of enhanced condensation and/or evaporation, while the pCO_2 of the cave atmosphere undergoes slight variations during the year. The cave is known for its breezes, and air moves upstream during the summer and downstream during the winter throughout the cave. This behavior is consistent with feeding waters supplied by condensation processes, which are higher but with a lower level of pCO_2 during the cold and wet seasons (winters), while evaporation prevails during the warmer and drier ones (summer) when the pCO_2 is higher (c.f. Banner et al., 2007). Therefore, the transformation from rounded to quite or even totally parallelepiped was mainly induced by the solution-redeposition and recrystallization of the already formed speleothem, while the precipitation of new calcite played a second-order role.

These pieces of evidence confirm that the external water films must flow very slowly or even sometimes be stationary, thus allowing deposition or solution processes to occur, even if calcite saturation levels of the feeding solution change very little. In fact, only extremely low supersaturation can induce an epitaxial growth over the pre-existing monocrystalline structure of the speleothem. In this manner, the soda straw is obliged to gradually transform its cross section from round to rhombic, as required by the crystalline structure of calcite.

However, if the degree of supersaturation is not constant along the whole surface, necessarily the soda straw will become larger at its top and progressively narrow towards its tip as downward movement and precipitation progressively decrease the calcium carbonate content of the solution. This is not the case of the parallelepiped straws. At least some of the time, the upper part of the speleothem must be in contact with slightly undersaturated water that progressively increases its carbonate concentration by solubilizing part of the already existing tube's external structure during its slow motion downward. This temporal variation of the extent of the undersaturated area along the soda straw is consistent with the near constant horizontal cross section dimensions along the C axis of the whole speleothem.

It would be hard to justify this complex behavior by the arrival of seepage water over the external surface of the tube at its attachment point, but this may be compatible with active condensation that always brings undersaturated water in contact with a speleothem's surface. In fact, the normal change in intensity and location (preferred direction) of these phenomena during the year, moving, expanding or reducing the respective areas of under-saturation and oversaturation, can easily explain such in-time and -space variations (Fig. 10).

The relative rarity of parallelepiped soda straws relative to the already very rare pyramidal straws is probably caused by the unique combination of variables required for them to grow. Development of parallelepiped soda straws requires
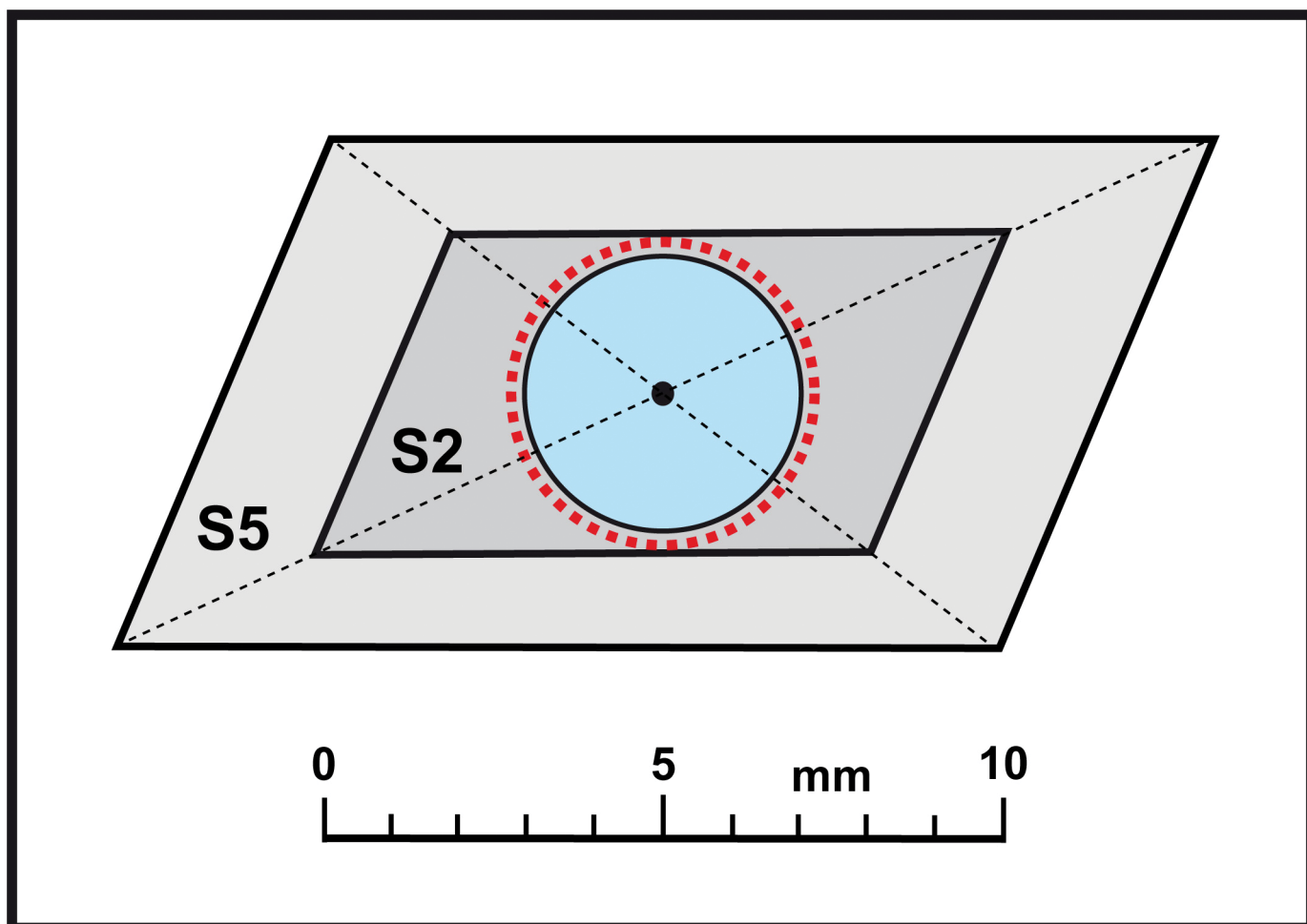
Figure 9. The rounded section of a normal soda straw (red dots) compared with those of the largest (S5) and the smallest (S2) available samples. The blue circle represents the feeding tube of S5, while the black one is that of S2.

air current-driven changes in condensation/evaporation processes that are unique to each speleothem because local air currents are dependent upon the baffling effects of surrounding speleothems and wall geometries. These conditions presumably supplied the necessary variability in time and space of the degree of saturation and feeding rate. In addition, we noticed that if the condensation on a tubular soda straw's 0.1 mm-thick external walls is maintained in the same area for enough time, a hole will be produced, and feeding water would spill out from the internal tube, thus end growth as a typical soda straw.

The final step in the development of the sampled square soda straws was the partial masking of their rhombic shapes by thin, uneven layers of polycrystalline calcite (Figs. 3C and 4). This final stage may have started prior to their falling to the cave floor but probably developed after breakage as the fragments sat on the still-growing flowstone. This final stage was characterized by a sudden increase in supersaturation, which induced new nucleation processes and creation of the thin layers of polycrystalline calcite with palisade structures. This overgrowth partially masked the monocrystalline structure of the speleothem and cemented a few of them to the flowstone floor. This outer crust is very thin (never exceeding 2−3 mm) and suggests this last stage was relatively short. Nonetheless, the achieved supersaturation must be far higher than that in the previous stages, which was always characterized by monocrystalline deposit.

Final remarks

The square soda straws recently found in the Dry Cave are sub-types of stalactites that can be subdivided into two different groups: pyramidal and parallelepiped ones. Their rhombic cross sections and tapering angles distinguish them from normal conical stalactites and from each other. Typical stalactites are characterized by a tapering angle normally ranging between 3° and 5° (Fig. 11). The pyramidal ones are the limit structure for this type of speleothem when supersaturation is kept to a minimum under stationary conditions. This limit is characterized by a tapering degree close to 1.6°, 2−3 times lower than that of the normal stalactites. Only non-stationary conditions may justify the development of quasi- to true-parallelepiped soda straws, characterized by a tapering degree 5−10 times lower than the pyramidal ones
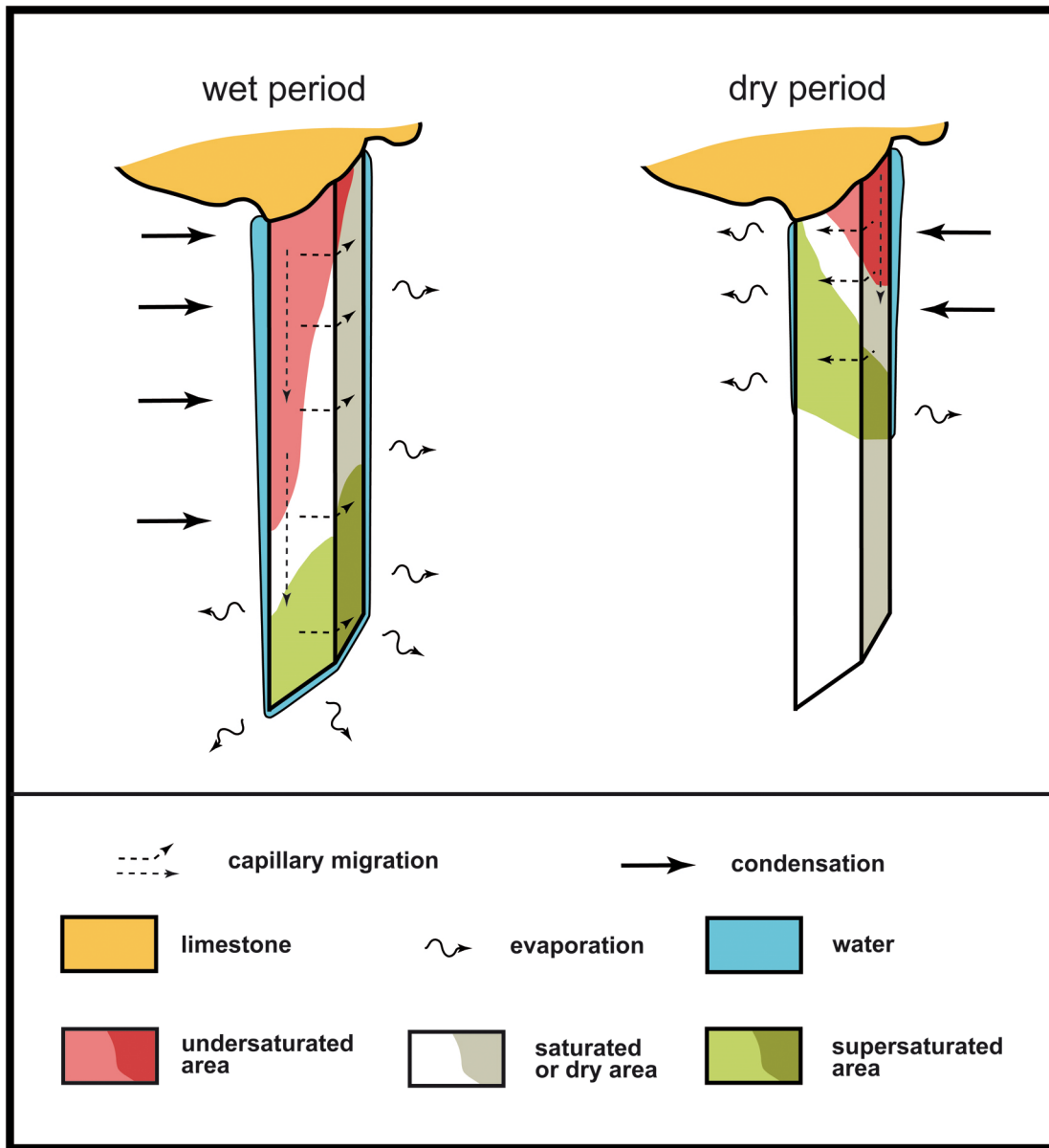
Figure 10. Sketch of two of the possible migrations of the different saturation areas over a square soda straw as a function of the wind direction because it controls the most-likely locations of condensation and evaporation.

(0.3°−0.1°). In fact, very peculiar hydro-dynamical and hydro-chemical conditions are required to justify the genesis of the parallelepiped soda straws. Firstly, it is necessary for a film of condensation water to flow very slowly, or even sometimes be stationary, over the external surface of a tubular straw for a rather long interval of time. Moreover, the concentration of calcium carbonate in this water must regularly fluctuate from slightly under-saturation to slightly super-saturation, never raising or lowering to a significant degree in either direction. This is required to maintain the process of solution/re-deposition, which slowly transformed the previous rounded monocrystalline structure into an elongated, single euhedral crystal with a rhombic cross section.

A factor which may easily allow slight swing of the semi-stationary saturation condition is the CO_2 content in the cave atmosphere, which is normally subject to slight changes every 12 hours (from day to night and vice versa) and seasonally to a greater extent (from winter to summer). The diffusions from air to water and the reverse are extremely fast processes; thus, even a small change in the partial pressure of CO_2 is immediately reflected in the carbon dioxide concentration of stationary or slowly moving water films, which in turn affects the saturation degree with respect to calcite. Presently no data are available on CO_2 content and its possible daily or seasonal variation(s) within Dry Cave. Therefore, it is impossible to state if this parameter is really the principal or at least one of those controlling the evolution of the parallelepiped soda straw even if this seems to be quite reasonable.
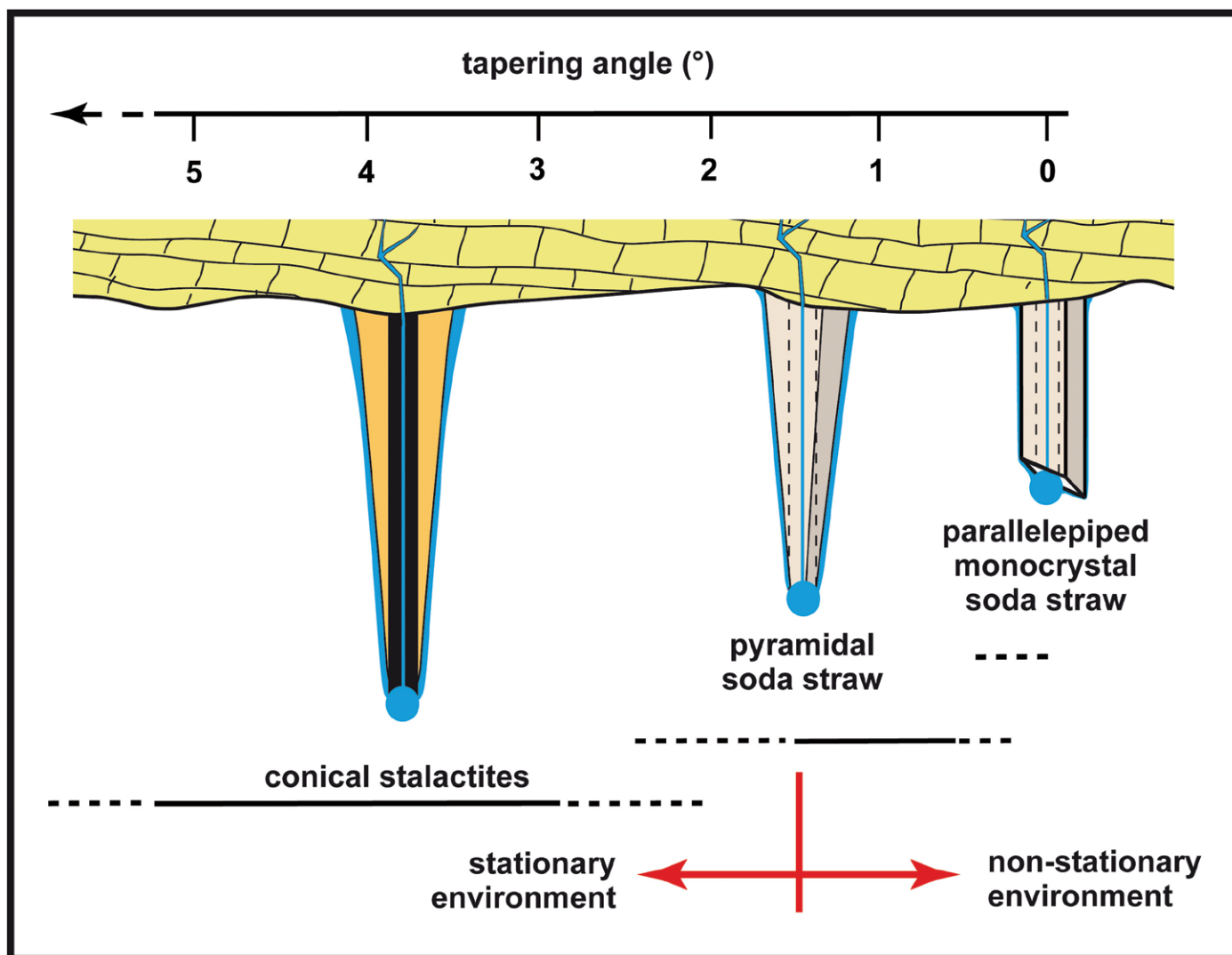
Figure 11. Stalactite sub-types are, in large part, defined by the tapering degree. Conical stalactites have tapering angles greater than 2.5° and commonly in excess of 5°. Pyramidal square soda straws have tapering angles of 0.1° to 2.0°, but for tapering values lower than 1.6°, a non-stationary environment is probably required. Finally, the perfect parallelepiped stalactites, first reported herein, are the end member with a tapering angle of 0° (null).

In the future, the role of pCO_2, but also our principally speculative genetic mechanism, should be confirmed by experimental measurements carried out on site. The area where the square straws are growing should be continuously monitored not only to achieve the in-time evolution of the local microclimatic data (temperature, relative humidity, pCO_2, direction and intensity of air movements, etc.). Moreover, temporal migrations of undersaturated, saturated and supersaturated areas should be monitored over the external surface of these speleothems by means of some chemical analyses.

In any case, it must be noted that 20 years ago the common feeling was that all speleothem types and subtypes were known (Hill and Forti, 1997). However, only stationary conditions were taken into consideration to define their genesis, and it is now recognized that non-stationary conditions can produce a diverse array of sub-types not previously known or expected. In the last few years, explorations made in remote corners of our planet have resulted in documentation of novel speleothems, most of them displaying characteristics that could only have arisen under non-stationary conditions (Camporeale and Ridolfi, 2012; Vesipa et al., 2015; Forti et al., 2016; Badino et al., 2017; Calaforra and Forti, 2019).

These new findings suggest that the underground world is much more complex than supposed; and therefore, it is highly probable that in the next few years, new strange speleothems will be discovered, or some of those, presently supposed to be exclusive of a single cave, will eventually reveal to be rather common. This shows that the study of caves and speleothems will remain a research field full of discovery and satisfaction for cavers who devote themselves to it.

References

Badino, G., Calaforra, J.M., De Waele, J., and Forti, P., 2017, An Hypothesis On The Evolution of Complex Flowstones, *in* Proceedings 17th International Congress of Speleology, Sydney, v. 2, p. 320−324.

Banner, J.L, Guilfoyle, A., James, E.W., Stern L.A., and Musgrove, M., 2007, Seasonal variations in modern speleothem calcite growth in Central Texas, U.S.A.: Journal of Sedimentary Research, v. 77, no. 8, p. 615−622. https://doi.org/10.2110/jsr.2007.065.

Basset, W.A., and Basset, A.M., 1962, Hexagonal stalactite from Rushmore cave, South Dakota: National Speleological Society Bulletin, v. 24, p. 88−94.

Calaforra, J.M., and Forti, P., 2019, The climate driven peculiar speleothems of the Natuturingam Cave (Puerto Princesa Underground River, Palawan, Philippines): a review: Atti e Memorie Comm. Grotte E. Boegan, v. 48, p. 3–22.

Camporeale, C., and Ridolfi, L., 2012, Hydrodynamic-driven stability analysis of morphological patterns on stalactites and implications for cave paleoflow reconstruction: Physical Review Letters, v. 108, p. 238501 https://doi.org/10.1103/PhysRevLett.108.238501.

Curl, R.L., 1973, Minimum diameter of stalactites: National Speleological Society Bulletin, v. 34, no. 4, p. 129.

Fairchild, I.J., and Baker, A., 2012, Speleothem Science: From Processes to Past Environments: West Sussex, UK, Wiley-Blackwell, 432 p. https://doi.org/10.1002/9781444361094.

Forti, P., Badino, G., Calaforra, J.M., and De Waele, J., 2016, The ribbed drapery of the Puerto Princesa Underground River (Palawan, Philippines): morphology and genesis: International Journal of Speleology, v. 46, no. 1, p. 93−97. https://doi.org/10.5038/1827-806X.46.1.2011.

Franke, H.W., 1965, The theory behind stalagmite shapes: Studies in Speleology, v. 1, no. 2/3, p. 89−95.

García-Ruiz, J.M., Villasuso, R., Ayora, C., Canals, A., and Otálora, F., 2007, Formation of natural gypsum megacrystals in Naica, Mexico: Geology, v. 35, p. 327–330. https://doi.org/10.1130/G23393A.1.

Halliday, W.R., 1959, Holocrystalline Speleothems: National Speleological Society Bulletin, v. 21, p. 15−20.

Hill, C.A., and Forti, P., 1997, Cave Minerals of the World: National Speleological Society, 424 p.

Mullin, J.W., 1997, Crystallization, 3rd ed.: London, Butterworth-Heinemann, 527 p. https://doi.org/10.1002/cite.330701126.

Price, P.H., and Heck, E.T., 1939, Greenbrier County: West Virginia Geological Survey County Reports, 846 p.

Short, M.B., Baygents, J.C., and Goldstein, R.E., 2005a, Stalactite growth as a free-boundary problem: Physics of Fluids, v. 17, no. 8, p. 083101. https://doi.org/10.1063/1.2006027.

Short, M.B., Baygents, J.C., Beck, J.W., Stone, D.A., Toomey III, R.S., and Goldstein, R.E., 2005b, Stalactite growth as a free-boundary problem: a geometric law and its platonic ideal: Physical Review Letters, v. 94, no. 1, p. 018501. https://doi.org/10.1103/PhysRevLett.94.018501.

Springer G., 2019, Dry Cave: Beyond the Bitter End, The West Virginia Caver, v. 37, no. 4, p. 3−4.

Vesipa R., Camporeale C. and Ridolfi L., 2015, Thin-film-induced morphological instabilities over calcite surfaces, *in* Proceedings Royal Publishing Society A, v. 471, no. 2176, p. 20150031. https://doi.org/10.1098/rspa.2015.0031

White W.B., 1976, Cave minerals and speleothems, *in* Ford T.D., Cullingford C.H., eds., The Science of Speleology: London, Academic Press, p. 267−327.

LATERAL FERRUGINOUS GROUNDWATER TRANSFER AS THE ORIGIN OF THE IRON CRUSTS IN CAVES: A CASE STUDY

Cristina Fonollá[1,C], Eugenio Sanz[1], and Ignacio Menéndez-Pidal[1]

ABSTRACT

The iron crusts appearing in all sections of the lower gallery of the Majada del Cura cave (Soria, Spain) consist of iron oxides, hydroxides, and to a lesser extent, manganese; the predominant mineral is goethite. The genesis of goethite is associated with the hydrogeomorphological evolution of the hypogeum river, which has received, upstream from explored cavities, lateral transfer of slightly ferruginous groundwater from the anaerobic environment of the Utrillas facies. The Utrillas facies connects to the cave only through the cave's lower gallery but not from the high gallery. Based on preexisting knowledge of the geomorphological history and the decrease in karstic base level, this connection has existed since at least the Middle Pleistocene. The torrential character of the river and the aerobic conditions cause precipitation by oxidation of Fe^{+2} with little bacterial participation, and the formation of mineral species is compatible with this oxidizing environment.

Introduction and Objectives

Iron and Manganese oxides and hydroxide deposits appear frequently in cavities (Hill and Forti, 1997), and the mineralogy of these deposits can be quite complex (Onac and Forti, 2011a; Post, 1999; White et al., 2009). In past decades, these types of speleothems have been studied in many cavities (among others: Crabtree, 1962; Moore, 1981; Gascoine, 1982; Hill, 1982; Kashima, 1983; Dyson and James, 1981; Peck, 1986; Onac and Forti, 2011b; White et al., 2009; Frierdich et al., 2011; Carmichael et al., 2013; Yusta et al., 2009; Rossi et al., 2010, Rossi et al., 2016; Gázquez et al., 2011; Gázquez et al., 2012). In those works, the incrustations are studied from different perspectives such as mineralogy, speleogenesis, and paleoenvironment. These works address the origin of the iron or manganese present in the crusts.

For a long time, it was thought that the formation of mineral deposits in caves and speleothems were mainly controlled by abiotic processes as a result of the cave's environmental conditions and changes in redox conditions (Barton and Northup, 2007; Engel et al., 2004; Northup and Lavoie, 2001). However, according to the most recent microbiological investigations, it has been proven that deposition of iron and manganese is often governed by microorganisms, mainly bacteria, which metabolize by the processes of Fe and Mn mobilization from sediments, as well as through oxidation and deposition (Skinner and Fitzpatrick, 1992; Hose et al., 2000; Sommers et al., 2002; Northup and Lavoie, 2001, Northup et al., 2003; Spilde et al., 2005; Boston et al., 2006, Boston et al., 2009; Hill and Forti, 2007; Hazel and Northup, 2007).

The objective of this work is the macroscopic, chemical, and mineralogical characterization of the iron and manganese crusts of the Majada del Cura cave. The cave's relationship with the hydrogeological and hydrogeochemical characteristics of the karst and the geological formations of the environment has allowed the construction of a genetic model of the crusts.

This work also aims to limit this model to the past as much as possible. For this, it has been fundamental to relate the regional external geomorphology to the altitudinal arrangement of caves and springs, as well as the altitudinal arrangement of sandy formations to ferruginous underground waters and the dating of calcareous tufa and cave sediments. Thus, the main characteristics of the paleohydrogeological evolution of the aquifer are determined, showing the relationship that this evolution has had with the hydrodynamics of the karstic aquifer and the formation of the iron crusts.

Methodology

During explorations of the Majada del Cura cave, different types of iron precipitates and their macroscopic characteristics have been described. Their distribution within the hydrological and sedimentological context of the karstic apparatus has been analyzed. The other known cavities of this Pico Frentes and Sierra Llana karst have also been explored (Fig. 2) in case they present similar ferruginous crusts.

To analyze the geochemistry and mineralogy of the iron crusts, five representative samples were taken, three of the patina of iron on pebbles (CF-1, CF-2 and CF-3), one of a crust on a speleothem (C-1) and another corresponding to a current precipitate (P1) in a puddle of overflow water (Fig. 4-F). Several analytical techniques were employed and are briefly described below. The quantitative chemical analyses of samples P1 and C1 were conducted through X-Ray

[1]Geology Laboratory. Department of Engineering and Land Morphology. Esc. Tec. Sup de Ing. de Caminos, C.C. y P.P. (School of Civil Engineering), UNIVERSIDAD POLITÉCNICA DE MADRID (U.P.M.), C/ Profesor Aranguren 3, 28040 Madrid, Spain
[C] Corresponding author: cristina.fonolla@upm.es

Fluorescence (XRF), a multipurpose X-ray diffraction Panalytical with a Wavelength Dispersive X-ray Fluorescence (WDXRF) spectrometer. Results of the analyses are listed in Table 2. X-Ray Diffraction (XRD) equipment, "Bruker D8 Advance", for powder samples was used to identify the mineralogical composition of the crystalline phases present in the five samples (Table 1).

Since it was difficult to visually isolate the iron crusts completely from the surface on which they formed, the constituent minerals of the crusts and iron mineralization were identified through images (Fig. 4 to Fig. 6) obtained with a scanning electron microscope (SEM/EDS) model JEOL JSM-820 that has an energy-dispersive X-ray detector (EDX) attached. The EDX was used to perform semi quantitative analyses of several zones of the crusts and of the substrate in contact with the crusts. Microprobe analyses (Table 3) confirmed that the crusts also contained manganese oxides. All the analyses have been carried out in the Technical Services Area of the Complutense University of Madrid, (Spain).

Inside the active cave, the iron crusts have been deposited on the surfaces of all forms of karstic erosion, as well as in the current detrital sediments and in the ancient levels hung by paleogours associated with the subterranean river. In recognizing these sediments of detrital origin, recycled particles from the Utrillas facies were observed, which do not outcrop in the vicinity of the cave, suggesting that those particles have undoubtedly been transported upstream by the hypogeum river through conduits that are, for the moment, inaccessible. This issue was important because it has been known for a long time that this facies contains ferruginous groundwater in the area, and this could constitute the possible source of iron crust. Since there are no methods available to create boreholes, it has been studied first, and the descriptive geometry of the structural contour suggests the possibility that this facies was in depth in hydraulic connection with the cave. A hydrogeochemical study of the area around the karstic apparatus was initiated to evaluate the distribution and concentration of the ferruginous groundwater in these sedimentary facies that could explain the origin of the iron in the crusts. Chemical analyses were obtained from 140 boreholes and wells corresponding to the municipal areas of 10 population centers located in the lower parts of the mountain. The total iron concentration (iron in solution plus iron in suspension) present in these boreholes and wells was measured at the Territorial Service of the Ministry of Health in the province of Soria by the method of atomic absorption spectrophotometry (Servicio Territorial de Sanidad, 1995-1997). The iron content of the effluent streams that circulated during the dry season due to the Weald and Utrillas facies was also analyzed with portable field equipment.

Regarding the current iron precipitation processes, some specific measurements have been made in the underground river, in different hydrological conditions, on the iron content, pH, electrical conductivity and temperature. A historical series of geochemical analyses of the Fuentetoba spring water measuring iron content have been conducted to determine whether they indicated significant concentrations.

To detect the possible presence of bacterial groups in the groundwater, as well as to determine the aggressiveness of these bacteria (indicated by the time it takes for the reaction to appear) and their possible influence on the formation of iron patinas of iron and manganese, tests were carried out following the B.A.R.T method (Biological Activity Reaction Tests) designed by Cullimore (1992). Tubes were used, each of which contained a crystallized pellet of chemicals at the bottom and a free sphere. A tube was filled with water to the upper mark (15mL), causing the sphere to float and isolating the upper medium (aerobic) from the lower medium (anaerobic). For 15 days, the reactions that occurred in the water and in the pearl were observed (Table 4) and identified with those defined by the manufacturer.

On the walls cut by the erosion of the speleothems mentioned of paleogours, the alternation of clear and dark 1 millimeter calcite layers depending on their iron content were observed in detail. These layers revealed that the geochemical precipitation processes of the iron were associated with the river starting from past epochs to the present. It was interesting to date these chemical sediments, and, in this way, two samples were taken from the two levels of paleogours located at different heights, to determine their age as indicated by the decay of radioactive isotopes of uranium/thorium (U/Th) (Table 6). These tests have been carried out in the Institute of Earth Sciences "Jaime Almera" of the CSIC through ICP-MS (Hellstrom, 2003).

Table 1. Mineralogical semiquantitative analysis of mineral phases by dust XRD.

Sample Name	Mineral Phases, %							
	Quartz	Alkali Feldspar	Phyllosilicates	Calcite	Goethite	Lepidocrocite	Hematite	Magnetite
C-1	58	11	25	···	3	1	1	1
CF-1	46	5	12	24	10	···	2	1
CF-2	1	···	···	97	1	···	···	1
CF-3	49	11	20	17	1	···	1	1
P-1	66	5	14	1	11	···	2	1

The characteristics of active and abandoned conduits and the integration of the external geomorphology with the dating of the paleogours terraces present in the cave with the underground river, and of the calcareous tufa associated with the upwellings, have contributed to a better understanding of the speleogenesis of the system and propose an evolution of the karstic aquifer. In this sense, the calcareous tufa of these springs have been sampled (Fig. 3A, Fig. 4 and Fig. 10A) to determine their age by U/Th by means of unbalance series. This was completed at the Institute of Earth Sciences "Jaime Almera" of CSIC through ICP/MS (Hellstrom, 2003).

Geological, Geomorphological, and Hydrogeological Setting

The Majada del Cura cave (UTM 30N European 1950 X (m) = 0533288 long, Y (m) = 4626421 latitude) is found in the eastern end of the Sierra of Cabrejas, which belongs to the septentrional area of the Iberian Range (Soria, NE of Spain). The cave was discovered in 2002 by speleological groups Deportes Espeleo and Terrasub (Sanz et al., 2012), and it is still in the exploration phase. The cave's entrance is located in a high plateau at 1,240 m.a.s. (called Sierra Llana) and extends more than 3.5 km with an E-W direction (Fig. 1).

The explored cavities seem to present two macro-stages in the installation of the networks and phases of karstification. To these two macro-stages correspond at least the two levels of well-defined main galleries:

The first level of galleries and networks is hanging, made of fossil, predominantly horizontal, and has large dimensions. It is located near the level (−20m) of the mouth of entrance or towards the height 1,220 m.

In the second level, another active network links to the previous one through some galleries inclined at about forty degrees. This gallery is sub horizontal, and the channel of a hypogean river runs with a longitudinal slope inclined east towards its drainage point (Fuentetoba). It is a profile of successive backwaters and steps of rapids and waterfalls. We could place it towards the level -50m (1,190m).

From the stratigraphic point of view, the ancient materials in the area belong to the Weald facies (Lower Cretaceous), of detritic nature and about 300m thick.

Above these sediments is a stratigraphic unit of the Middle Cretaceous, known as the "Utrillas facies." This facies is widespread in much of the Iberian Peninsula, and by extension this term is applied to the diachronic section that emerges throughout the Iberian Cordillera, which represents the sediments of predominantly fluvial facies Albian aged; although there were also marshy areas (lignites) and sediments of wind origin. The sediments of quartz sands predominate with a small proportion of feldspar grains that were subsequently altered to kaolin. At its base, part of the Aptian can be represented, and on its roof, the Cenomanian. It sits discordantly on Paleozoic, Triassic, Jurassic, or continental Lower Cretaceous ("Weald facies") materials and gives rise to a Regional Discontinuity Surface.

At this site, the Utrillas facies is 576 m thick, and it can be differentiated into two units: a lower unit containing 200m of sandstone and a conglomerate domain over lutites, as well as an upper 376m unit of medium thickness conglomerate sandstone layers interspersed in a thick series of lutites. These layers of thick sands to conglomerates are rich in quartz and K-feldspar, and its grey color results from large amounts of type I organic matter (lacustrine) in an immature state, but very close to the hydrocarbon generation window that fills the intergranular porosity. Normal samples have OIL = 1.5 and almost 4.0 mg/g of rock of organic matter in the form of hydrocarbons in liquid state (Marfil et al., 1992). This tar sandstone was exploited as an asphalt mine (average content of 8%) in the 19th and early 20th centuries through a gallery up to 50m deep in the core of the same anticline where Majada del Cura cave developed.

Both the Weald and the Utrillas facies have a similar hydrogeological behavior: they constitute a detritic aquifer where the numerous intercalations of lutites limit their permeability or confine it in some sectors. The presence of ferruginous cement in
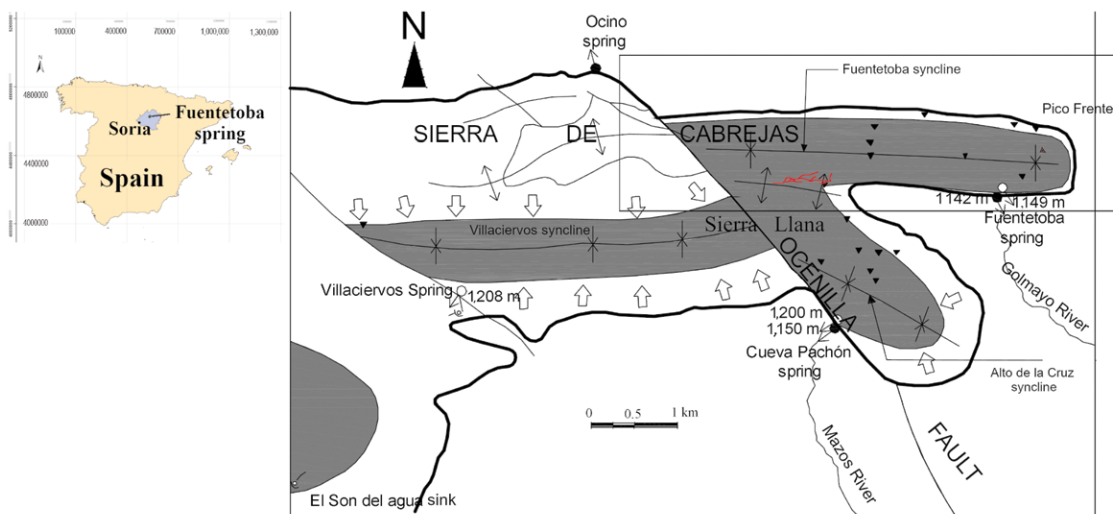

Figure 1. The Majada del Cura cave location map (Sanz et al., 2012).

the sandstones is important, and ferruginous crusts of iron hydroxides associated with laminations and bedding surfaces are frequent (Fig. 10C). There are even small limonite and goethite deposits that have been exploited in the past and with local interest. All of this contributes to the fact that groundwaters are naturally contaminated by the presence of iron, which might jeopardize these geological formations as useful aquifers for human supply (Yélamos and Sanz, 1994; Sanz and Martínez, 2004). The iron content is related to the degree of aeration and oxygenation in aquifers: the upper part is hydrodynamically more active and aerobic; and therefore, has less iron (and vice versa). Likewise, the more permeable materials (more aerated) have less iron, and the less permeable ones have more iron. The iron content of the streams increases in the summer since in the dry season the underground component of the water currents has more influence (Sanz and Martínez, 2004).
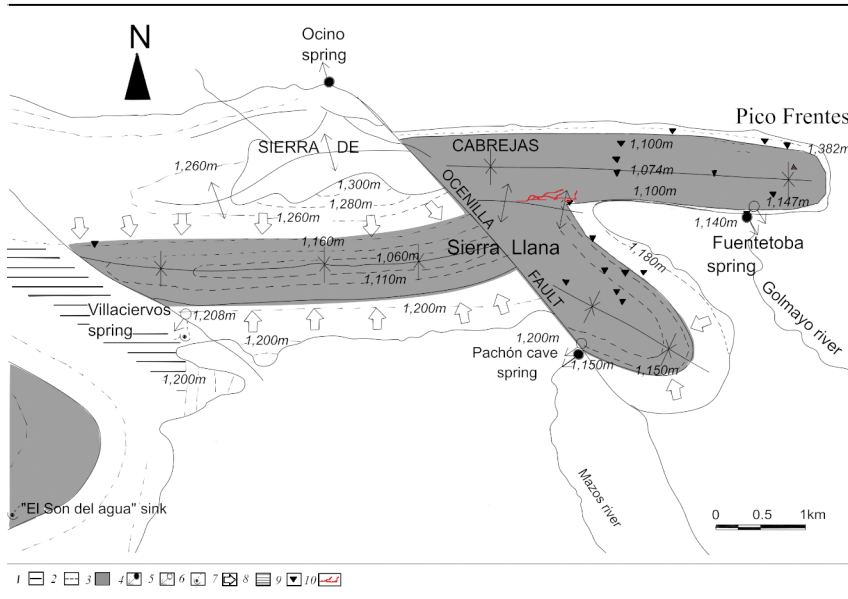
Above the sands of the Utrillas facies is the Cenomanian limestone, which is more or less, sandy and marly; fossiliferous marls and clayey limestones Turonian aged serve as the impermeable base of the karst aquifer where the cave is located. Concordant with the Turonian are 100m of Coniacian nodular limestones that, together with the 120m thick massive Santonian-Campanian limestones, stand out morphologically in the relief, giving rise to the cliffs of the northern edge of the Pico Frentes and Sierra Llana. The cave is excavated in these carbonaceous rocks, perfectly following the direction and dip of the layers of geological contact between marls and limestones near the axis of an east-west direction anticline. These limestones make up the karstic aquifer of Pico Frentes (Rosas et al., 2016; Sanz et al., 2016), a highly developed karst system that is constituted by a succession of synclines displaced by the strike-slip Ocenilla fault (Fig. 2). The aquifer drains through the source of the Mazos river and Fuentetoba spring. This last spring has about 200 L/ s of medium flow and is highly variable (Rosas et al., 2016).

It seems that the axis of the Fuentetoba anticline, at least from the Ocenilla fault, influences the hydrogeological organization of the karstic massif, contributing to the division of the drainage. In the north, the flow is directed towards Fuentetoba spring and in the south, towards the source of the Mazos river and other upwelling waters located at the head of the Golmayo river ravine.

The explored cavities present two levels of

Figure 2. Hydrogeological organization of the karst system (Rosas et al., 2016). 1. Limestones-marls contact outcrop. 2. Contour lines limestones-marls contact in Pico Frentes aquifer. 3. Permanently saturated zone. 4. Spring, perennial. 5. Spring, intermittent. 6. Sink. 7. Groundwater flow in the peripheral of the saturation zone. 8. Groundwater divide. 9. Caves and potholes. 10. The Majada del Cura cave.
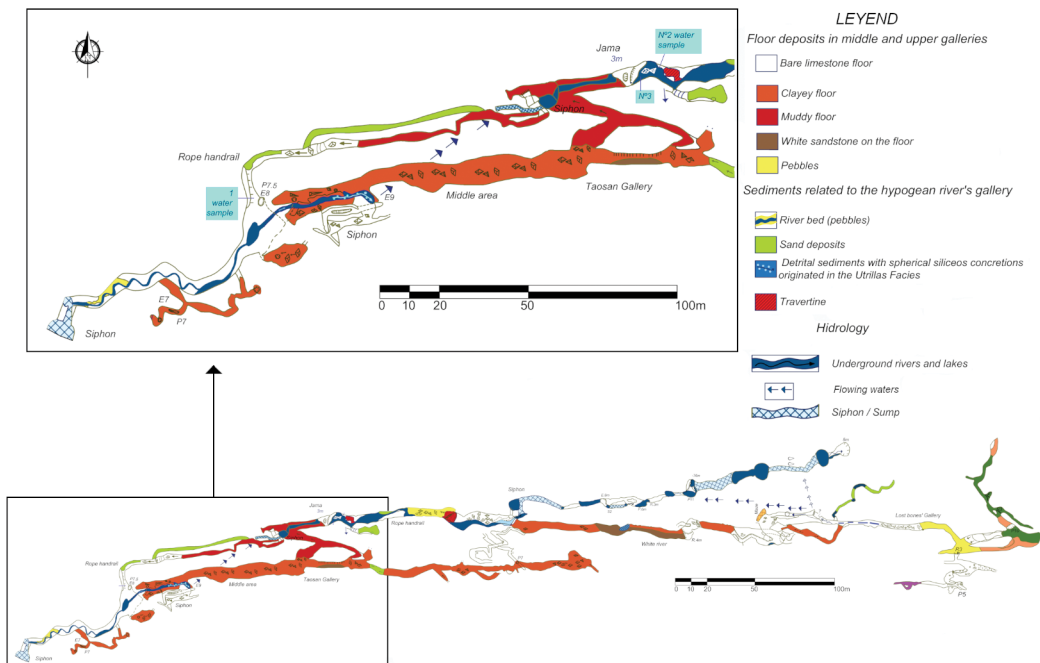

Figure 3. Current topography. La Majada del Cura cave (Soria). Ferruginous crusts are found in the active gallery.

well-defined main galleries that are superimposed along the same geological contact that dips between 45º and 65º towards the north. The first gallery is a hanging, huge fossil and is predominantly horizontal. In the second level, an active network exists that links to the previous one through some inclined passages. This gallery is active and through it runs a hypogeum river with a slope inclined to the east, towards its drainage point (Fuentetoba spring). It is a profile of successive backwaters and steps of rapids and waterfalls (Figure 3).

The Sierra of Cabrejas, from a geomorphological point of view, was affected by a long stage of denudation during the Upper Neogene, with levelling and generalized flattening towards the 1,250m height, although with a gently dipping slope towards the south; It is an erosion surface of the Astaracian (Benito-Calvo and Pérez-González, 2007). Regionally, Benito-Calvo and Pérez-González (2007) locate the beginning of the exhumation of the previous surface; and therefore, the beginning of the incision of the drainage at the end of the Turonian. Late, on this surface, a relict or fossil surface drainage network was installed (Pliocene and throughout the Quaternary). It is shallow and incipient that is conserved notched in the rock in some areas. There are doline fields, some uvalas, and karren fields. The subsequent erosive phases led to the lowering of the relief of the limestone massif to the level 1,030-1,000m, which is the altitude of the Douro river to the north of this mountain range (Sanz, 1992).

Results

Macroscopic description of iron crusts and their geological and hydrogeological context

The iron and manganese crusts of the cave are located on floors, walls, and ceilings of the active gallery (they are not present in the upper gallery), continuously covering a large part of the surfaces with a thin black or brown layer between 0.01 and 4 mm thick. They occur mainly in the upstream westernmost part of the underground river, losing some importance in the eastern lower sector, according to groundwater flow direction. Through the course of the underground river and below the minimum low water level, no ferruginous incrustations are formed, and the rock appears nude with its natural cream color. The originating agent of the ferruginous incrustations is considered to be the river since the habitual levels of current floods are marked and distinguished by the different intensities of coloration on the channel walls, with the intensity increasing as the height of water increases (Fig. 4A). There are also horizontal paleo-levels located at higher elevations of the river and lakes, which sometimes number up to six. They are drawn by horizontal lines of iron oxides on the walls that indicate the successive pulses of embedding of the river. At some points, the dark deposits of iron have fallen off.

Ferruginous precipitates constitute crusts of consolidated material. Their surface is smooth and adapts to all kinds of erosion forms and sediments (from the past and present) in the active cave. Some different types of sediments include:
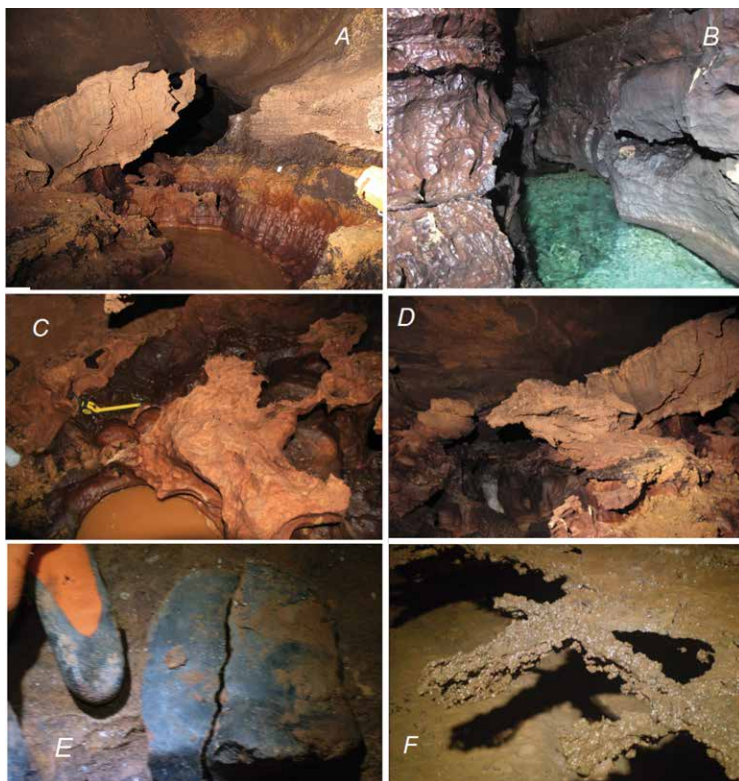

Figure 4. Ferruginous crusts and deposits in the active gallery of The Majada del Cura cave.

1. Fine sheets of iron covering forms of corrosion in the substrate rock (Fig. 4B).
2. Patches of black crust of 1-2 cm on the surfaces of paleogours. From here sample C-1 was taken (Fig. 4C).
3. Iron sheets of 0.1 to 2 cm covering a huge yellow clay lump no more than 5 cm thick attached to the walls of the gallery and located at different heights and with variable dimensions that are related to recent floods (Fig. 4D).
4. Pebbles covered in a black patina on the outer side of 1 mm thick (Fig. 4E). It affects gravels and pebbles deposited between clays corresponding to sediments of recent floods located between the current channel level and up to 1 m above. From here, the samples CF-1, CF-2 and CF-3 were taken.
5. Ferruginous precipitates associated with current stagnant flood waters located 1 m above the current channel. They are lattices of calcite and floating iron supported on the edges of the banks (Fig. 4F). From here, the sample P-1 was taken.
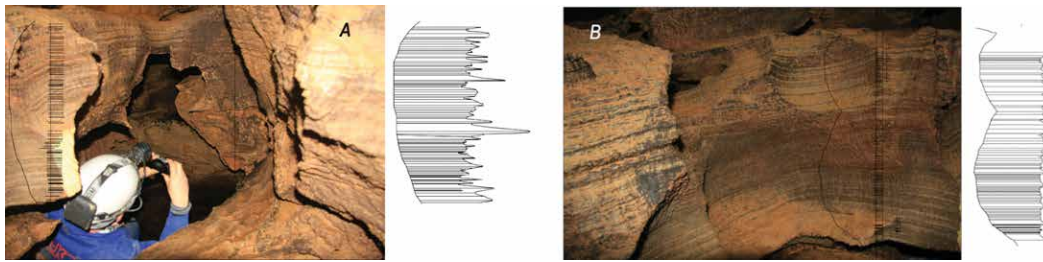
Figure 5. Iron-Mn external lamination in gours. 5A Fresh section of the gours (above the helmet) does not exhibit Fe-Mn lamination. Fig. 5B Potholes have affected paleogours.

In the erosion sections of potholes that affect paleogours, in the small layers of growth of these speleothems, an alternation of light 1 millimeter layers of calcite and other dark layers with higher iron content are observed. This different content of iron is superficially revealed in a patent manner (Fig. 5A).

The clear layers of calcite are thicker, about 5 or 6 times more than dark layers. With cuts of 0.5 m in Figure 5A, 65 tiny layers can be counted, and in Figure 5B with cuts of 5 m, 99 tiny layers can be counted.

Geochemical and mineralogical results of iron crusts

Semi quantitative mineralogical analyses of the five samples by powder XRD were used to detect the crystalline phases of iron oxides and hydroxides, hematite (1-2%), goethite (1-11%), magnetite (1%), and lepidocrocite (1%). Due to the low crystallinity of the crusts, the X-ray diffractograms were poorly defined. Other minerals present included quartz, potassium feldspar, and phyllosilicates (clay minerals) (Table 1).

Iron and manganese oxides have been detected in the crusts by means of X-ray fluorescence in samples C1 (paleogours) and P1 (Table 2); the percentages of manganese in the total sample are small. However, higher values have been detected in the punctual analysis of the cortices with the EDX microprobe in all samples (Table 3).

The samples of pebbles collected in the current river have crusts of iron oxides (77.73 - 4%) and manganese (25.72-10.47%), and their chemical composition varies depending on the area of the crust where the microanalysis was carried out. Some crusts have formed on carbonate clasts (CF-2 and CF-3) and others on clay minerals, quartz, and feldspars (CF-1).

In the area outside the paleogours (sample C1, Fig. 6-B), a network of filaments was observed that covers the surface of the sample, probably belonging to ferruginous bacteria, and rounded deposits that may be the result of their biological activity. In a cross-section, the chemical composition of the crust was analyzed with a microprobe that detected a matrix of iron and manganese oxides, with clay and quartz minerals that include quartz clasts (samples C1-3-SP1 to SP5). The composition of the material in contact with the crust of iron includes iron oxides, alumina-silicates, and quartz.

The last sample analyzed (P-1) is formed by iron and manganese oxides with quartz fragments in some areas, depending on where the analysis was carried out. Rounded goethite textures were photographed. An orange paste of clay minerals, iron oxides, and quartz was deposited on the iron crusts (Figures 6 to 8).

Result on the current presence of iron bacteria

The cultures used were I.R.B (iron related bacteria), S.L.Y.M. (slime forming bacteria), T.A.H. (total aerobic bacteria) and S.R.B. (sulfate reducing bacteria). The reactions that occurred are summarized in Table 4. The 1 HAB/TAB reaction indicates the existence of aerobic bacteria, with a population <61,000 cfu/mL (cfu = cells) and moderate activity. The I.R.B have a population < 10 cfu/mL and are not aggressive; reaction nº 5 indicates the existence of anaerobic Ferro-bacteria. The SLYM tubes contain general microflora, and its population of 500-2500 cfu/mL is moderate. Finally, the current sulfate reducing bacteria (S.R.B) from the water samples in zones Z2 and Z3 have a population of less than 20 cfu/mL, so they are considered non-aggressive. However, in zone 1, the population between the values of 925 to 1400 cfu/mL indicate a medium aggressiveness (Senderos, 2001), (Smith, 1995).

Results of chemical analyses of iron in the waters of the underground river and Fuentetoba spring

It has not been possible to perform periodic monitoring in the underground river and overflow ponds because of accessibility difficulties, but some specific measures carried out in two overflow ponds and in the hypogeum river (zones 1-3 of Fig. 3) of the active gallery of the cave do not present high concentrations of iron (Table 5). The pH is slightly alkaline, and

Table 2. Analysis of oxides in weight percentage of samples C1 y P1, XRF.

Sample Name	Oxides																		
	Fe_2O_3	CaO	SiO_2	MgO	Al_2O_3	K_2O	Na_2O	Cr_2O3	MnO	TiO_2	V_2O_5	SnO_2	P_2O_5	SrO_2	ZrO_2	SO_3	Cl	ZnO	CoO
C1	11.17	0.99	62.14	1.10	19.52	3.11	0.30	0.01	0.12	0.90	0.04	···	0.25	···	0.11	0.08	0.08	0.01	0.01
P1	32.54	1.37	51.93	0.50	9.83	1.44	0.20	0.20	0.62	0.79	0.03	0.01	0.30	···	0.26	0.05	0.07	0.01	···

Table 3. Analysis of mayor elements by weight percentage (EDX).

Sample	O, %w	Fe, %w	Mn, %w	Mg, %w	Si, %w	C, %w	Al, %w	Ca, %w	K, %w	Description
C-1-3-SP1	46.74				53.26					Upper crust, Quartz
C-1-3-SP2	24.04	73.28			2.68					Superficial crust, matrix
C-1-3-SP3	38.30	49.83			3.04	7.16	1.67			Superficial crust, matrix
C-1-3-SP4	38.83	28.70	19.85			8.28	2.11	2.24		Superficial crust, matrix
C-1-3-SP5	28.94	29.94	26.12		6.47		4.04	4.50		Superficial crust, matrix
C-1-4-SP1	44.91	20.08			32.11		2.90			Clays, inner zone, dark
C-1-4-SP2	43.68	22.45			28.48		5.40			Clays, inner zone, light
C-1-5-SP1	54.30	11.08			13.15	10.58	8.36		2.53	Upper zone
CF-1-2-SP1	22.27	77.73								Dark matrix, iron oxide
CF-1-2-SP2	29.27	40.25	18.53		6.84		5.12			White spheres
CF-1-2-SP3	22.27	77.73								Dark matrix, iron oxide
CF-1-3-SP3	48.15	15.00	16.59		3.95	11.83	2.47	2.01		White spheres
CF-1-4-SP1	53.26				46.74					Quartz matrix between spheres
CF-1-4-SP2	45.72	19.58	13.81		7.69	9.31	1.97	1.92		White spheres
CF-1-5-SP1	46.63	12.05	25.72		15.61					Yellowish inner zone
CF-1-5-SP2	32.96	50.92			16.12					Dark minerals (Yellowish inner zone)
CF-1-5-SP3	42.00	25.59			23.35		9.07			White matrix between dark minerals (inner zone)
CF-1-6-SP1	40.10	44.58			5.08	7.00	3.25			Detail CF-1-5-SP3, mineral
CF-1-6-SP2	22.27	77.73								Matrix, detail CF-1-5-SP3
CF-2-2-SP1	28.53							71.47		Inner part beneath iron crust, carbonate clast.
CF-2-3-SP1	53.26	46.74								Quartz clast in orange matrix over iron crust.
CF-2-3-SP2	46.10	9.60			25.58		5.14		3.58	Upper part, clays & iron oxides
CF-2-3-SP3	46.73	8.31			27.12		14.32		3.52	Upper part, clays & iron oxides
CF-2-3-SP4	45.92	10.51			25.65		14.63		3.29	Upper part, clays & iron oxides
CF-2-4-SP1	40.66		22.96		19.72		9.89	6.76		Upper part., over carbonate
CF-2-4-SP2	55.48		10.47		13.72	11.37	5.99	2.97		Upper part., over carbonate
CF-2-5-SP1	55.17		13.62		7.37	13.45	5.76	4.62		Upper part., over carbonate, zoom
CF-3-1-SP1	35.25	36.18			14.76		7.65		6.16	Inner part, Orange-brown zone
CF-3-1-SP2	44.33	13.93			24.37		13.17		4.21	Inner part, Orange-brown zone
CF-3-2-SP1	46.98	5.40	23.23		6.38	9.72	4.84	2.56	0.89	Upper part, iron crust
CF-3-2-SP2	49.28	4.00	23.15		5.66	11.42	3.92	2.56		Upper part, iron crust, dark
P1-1-SP1	25.95	68.50			5.55					Cross-section

Table 3. (Continued).

Sample	O, %w	Fe, %w	Mn, %w	Mg, %w	Si, %w	C, %w	Al, %w	Ca, %w	K, %w	Description
P1-1-SP2	35.34	33.44	8.67		19.24			3.31		Cross-section
P1-1-SP3	26.04	68.26			5.70					Cross-section
P1-1-SP4	26.08	68.16			5.75					Cross-section
P1-1-SP5	53.26				46.74					Quartz, grain detail
P1-1-SP6	28.98	60.89			10.13					Cross-section
P1-1-SP7	22.27	77.73								Cross-section
P1-2-SP1	36.20	51.68	1.59		2.04	6.23	2.26			Goethite, iron oxide detail
P1-3-SP1	53.26				46.74					Upper orange zone, over iron oxides, Quartz
P1-3-SP2	53.26				46.74					Upper orange zone, over iron oxides, Quartz
P1-3-SP3	40.94			2.82	17.40		7.67	31.17		Upper orange zone, over iron oxides, Quartz
P1-3-SP4	47.56	10.96			30.08		11.40			Upper orange zone, over iron oxides, Quartz

the river temperature is about 8°C. The conductivity of the river is 300 μS/cm, and the conductivity of lakes is 700 μS/cm. The measurements in Fuentetoba spring have been more continuous. The Fuentetoba spring is the point of exit of the underground river and located 2 km to the west of this known stretch of cave. There have been 23 semester chemical analyses throughout 2001- 2018 (CH Duero). According to these analyses, the water is calcium-bicarbonate facies and poorly mineralized, where bicarbonates (between 200 μg/L and 42 μg/L) and calcium (between 43 and 97 μg/L) represent more than 95% of the ionic content. During certain summer months, the iron concentration can range from as high as 100 μg/L to less than 0.01 g/L. Of all the ions present in the water, the concentration of the iron ion shows the most pronounced seasonal variation. It should be noted that the analyzed iron is in solution and not of total iron, which is probably greater, as is the case with the results of the analysis of the water points located in the geological facies of Weald and Utrillas. The sulphate content varies from between 4 to 12 μg/L. The conductivity normally ranges from between 300 to 400 μS/cm, the temperature from between 7°C to 13°C and the pH from between 7.3 to 8.4 (Table 5).

The ferruginous groundwaters of the Utrillas and Weald facies

It has not been possible to obtain information from an immediate borehole to the cave, but it is possible to collect samples from the area around the karstic system of Pico Frentes. There is only a relatively close borehole that reaches the Utrillas, crossing the limestone of the Pico Frentes syncline and detecting ferruginous waters.

As shown on Figure 9, the presence of iron in the groundwater of the Facies Utrillas and Weald is widespread. Since a significant part of the registered water points (at least 30% of the boreholes) presents significant quantities of iron at almost 25% above 200 μg/L, which marks the limit of potability for human consumption according to the current Spanish regulations, the iron is a real problem when looking for human supply captures in the area (Fig. 10). Results of dissolved iron concentrations in the water show that they range between a minimum value of 0 mg/L and a maximum of 22.7 mg/L of total iron, depending on the depth of the borehole and the underlying lithology. In addition, there are several streams that drain these facies and present ferruginous water in low water level.

Another interesting aspect is that the concentration of iron increases with the depth of circulation of the groundwater due to the lower presence of dissolved oxygen. This causes water's oxidation potential to decrease and reduced iron species to predominate, which do not precipitate easily due to their high solubility. This makes the water of the streams have less iron content than the springs and less iron than the water extracted from the boreholes via wells or pumping. In addition, in these boreholes, it has been possible to establish how the iron increases up
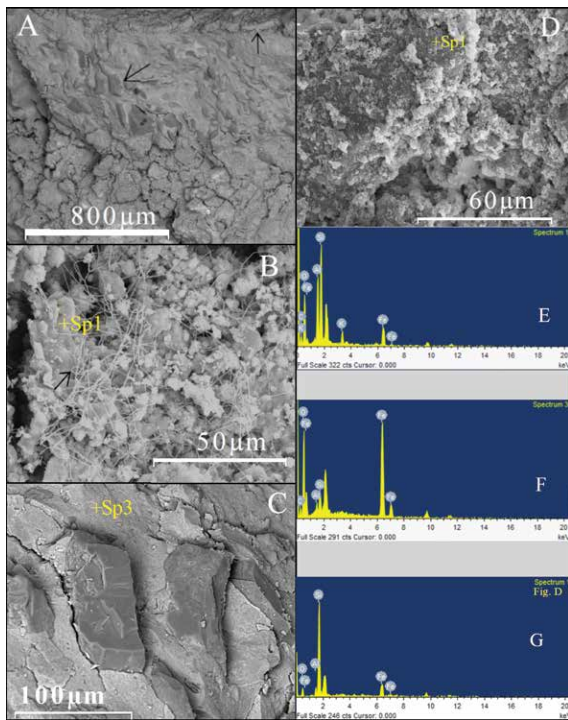
Figure 6. Group of documentary photos: (A) Photographs of a section of the paleogours crusts, sample C1, (B) outer surface of the bark with filaments belonging to bacteria, sp1 EDX micro analysis (E), (C) Most inner zone of the crust, with quartz clasts embedded in a matrix of iron oxides and aluminium-silicates (EDX analysis in F). (D) Internal, granular zone composed of oxides of Fe, Si and clays. In (G) sp1 EDX microanalysis.

to 50 m, as seen in the map of the Figure 9, reaching values of up to 20 µg/L of total iron. The content of iron also varies seasonally, depending on whether the water is low or high, so that iron increases in low waters where the influence of groundwater discharges in Utrillas and in Weald. The iron content is greater in the springs, especially in the streams. This has also been observed in Fuentetoba spring.

The hydraulic connection of the Utrillas facies with the active gallery of the Majada del Cura cave in depth

The 40 m vertical displacement of the Ocenilla fault allows the deep intersection of the Utrillas facies of the footwall block of the west with the karstified limestones of the hanging wall block. Much of this underground intersection is located in the saturated zone and allows the hydraulic connection between these two hydro-stratigraphic formations of different permeability along two short sections (400m approximately in total) that are deduced by means of descriptive geometry and represented schematically (Fig. 2). Prolonging the gallery according to its westward direction following the stratification planes on which it faithfully fits, the western end of the active gallery is located at about 300 m of distance of the stretch of the fault, where the deep Utrillas facies are foreseeably located. This stretch of cave is still unexplored and may be inaccessible, but it is where the water flow comes from. This connection between the Utrillas and the cave has been verified in a reliable way by the existence of sediments from the deposits of avenues of the cave's underground river, where most sediments are limestone sands, although 10% are highly abrasive sands and pebbles of quartz and quartzite, exactly like those of the Utrillas facies. In addition, some spherical nodules of quartz aggregates only appear in this stratigraphic facies (Fig. 10-A).

Ancient deposits of the river with the presence of iron

On the outside of the karstic system, the limestones precipitated in Fuentetoba spring are a reddish color, and this is a sign of the presence of iron in its waters. Nevertheless, inside the cave, there are speleothems of paleogours, and when the speleothems have been eroded alternating clear and dark 1 millimeter calcite layers, with lower and higher
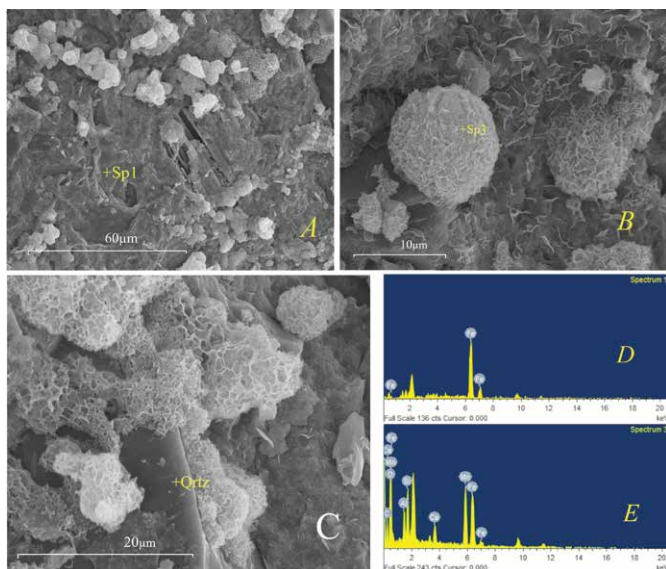

Figure 7. .Sample CF-1 Photographs of SEM (A) general view of the crust section, dark matrix of Fe oxides, EDX analysis at (D), (B) expansion of the Fe and Mn oxide spheres, composition in the EDX (E) microanalysis; (C) detail of a quartz crystal surrounded by Fe and Mn oxides.

iron content respectively, are observed. In the past, each waterfall jump conditioned the formation of gours barriers, leading to a lacustrine phase more important than the current one, with the succession of lakes one after the other. Some of these gours barriers subsist half eroded, but others have been hung as terraces, or as rock ledge, well welded to the walls of the sections cut in later erosive phases. The lower active network of the river cave has two generations of dripstone stalagmite located between 0.5 and 5m above the current channel and associated with gours barriers. They appear as two levels of terraces, especially on the current steps or slope breaks where there are cascades and waterfalls and where the agitation of the water favored the precipitation of calcium carbonate.

Two samples with U/Th have been dated, one corresponding to a low-intermediate paleogours terrace where the contamination by Th 232 is relatively low and constitutes a reliable data (sample nº. 1 of Table 6). Sample Nº. 2 is from a high terrace of paleogours, and its age exceeds the limit of the method of > 350,000 years. These crusts bear witness to an old encrusting circulation corresponding to 188,000 BP on the lower terrace and more than 350.00 BP on the upper
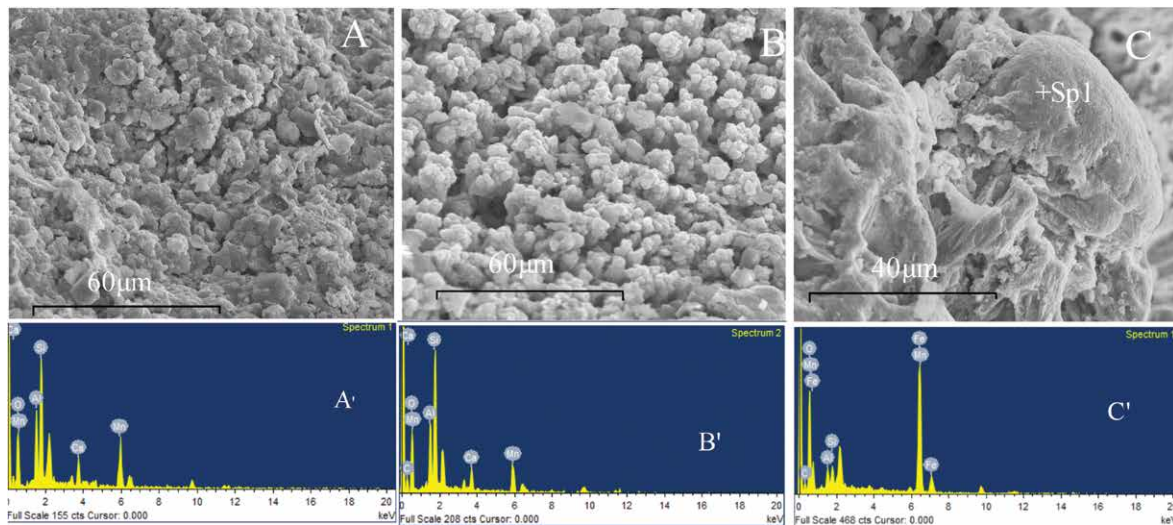
Figure 8. Photographs SEM (A) sample pebble CF-2 ridge oxides from the inner zone of the crust, in contact with the carbonate, EDX analysis (A'). (B) CF-3 ridge Fe and Mn oxides, EDX microanalysis (B'), (C) shows P-1 crystal detail of goethite (goethite), (C') EDX microanalysis.

terrace (within the middle-upper Pleistocene).

Age of the calcareous tufa from Fuentetoba spring

Samples dated with U/Th offer a variable degree of reliability (Table 7), excluding problematic cases (italics in Table 7).

The sample No. 3A was collected in the calcareous tufa of the Mazos river and contaminated by Th232. Therefore, the value of the dating is approximate. However, sample No. 4 is slightly contaminated, collected in the calcareous tufa of La Monjía, and located a few hundred meters from Fuentetoba spring. At a higher level, they are also part of Fuentetoba spring and gives an age close to the method limit > 350,000 years. Finally, the sample No. 10A was collected in the calcareous tufa next to Fuentetoba spring. Based on analysis, it gives an age of 252,304 years +70,511/−42,615.

Other samples taken contained so much residue that it was impossible to date them. These included samples from the calcareous tufa of Pachón cave, the spring of the Mazos river (sample No. 11B) and a column of clay located in an intermediate section of the second level of the Majada del Cura cave.

Table 4. B.A.R.T. tests results for selected sampling stations.

| | Reaction and Days to Reaction | | | | | | | |
| | I.R.B. | | S.L.Y.M. | | T.A.B. | | S.R.B. | |
Sample Name	Reaction	Day	Reaction	Day	Reaction	Day	Reaction	Day
Rope handrails - Z.1	5	10	N	N	1	3	2	6
'Algaes'- Z.2	N	N	3	6	1	3	U	U
Hypogean river -Z.3	N	N	2	5	1	3	N	N

Note: Samples were collected in spring time.
No reaction = N
Reaction unknown = U

Table 5. Temperature, pH and iron concentration from water samples collected from La Majada del Cura cave (Spain).

Sample name	Temperature, °C	pH	Iron concentration, ppm	
Rope handrails - Z.1	11.4	7.30	0.00	
'Algaes'- Z.2	11.4	7.25	0.00	
Hypogean river - Z.3	10.9	7.24	0.40[a]	0.00[b]

[a] First test.
[b] Second test.

Table 6. Values of U/Th dating of two paleogours levels from The Majada del Cura cave (Spain).

Sample Name	Ref - Lab	U-238, ppm	Th-232, ppm	U-234/U-238	Th-230/Th-232	Th-230/U-234	Nominal Date, BP
1	1512	0.29	0.10	1.11 ± 0.02	8.596 ± 0.458	0.84 ± 0.03	188,808 + 17,060 − 14,853
2	2712	0.25	0.38	1.01 ± 0.03	2.011 ± 0.065	0.97 ± 0.04	> 350,000

Table 7. Values of U/Th dating of samples, calcareous tufa from Soria (Spain), 2012.

Sample Number		Ref - Lab	U-238, ppm	Th-232, ppm	U-234/ U-238	Th-230/ Th-232	Th-230/ U-234	Nominal Date, BP
3A	Tufa-Mazos River	1612	0.32	0.16	1.04 ± 0.02	1.953 ± 0.082	0.30 ± 0.01	38,858 + 1,660 − 1,635
4	Tufa-La Monjía	1412	0.35	0.20	1.08 ± 0.02	5.808 ± 0.232	0.98 ± 0.03	335,683 + 98,854 − 52,534
10 A	Tufa-Fuentetoba spring	3312	0.34	0.33	1.01 ± 0.02	2.927 ± 0.186	0.05	252,304 + 70,511 − 42,615

Discussion

Hydrogeochemical model of the crust's formation.

As it is known, the main source of iron and manganese in karst comes from the host rock or the surrounding lithologies that contain these elements, which have been transported to the caves by water. The greatest variety of iron and manganese compounds are produced in carbonate rocks since these rocks and the products of their weathering ("terra rossa" in Mediterranean climates, for example) are enriched in minerals with iron and manganese. This is more unusual in other lithologies, such as gypsum, where the allochthonous origin is more frequent (Osborne, 1978; Peck, 1986; Bosák et al., 2002). Kashima (1983) mentions several caves where the manganese comes from alteration soils that have then been transported by infiltration. In Pauler Cave (Illinois, USA), iron and manganese deposits are deposited by filtrations and streams (Frierdich et al., 2011). Gascoine (1982) locates the origin of iron and manganese in the schists that are above the limestone of the cave and that, due to being transported by water, suffer oxidation near the input points. In Lechuguilla Cave (USA), water entering the cave as filtration is a potential source of dissolved manganese (Levy, 2007). Moore (1981) studies the case where the source of manganese is the reduced waters outside the cave due to the presence of vegetable particles. The origin of the manganese and iron that
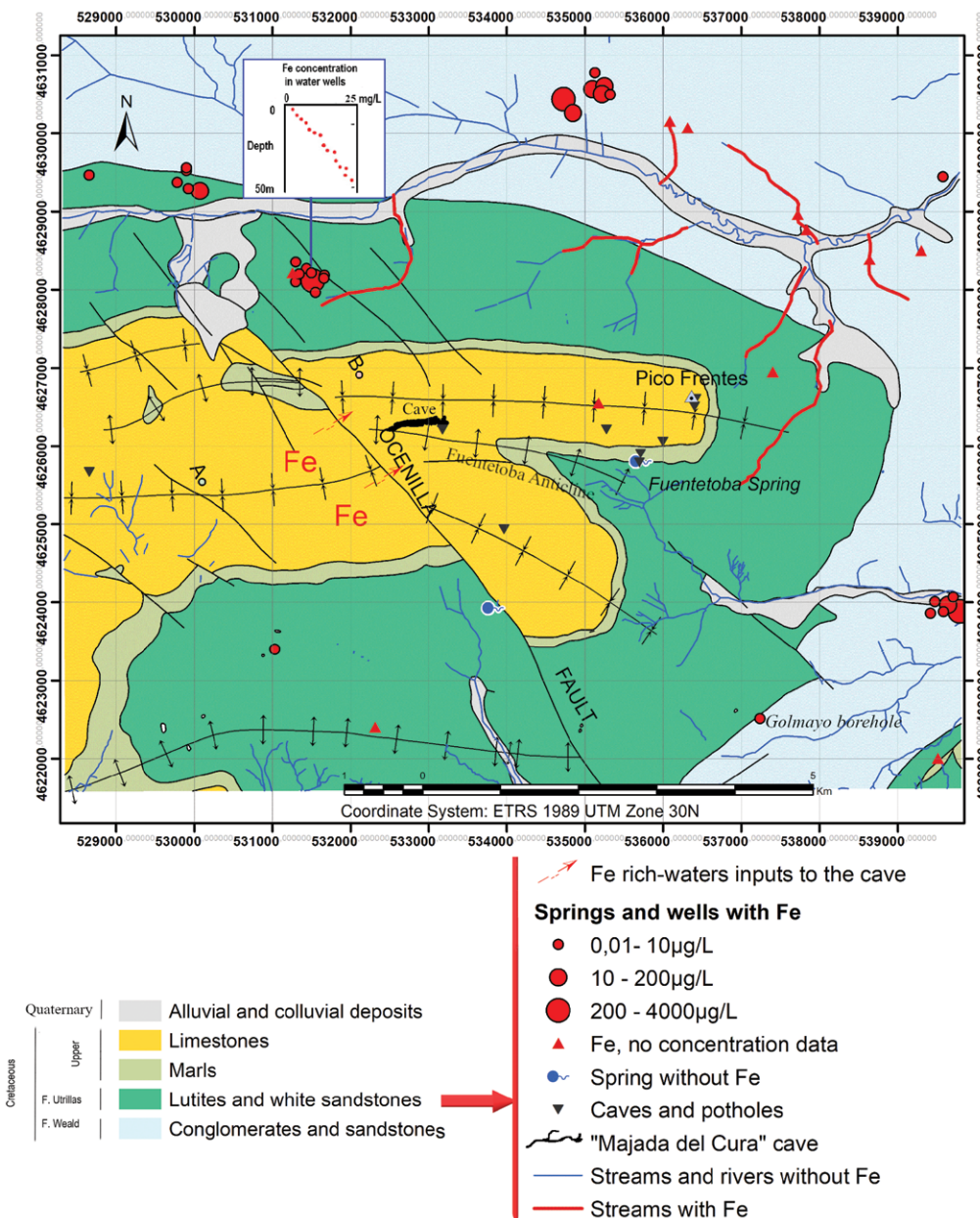

Figure 9. Hidrogeologycal map simplified from "Geological map hoja nº 349, Cabrejas del Pinar (MAGNA)", springs and wells contain ferruginous water in Facies Weald and Utrillas.
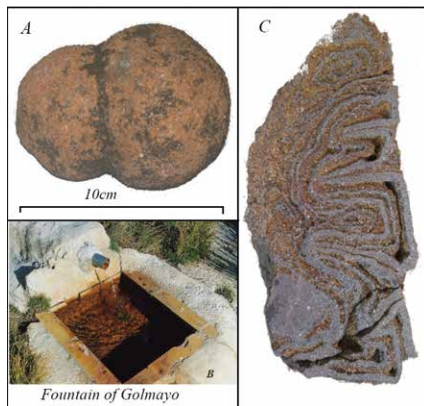
Figure 10. (A) Quartz nodules from Utrillas Facies, are transported by the hypogean river. (B) Ferruginous water from an artesian well in Utrillas Facies (Golmayo, Soria). (C) Convolute ferruginous lamination found in the Utrillas Facies.
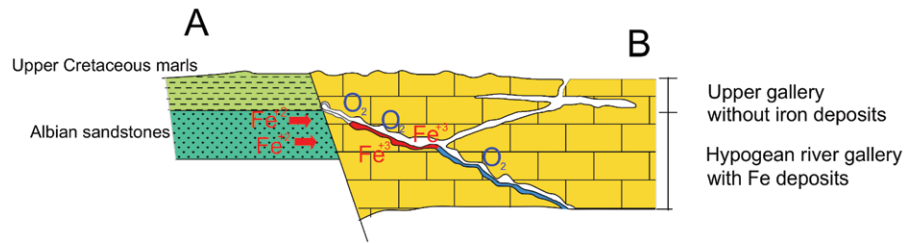

Figure 11. Cross section, footwall (A) Utrillas' sandstones seep water with Fe^{2+} into an oxidizing environment, downstream, to the limestones hanging wall (B) where Fe^{3+} will precipitate in form of oxides-hydroxides of iron.

gave rise to the formation of the crusts of El Soplao Cave is related to the mobilization of these metals, present in the polymetallic sulphide mineralization of the host rock (Rossi et al., 2010). In other cases, the source is siderite nodules in limestones (Yusta et al., 2009). White et al. (2009) quotes pebble patinas of Mn and Fe that come from enrichment of Mn content in streams coming from upstream in non-karstic basins (Northup, 2003). On other occasions, these deposits are the result of enrichment of Fe and Mn through microbial oxidation of leachate from altered bedrock. In other words, they are a result of microbial alteration of the bedrock in vadose conditions. In coastal environments, Allouc and Harmelin (2001) attributes the origin of the biosedimentary deposits of Mn from the interaction of silt with microorganisms and Mn dissolved in seawater. The formation of microbial ferromanganesiferous Frutexites is also mentioned due to the entry of Fe and Mn rich freshwaters into submarine caves (Guido et al., 2016).

In contrast to studies of caves in other regions, the example explained here has the source of Fe in the transfer of ferruginous groundwater from a detrital aquifer in hydraulic connection with the Majada del Cura cave.

The abundance of iron precipitates in the Majada del Cura cave does not occur in the other caves and shafts of this karst system or in others in the region. In addition, the characteristics of the terra rossa, an underdeveloped soil with poor plant cover present outside this and the rest of the other caves, do not seem to favor the export of the Fe^{2+} ion. Apparently, there are no other possible sources of iron within karst systems in the area, such as mineralization in known iron deposits or elevated metal contents in the Cretaceous limestones. However, the presence of iron in this cave is not surprising since this cave is the only one that seems to be linked to the mobilization of the ferruginous underground water, with high concentrations associated with the sediments of the Facies Utrillas that, as it has been seen, have been in hydraulic connection with the active gallery through the Ocenilla fault at about 40-50 m deep. For this reason, the high gallery located above this level had no possibility of this iron source; and therefore, lacks iron crusts. As the hypogean network was fitted with time throughout the evolution of the karst, the gallery was connected with the Utrillas until the present. It must be admitted that this hydrogeochemical process is relatively modern within the speleogenetic context of the system, whose beginning dates back to the Miocene (Sanz et al., 2012) but includes at least the Middle Pleistocene until today, as it is deduced from the level and chronology of paleogours levels with speleothems influenced by the ferruginous environment.

The trace of this cave should be extended upstream, adjusting to the Ocenilla's fault plane, redirecting flows from the Villaciervos syncline and acting as the Utrillas reception gallery at a depth where it is assumed to be under anoxic conditions. Apart from the very ferruginous groundwater incorporated into the river, there is a possibility that these facies provide sands and particles of iron ores in the flood drains of the river. From another point of view, both these sandy sediments and the ferruginous waters of the Utrillas facies also behave in some way as natural water tracers in the groundwater low of the karstic system.

In the precipitation of iron, the chemical composition of the water is a determining factor, in that some units of parts per million of iron in solution assure the formation of scale, and small changes in the pH can favor it. In the few analyses carried out in situ in the stream during low water, no significant concentrations of iron have been detected, but this does not mean that there are not any in other situations or within the inaccessible upstream conducts, closer to the facies Utrillas and where a greater influence of ferruginous discharges to the system is expected. The high iron content sporadically detected in the outlet water of the karst system in Fuentetoba spring indicates that inside the karst system, there must be important entries of ferruginous waters. In fact, although the concentration of iron is not very high, it is enough to cause the precipitation of scales and crusts.

Although the chemical composition is very important, it is not the only factor, since in our case, it is also influenced by the torrential regime of the underground river and its great speed, turbulence, and water aeration in cascades and

waterfalls that favor the release of carbon dioxide and the water oxygenation, favoring the precipitation of iron carbonates and hydroxides, respectively. This underground torrent acts as a real oxygenation reactor of the aquifer, stirring the water at high speed, favoring air-water contact, and producing a mechanism of natural de-ironing of the water with more soluble Fe^{2+} from the Utrillas upstream. Fe^{3+} will precipitate completely in the form of ferric hydroxide, provided that the water is around pH = 8 under aerobic conditions (which is the case). The presence of goethite as the most abundant mineral in iron crusts and other mineral species of iron oxides, such as hematite and magnetite, is perfectly compatible with this oxidizing environment (Fig. 11).

Thus, under these conditions, autoxidation of iron occurs, changing from soluble to insoluble forms.

For example, in the case of oxidation of the ferrous bicarbonate, soluble in the presence of water and in an aerobic medium, it passes to Fe III hydroxide, insoluble (only soluble with pH < 2):

$$2\,Fe\,(HCO_3)_2 + H_2O + \tfrac{1}{2}\,O_2 \rightarrow 2\,Fe\,(OH)_3 + 4\,CO_2$$
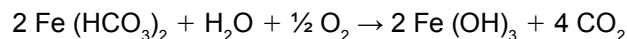
This reaction is modified (adapted) from Cullimore & McCann (1977).

$2Fe\,(HCO_3)_2$ is soluble, while $Fe\,(OH)_3$ is only soluble with pH < 2,2

In the same way, soluble manganese can be insolubilized:

$$2\,Mn\,(HCO_3)_2 + O_2 + 2\,H_2O \rightarrow 2\,Mn(OH)_4\downarrow + 4\,CO_2\uparrow$$
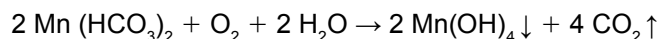
The fluctuation of the hypogean river level reaches over 1.5 m in some areas. These variations have been, and are, important, as observed directly. In periods of high rainfall, ponds and siphons are filled, and there are larger discharges in the Fuentetoba spring. When the level of the hypogean river goes down, the water of the wet walls and the flood ponds evaporates, favoring the precipitation of carbonates and the oxidation of iron in the form of sheets and crusts on the walls and on the pebbles and sediments dragged in by the water.

It is widely known that iron and manganese compounds are extremely sensitive to changes in pH and Eh in water environments, and they oxidize when geochemical conditions change from anaerobic to aerobic, resulting in mineral precipitation (Skinner and Fitzpatrick, 1992). This can happen under natural conditions or by anthropogenic action. An example of this is the precipitates that iron and manganese biochemists provoked by mining activity, which occurred in the cave area of Zoloushka (Ukraine/Moldova), where the works of drainage in a gypsum quarry meant the opening of a karst aquifer and the consequent hydrogeochemical changes in the water environment of a cave (Kotula et al.,2019). Our case is somewhat similar, but due to natural causes: a detrital aquifer with ferruginous groundwater under anaerobic conditions since it is isolated from the surface by impermeable layers. The aquifer drains locally through a cave of a karstic aquifer that it is in contact with. It is assumed that this implies radical changes in the hydrogeochemical environment, which goes from reduction in the detrital aquifer to oxidative conditions within the cave.

In the past, during the middle and lower Pleistocene, and in at least two warm periods where the underground river flow was precarious, the generation of gours was favored. These speleothems developed in environments influenced by the ferruginous environment of the Utrillas since the level has barely changed by a few meters compared to the current channel. The enrichment of the iron by clear seasonal influence is observed, in such a way that the thinner and darker layers in the surface by oxidation of the iron carbonates (sample 5) were deposited safely in low water, when the water of the gours would be with less volume, supersaturated, and in a more oxidizing medium, although it is supposed to be a more toxic medium with the precipitation of iron carbonate (siderite) colorless. The subsequent exudation of iron, or the oxidation of the siderite, make it migrate to the surface, enriching itself in oxides of iron from siderite.

$$2\,Fe\,(HCO_3)_2 + H_2O + \tfrac{1}{2}\,O_2 \rightarrow 2\,Fe\,(OH)_3 + 4\,CO_2$$
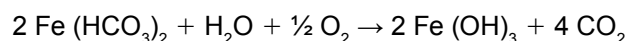
The geomorphological evolution and the presence of iron crusts in the caves

A period of several million years separates us from the generating processes of this cave, combining the syngenetic and paragenetic galleries inside the same underground network. In fact, a slow movement of age surely fini-tertiary period modelled a paragenetic gallery with dense red clay filling. Over time, in these paragenetic galleries, the circulation of water would disappear due to the lowering of the phreatic level, and they were suspended on other new synergic galleries re-excavated and active. During the initial stages, the underground flow was above the sands with ferruginous groundwaters of the Utrillas facies that did not intervene in the hydrogeological scheme. But once the karstic base level was lowered, the connection was made effective through the low gallery.

When did this hydraulic connection start? It is unknown with precision, but it can be affirmed that it is determined by the age of the paleogours and the calcareous tufa associated with the upwelling of Fuentetoba that has worked as an upwelling zone related to low galleries until now. The flow has been directed and concentrated towards the lower area of the south flank of the permeable contact syncline (limestone) and waterproof (Turonian marls). The Fuentetoba spring is currently the lowest point of this contact, and it should have remained the main point of stable drainage throughout much of the Quaternary period. Only here do the calcareous tufa deposits not exist in the entire northern flank and

the rest of the periclinal closure, where the contact is at the highest level. Therefore, this upwelling should have been selected from at least the Middle Pleistocene and shows the large volume of calcareous tufa associated. Therefore, the formation of the crusts should be related to this final paleohydrogeological phase. The depth of the hypogeum river between the paleogours terraces dating from 188,000 BP and the current course does not usually exceed 4m, which indicates the little incision of the river.

Conclusions

Most of the origin of crusts and inlays of iron in the caves are associated with sources with rocks or nearby mineral deposits with high iron content, but in the case studied, it is a transfer of ferruginous water from an anaerobic environment that, due to a tectonic accident, passes to the underground river of a cave. The aeration of water by the torrential character of the hypogeum river favors the chemical precipitation in oxidizing medium of oxides and hydroxides of iron. This process has only worked from the hydraulic connection of the network of active lower galleries with the sands with ferruginous groundwaters of the Utrillas facies since at least the Middle Pleistocene, where the hydrogeological configuration was similar to the current one.

Acknowledgements

References

Allouc, J., and Harmelin, J. G., 2001, Mn-Fe deposits in shallow cryptic marine environment: Examples in Northwestern Mediterranean submarine caves: Bulletin de la Société Geologique de France, v. 172, p. 765−778. https://doi.org/10.2113/172.6.765

Barton, H.A., and Northup, D.E., 2007, Geomicrobiology in cave environments: Past, current and future perspectives: Journal of Cave and Karst Studies, v. 69, p. 163–178.

Benito-Calvo, A., and Pérez-González, A. ,2007. Erosion surfaces and Neogene landscape evolution in the NE Duero Basin (north-central Spain): Geomorphology, v. 88, Issues 3–4, p. 226−241. https://doi.org/10.1016/j.geomorph.2006.11.005.

Beltrán Cabrera, F.J., Ríos Mitchell, J.M., and Ríos Aragüés, L.M., 1980. Mapa Geológico de la hoja no 349, Cabrejas del Pinar. IGME Escala 1:50.000, Shape files.

Bosák, P., Bella, P., Cilek, V., Ford, D.C., Hercman, H., Kadlec, J., Osborne, A., and Pruner, P., 2002, Ochtiná Aragonite Cave (Western Carpathians, Slovakia): Morphology, Mineralogyof the Fill and Genesis: Geologica Carpathica, v. 53, p. 399−410.

Boston, P.J., Spilde, M.N., Northup, D.E., Rosales-Lagarde, L., and Stafford, K., 2006, Subsurface sulfur systems: Production and preservation of distinctive biogenic signatures in sulfur, iron, manganese, and carbonate cave systems: Geochimica et Cosmochimica Acta, v. 70, p. A60, https://doi:10.1016/j.gca.2006.06.225

Boston, P.J., Spilde, M.N., Northup, D.E., Curry, M.C., Melim, L.A., and Rosales-Lagarde, L. 2009. Microorganisms as speleogenetic agents: Geochemical diversity but geomicrobial unity, in, Klimchouk, A.B. and Ford, D.C., eds., Hypogene Speleogenesis and Karst Hydrology of Artesian Basins, Ukrainian Inst. Speleology and Karstology Special Paper 1, p 51−58.

Carmichael, M.J., Carmichael, S.K., Santelli, C.M., Strom, A., and Bräuer, S.L., 2013, Mn (II)-oxidizing Bacteria are Abundant and Environmentally Relevant Members of Ferromanganese Deposits in Caves of the Upper Tennessee River Basin: Geomicrobiology Journal, v. 30, p. 779, https://doi.org/10.1080/01490451.2013.769651

CH Duero (Confederación Hidrográfica del Duero) http://www.mirame.chduero.es/DMADuero_09_Viewer/viewerShow.do;jsessionid=-C0858653A78DE4AA03598E6B84E6C3F2?action=showViewer

Crabtree, P.W., 1962. Bog ore from Black Reef Cave: Cave Science, v. 4, p. 360−361.

Cullimore, D.R., and McCann,1977, The Identification, Evolution and Control of Iron bacteria, in Skinner, F.A. and Sewan, J.M., eds., Groundwater, Aquatic Microbiology: New York, Academic Press, p. 219−261.

Cullimore, D.R., 1992, Practical Manual of Groundwater Microbiology, Lewis Publishers, 412 p.

Dyson, H.J., and James, J.M., 1981, The incidence of iron bacteria in an Australian cave, in Beck, B.F. ed., Proceedings of the 8th International Congress of Speleology, v. 1, p. 79–81.

Engel, A.S., Stern, L.A., and Bennett, P.C., 2004, Microbial contributions to cave formation: New insights into sulfuric acid Speleogenesis: Geology, v. 32, p. 369. https://doi:10.1130/G20288.1

Frierdich, A.J., Hasenmueller, E.A., and Catalano, J.G., 2011, Composition and structure of nanocrystalline Fe and Mn oxide cave deposits: Implications for trace element mobility in karst systems: Chemical Geology, v. 284, p. 82–96. https://doi.org/10.1016/j.chemgeo.2011.02.009

Gascoine, W., 1982. The formation of black deposits in some caves of South East Wales. Cave Science, v. 9, no. 3, p. 167−175.

Gázquez, F., Calaforra, J.M., and Forti, P., 2011, Black Mn-Fe Crusts as Markers of Abrupt Palaeoenvironmental Changes in El Soplao Cave (Cantabria, Spain): International Journal of Speleology, v. 40, p. 163–169, https://doi:10.5038/1827-806X.40.2.8

Gázquez, F., Calaforra, J.M., and Rull, F., 2012, Boxwork and ferromanganese coatings in hypogenic caves: An example from Sima de la Higuera Cave (Murcia, SE Spain): Geomorphology, v. 177–178, p. 158–166. https://doi.org/10.1016/j.geomorph.2012.07.022

Guido, A., Rosso, A., Sanfilippo, R., Russo, F., and Mastandrea, A., 2016, Frutexites from microbial/metazoan bioconstructions of recent and Pleistocene marine caves (Sicily, Italy): Palaeogeography, Palaeoclimatology, Palaeoecology, v. 453, p. 127–138. https://doi:10.1016/j.palaeo.2016.04.025

Hellstrom, J. ,2003. Rapid and accurate U/Th dating using parallel ion-counting multi-collector ICP-MS: Journal of Analytical Atomic Spectrometry, v. 18, p. 1346−1351. https://doi.org/10.1039/B308781F

Hill C.A., 1982, Origin of black deposits in caves: National Speleological Society Bulletin, v. 44, p. 15−19.

Hill, C.A., and Forti, P., 1997, Cave minerals of the World 2: National Speleological Society.

Hill, C.A., Forti, P., 2007, Cave mineralogy and the NSS: Past, present, future: Journal of Cave and Karst Studies, v. 69, p. 35–45.

Hose, L.D., Palmer, A.N., Palmer, M.V., Northup, D.E., Boston, P.J., and DuChene, H.R., 2000, Microbiology and geochemistry in a hydrogen-sulphide-rich karst environment: Chemical Geology, v. 169, p. 399–423. https://doi:10.1016/S0009-2541(00)00217-5

Kashima, N., 1983, On the wad-minerals from the cavern environment: International Journal of Speleology, v. 13, p. 67–71. http://dx.doi.org/10.5038/1827-806X.13.1.5

Kotula, P., Andreychouk, V., Pawlyta, J., Marynowski, L., and Jendrzejewska, I., 2019, Genesis of iron and manganese sediments in Zoloushka Cave (Ukraine/Moldova) as revealed by δ13C organic carbon: International Journal of Speleology, v. 48, p. 221–235. https://doi.org/10.5038/1827-806X.48.3.2255

Levy, D.B., 2007, Oxidation-reduction chemistry of Lechuguilla Cave seepage: Journal of Cave and Karst Studies, v. 69, p. 351–358.

Marfil, R., Callaba, A., Gómez-Gras, D., 1992, Materia orgánica en la Fm. Arenas de Utrillas de Picofrentes (provincia de Soria): diagénesis mineral y orgánica: Geogaceta, v. 12, p. 43–46.

Moore, G.W., 1981. Origin of black deposits in caves, in Proceedings 8th International Congress of Speleology, Bowling Green I and II, p. 642−644.

Northup, D.E. and Lavoie, K.H., 2001, Geomicrobiology of Caves: A Review: Geomicrobiology Journal, v. 18, p. 199–222. https://doi:10.1080/01490450152467750

Northup, D.E., Barns, S.M., Yu, L.E., Spilde, M.N., Schelble, R.T., Dano, K.E, Crossey,

L.J., Connolly, C.A., Boston, P.J., Natvig, D.O. and Dahm, C.N., 2003, Diverse microbial communities inhabiting ferromanganese deposits in Lechuguilla and Spider Caves: Environmental Microbiology, v. 5, p. 1071–1086. https://doi.org/10.1046/j.1462-2920.2003.00500.x

Onac, B.P., and Forti, P., 2011a, Minerogenetic mechanisms occurring in the cave environment: An overview: International Journal of Speleology, v. 40, p. 79–98. http://dx.doi.org/10.5038/1827-806X.40.2.1

Onac, B.P., and Forti, P., 2011b, State of the art and challenges in cave minerals studies. Studia UBB Geologia, v. 56, no. 1, p. 33 – 42. https://doi.org/10.5038/1937-8602.56.1.4

Osborne, R.A.L., 1978, Structure, Sediments and Speleogenesis at Cliefden Caves, New South Wales: Helictite, v. 16, no. 1, p. 3–32.

Peck, S.B., 1986, Bacterial deposition of iron and manganese oxides in North American caves: National Speleological Society Bulletin, v. 48, no. 1, p. 26−30.

Post, J.E., 1999, Manganese oxide minerals: Crystal structures and economic and environmental significance, in Proceedings of the National Academy of Sciences of the United States of America, v. 96, p. 3447–3454. https://doi.org/10.1073/pnas.96.7.3447

Rosas, P., Sanz, E., and Menéndez-Pidal, I., 2016, Hidrogeología del Karst de Pico Frentes (Cordillera Ibérica, España): Estudios Geológicos, v. 72, no 1, p. 1−21. https://doi.org/10.3989/egeol.42132.375

Rossi, C., Lozano, R.P., Isanta, N., and Hellstrom, J., 2010, Manganese stromatolites in caves: El Soplao (Cantabria, Spain): Geology, v. 38, p. 1119–1122. https://doi:10.1130/G31283.1

Rossi, C., Villalaín, J.J., Lozano, R.P., and Hellstrom, J., 2016, Paleo-watertable definition using cave ferromanganese stromatolites and associated cave-wall notches (Sierra de Arnero, Spain): Geomorphology, v. 261, p. 57–75. https://doi:10.1016/j.geomorph.2016.02.023

Sanz, E., 1992, Relieve de la Sierra de Cabrejas. III Congreso geológico de España y I Congreso geológico iberoamericano de Geología: Salamanca, tomo, v. 3, p. 91−95.

Sanz, E., and Martínez, A., 2004, Hidroestratigrafía e hidrogeoquímica de la Facies Weald del Noroeste de la Cordillera Ibérica (Región de Pinares, Soria), VIII Simposio de Hidrogeología. Asociación Española de Hidrogeólogos. Zaragoza (España), p 155−164.

Sanz, E., López, J., Meneses, J.M., and Menéndez-Pidal, I., 2012, Guía geológica de la Sierra de Cabrejas y del Monumento Natural de la Fuentona (Soria) Diputación Provincial de Soria: Colección Temas Sorianos.

Sanz, E., Rosas, P., and Menéndez-Pidal, I., 2016, Drainage and siphoning of a karstic spring: A case study: Journal of Cave and Karst Studies, v. 78, no, 3, p. 183–197. https://doi:10.4311/2015ES0134.

Senderos, A. J., 2001, Estudio microbiológico de las incrustaciones y corrosiones en captaciones de agua subterránea: Universidad Complutense de Madrid. Facultad de Ciencias Geológicas. Tesis.

Servicio Territorial de Sanidad (Soria),1995−1997, Analítica de puntos de agua de la provincia de Soria.

Skinner, H.C.W., and Fitzpatrick, R.W., 1992, in Skinner, H.C.W. and Fitzpatrick, R.W. eds., Biomineralization processes of iron and manganese: modern and ancient environments: Caten Supplements, v. 21, p. 1–6.

Smith, S., 1995. Monitoring and Remediation Wells: Problem, Prevention, Maintenance and Rehabilitation: New York, Lewis Publishers, 183 p.

Sommers, M.G., Dollhopf, M.E., and Douglas, S., 2002, Freshwater Ferromanganese Stromatolites from Lake Vermilion, Minnesota: Microbial Culturing and Environmental Scanning Electron Microscopy Investigations: Geomicrobiology Journal, v. 19, p. 407–427, https://doi:10.1080/01490450290098513

Spilde, M.N., Northup, D.E., Boston, P.J., Schelble, R.T., Dano, K.E., Crossey, L.J., and Dahm, C.N., 2005, Geomicrobiology of Cave Ferromanganese Deposits: A Field and Laboratory Investigation: Geomicrobiology Journal, v. 22, p. 99–116, https://doi:10.1080/01490450590945889

White, W.B., Vito, C., and Scheetz, B.E., 2009, The mineralogy and trace element chemistry of black manganese oxide deposits from caves: Journal of Cave and Karst Studies, v. 71 no. 2, p. 136–143.

Yélamos, J.G. and y Sanz, E., 1994, Hidrogeoquímica de los manantiales sulfhídricos y ferruginosos de las facies Purbeck-Weald del noroeste de la Cordillera Ibérica (provincia de Soria): Estudios Geológicos, v. 50, no. 3-4 . https://doi.org/10.3989/egeol.94503-4319

Yusta, I., Castellano, A., Aranburu, A., and Velasco, F., 2009, Los depósitos de Mn-Al-Fe de la cueva de Lazalday (Zarate, Álava): composición química y mineralogía: Geogaceta, v. 47, p. 117–120.

VARIATION IN CEPHALIC NEUROMASTS SURFACE AND CAVE-DWELLING FISHES OF THE FAMILY AMBLYOPSIDAE (TELEOSTEI: PERCOPSIFORMES)

Daphne Soares[1,C] and Matthew L. Niemiller[2]

Abstract

Cave adaptation has led to unique sensory specializations to compensate for the lack of visual cues in aphotic subterranean habitats. As the role of vision is reduced or disappears, other sensory modalities become hypertrophied, allowing cave-adapted organisms to successfully detect and interact with their surrounding environment. The array of aquatic subterranean habitats, from fast-flowing streams and waterfalls, to quiet phreatic pools, presents a diverse palette to examine what possible sensory solutions have evolved against a backdrop of complete darkness. Mechanosensation is enhanced in many subterranean animals to such an extent that a longer appendage is recognized as a prominent troglomorphic adaptation in many metazoans. Fishes, however, not only interact with the environment using their fins, but also with specialized sensory organs to detect hydrodynamic events. We hypothesize that subterranean adaptation drives the hypertrophy of the mechanosensory lateral line, but that other environmental forces dictate the specific neuromast phenotype. To this end, we studied differences in the cephalic lateral line of the fishes in the North American family Amblyopsidae, which includes surface, cave-facultative, and cave-obligate species. None of the taxa we examined possessed canal neuromasts on the head. Primarily surface-dwelling species, *Chologaster cornuta* and *Forbesichthys agassizii*, possessed receded neuromasts throughout most of the head, with a few on papillae located in front of the nostrils and on ventral grooves on each side of the mouth. The cavefishes *Amyblopsis spelaea* and *Typhlichthys subterraneus* possessed papillate superficial neuromasts all over the head. We speculate that the change from the surface to the cave environment has led to papillate neuromasts in this group, which are likely shaped to detect the hydrodynamic characteristics of the boundary layer created by the swimming fish. Moving sensory organs from the surface of the body out into the boundary layer could increase sensitivity to high frequency stimuli created by prey, predators, and conspecifics.

Introduction

Water currents are a pervasive feature of all aquatic environments and provide obvious cues influencing fish behaviors. Fishes themselves can also create water displacement and pressure fluctuations (Kalmijn, 1989). Hydrodynamic stimuli provide important physical and biological information about the surrounding environment, and fishes have evolved a unique mechanosensory organ to detect hydrodynamic stimuli: the mechanosensory lateral line system (Bleckmann, 1994). The lateral line system is present in all fishes but varies in morphology and distribution.

The functional unit of the lateral line is the neuromast, which can be free standing on the skin (i.e., surface or superficial neuromasts) or in canals that are open to the environments via pores (i.e., canal neuromasts). The distribution of neuromasts across the body and head determines the ability of a fish to detect moving, as well as stationary, stimuli. Each object, be it a rock or a conspecific, creates a unique hydrodynamic signature. The information gained from these hydrodynamic images influences many aspects of fish behavior. For example, fish use their lateral line to examine novel objects (Teyke, 1990; de Perera, 2004), to detect prey (Hoekstra and Janssen, 1985; Janssen, 1999; Yoshizawa et al., 2010), to monitor the movement of conspecifics (Partridge et al., 1980; Faucher et al., 2010) and predators (McHenry et al., 2009), and to maintain position in flowing water (Sutterlin and Waddy, 1975; Montgomery et al., 1997). Superficial and canal neuromasts differ in function and performance but are overlapping in hydrodynamic selectivity. Physiological studies have shown that canal neuromasts respond to water movements that are produced by moving objects, such as prey, that is maximized in the direction of the canal axis (Denton and Gray, 1989; Montgomery et al., 1994). Canal neuromasts typically occur in a distinct line at the base of a canal that runs and extends over the head and flanks. In contrast, superficial neuromasts are located on the surface of the skin and preferentially respond to the velocity of water flow that is not orthogonal to their orientation axis (van Netten and Kroese, 1989; Coombs and Montgomery, 1994; Montgomery et al., 1994) and appear to be best suited to encode flow velocity (Baker and Montgomery, 1999; Van Trump and McHenry, 2013).

The principle sensory cell of the neuromast is the hair cell (Carton and Montgomery, 2004). These hair cells have a bundle of stereovilli that grow longer from one side of the apical surface to the other. A single true kinocilium occurs in the center on of the stereovilli bundle. The stereovilli of superficial hair cells are embedded in a gelatinous matrix called

[1] Biological Sciences, New Jersey Institute of Technology, 100 Summit Street, Newark NJ 07102
[2] Department of Biological Sciences, The University of Alabama in Huntsville, 301 Sparkman Drive NW, Huntsville, AL 35899
[C]Corresponding author: Soares@NJIT.edu

the cupula, and the cupula is drag-coupled to the surrounding water. The motion of the hair cell bundles in the neuromast generates electrical potentials that are transduced into action potentials in afferent neurons. The relationship between cupula displacement and the amplitude of the receptor potential is linear and can reach saturation (Ćurčić-Blake and van Netten, 2006). These signals provide the central nervous system with information about water flow around the body.

The evolution of the lateral line system can be crucial for fishes to adapt to novel environments. For example, several studies have noted that species living in quieter, low-flow habitats tend to have more superficial neuromasts than species living in higher-flow habitats (Coombs et al., 1988; Teyke, 1990; Janssen, 2004). A similar response has been documented in some cavefishes, where blind cave-dwelling taxa have more superficial neuromasts than in related surface-dwelling populations that retain a functional visual system (Poulson, 1963; Niemiller and Poulson, 2010; Yoshizawa et al., 2010, 2014). It is possible that rather than being related to flow regime, morphological characteristics of the lateral line system may be an adaptive response to living in perpetual darkness in subterranean habitats. In Mexican blind cavefish, *Astyanax mexicanus*, superficial neuromasts are longer and more sensitive than those of related surface fish (Teyke, 1990, Yoshizawa et al., 2014), which likely contributes to their ability to better detect flow. Although it is recognized that cavefishes generally exhibit hypertrophy of the lateral line system with respect to number and size of superficial neuromasts (Soares and a,b, 2013; Niemiller and Soares, 2015), studies on neuromast morphology of cavefishes are surprisingly few (Poulson, 1960; Dezfuli et al., 2009; Jiang et al., 2016), with the most intensive work on *Astyanax* (Teyke, 1990; Baker and Montgomery, 1999; Montgomery et al., 2001; Yoshizawa et al. 2010, 2014).

We are interested in cephalic neuromasts specifically because they are crucial for the fine-tuning locomotion necessary for catching prey (Müller and Schwartz, 1982; Bergman, 2004; Tittel et al., 1984; Hoekstra and Janssen, 1985; Janssen, 1990, 1996; Janssen et al., 1995; Janssen and Corcoran, 1998; Schwarz et al., 2011), and they may be organized in a conformation that leads to a mechanosensory fovea (Hoekstra and Janssen, 1986, Coughlin and Strickler, 1990). These neuromasts are very diverse in morphology and organization (Coombs et al., 1994; Beckmann et al., 2010), which are often related to the environment of the fish (Higgs and Furiman, 1998; Ahnelt et al., 2004; Schmitz et al., 2014). Consequently, neuromast phenotypes can be used as a diagnostic character for species delimitation (Kurawaka, 1977; Reno, 1966; Nelson, 1972; Gosline, 1974; Parin and Astakhov, 1982; Stephens, 1985; Webb, 1989b; Arai and Kato, 2003; Bergman, 2004). Functionally, cephalic neuromasts also contribute to rheotaxis (Baker and Montgomery, 1999; Janssen, 2004) and schooling (Blaxter et al., 1983; Janssen et al., 1995; Pitcher, 2001; Diaz et al., 2003),

Here, we examine and compare the morphology of cephalic neuromasts in a family of fishes that span the ecological gradient from surface to obligate cave inhabitation—the Amblyopsidae (Actinopterygii: Teleostei: Percopsiformes). The Amblyopsidae is comprised of six genera and nine species in eastern North America (Niemiller and Poulson, 2010; Chakrabarty et al., 2014; Armbruster et al., 2016). Although subterranean adaptation in fishes is quite common (Soares and Niemiller, 2013a.b; Niemiller and Soares, 2015; for phylogeny see: Niemiller et al., 2013a,b; Armbruster et al., 2016), this family is unusual in that most species in the family are stygobiotic (obligate subterranean). The swampfish (*Chologaster cornuta*) is a small, pigmented species that lives in swamps of the Atlantic Coastal Plain and is the only species in the family found only in surface habitats. All other recognized species are associated with karst terrain of the Interior Low or Ozark plateaus and are at least partially cave-adapted. The spring cavefishes, *Forbesichthys agassizii* and *F. papilliferus*, are facultative cave inhabitants generally occurring in spring-fed streams and also caves on occasion in the Interior Low Plateau karst region (Niemiller and Poulson, 2010). All of other species in the family are obligate inhabitants of caves and have evolved a suite of morphological, physiological, and behavioral characters associated with subterranean life, most notably degeneration of eyes and reduction of pigmentation (Niemiller and Poulson, 2010; Soares and Niemiller, 2013): Northern Cavefish (*Amblyopsis spelaea*), Hoosier Cavefish (*A. hoosieri*), Alabama Cavefish (*Speoplatyrhinus poulsoni*), Ozark Cavefish (*Troglichthys rosae*), Eigenmann's Cavefish (*Typhlichthys eigenmanni*), and Southern Cavefish (*Ty. subterraneus*). In this study, we describe the morphology of cephalic neuromasts using scanning electron microscopy in four species of amblyosids and compare among cave and surface taxa: *C. cornuta*, *F. agassizii*, *A. spelaea*, and *T. subterraneus*. We hypothesize that subterranean adaptation has lead to the hypertrophy of the cephalic mechanosensory lateral line in amblyopsid cavefishes.

Materials and Methods

Individuals of four amblyopsid species were collected under scientific permits issued by the states of Tennessee (no. 1605) and Kentucky (no. SC1211135), USA in April 2012. All individuals were approximately the same size (3 cm), presumably indicating comparable developmental age, and we were not able to differentiate the sex of the fish. We collected three individuals of *Forbesichthys agassizii* from a quiet pool (10 m², mean depth 0.6 m, mud/silt substrate with abundant vegetation) of a spring run fed by Jarrell's Spring, Coffee Co., Tennessee, USA; three individuals of *Chologaster cornuta* from Colly Creek, Bladen Co., NC; three individuals for each of the two cave-dwelling species: *Amblyopsis spelaea* from several quiet pools (20–150 m², mean depth 1 m, silt/sand/cobble substrate) in Under the Road Cave,

Breckinridge Co., Kentucky, USA and *Typhlichthys subterraneus* from several pools with some current (4–12 m², mean depth 0.5 m, cobble/bedrock substrate) in L&N Railroad Cave, Barren Co., Kentucky, USA.

Four fishes were used for histology. Fish were euthanized by prolonged immersion in tricaine methane sulfonate (MS222, 300 mg/L pH 7.2) then perfused with 0.9% NaCl followed by Alcohol-Formalin-Acetic acid (AFA). Fish were decapitated and heads were placed in AFA overnight. Heads were decalcified (RDO Gold, 20:1 ratio) under slow agitation until soft (1−2 days), were then embedded in paraffin (Paraplast X-tra) and cut at 10um thickness in a rotating microtome. Slides were rehydrated in a series of alcohol concentrations, stained with Cresyl violet for 5 minutes, rehydrated, cleared (Histoclear) and cover slipped with permount. Scanning electron microscopy (SEM) was used to differentiate and quantify the morphological features of superficial neuromasts among amblyopsid cavefishes.

Three fish of each species were euthanized by prolonged immersion in tricaine methane sulfonate (MS222, 300 mg/L pH 7.2). Whole specimens were fixed in 2.5% glutaraldehyde, 2% paraformaldehyde in 0.1M phosphate buffer. Fish were dehydrated in a series of increasingly concentrated ethanol baths before being critically point dried and spur coated with 5 nm of gold-palladium in a Denton Vacuum Desk II. SEM samples were imaged in an AMRAY 1620D (Bedford, MA, USA) scanning electron microscope at 10 kV–30 kV acceleration voltage. Scanning electron microscopy was performed at the Laboratory for Biological Ultrastructure at the University of Maryland. We defined the area of the neuromast as the surface that contains the entire footprint of the cupula and the sensory plate area, as the smaller region that contains only sterocilia. Measurements were done with ImageJ (open source, https://imagej.net). We sampled the entire head and operculum. We tested for differences in neuromast surface area, kinocilium length, and sensory plate neuromast area among species with analysis of variance followed by ad hoc Tukey HSD test using Vassarstats.net. Values reported are mean ± 1 standard deviation.

Figure 1. Lateral (A), ventral (B), and dorsal (C) SEM images of the head of *Forbesichthys agassizii*. Scale bar 1 mm.

Results

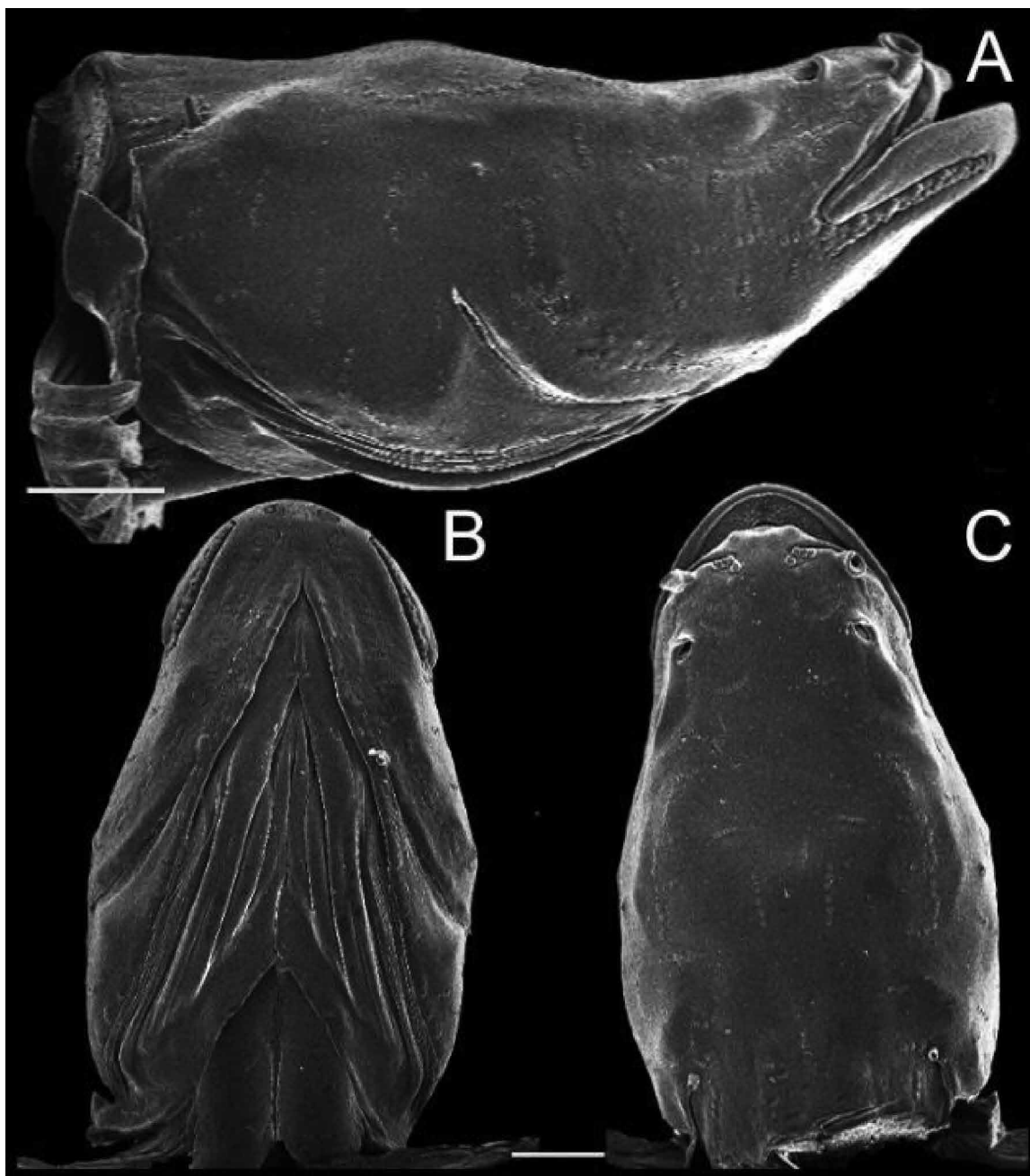The heads of *Forbesichthys agassizii* (Fig. 1)

Figure 2. Lateral (A), ventral (B), and dorsal (C) SEM images of the head of *Chologaster cornuta*. Scale bar 1 mm.

and *Chologaster cornuta* (Fig. 2, see Fig. 7) were covered with stitch-like structures, positioned dorsal-ventrally. The neuromasts on the dorsal and lateral part of the head were receded into pits. The ventral side of the jaw and rostrum in both of these species were populated with superficial neuromasts on papilla. The mandibular papillae were situated in grooves that run from the tip of the lower jaw to the edge of the mouth. The mean surface area of each superficial neuromast in *C. cornuta* was 272.9 $\pm$ 45.0 μm^2. The sensory plate, positioned in the center of the neuromast, was made up of hundreds of hair cells that occupy 131.7 $\pm$ 9.1 mm^2, or 48.3% of the neuromast area. The polarity, from shorter to longer, of the stereocilia was perpendicular to the long axis of the neuromast. The length of the kinocilium was 3.5 $\pm$ 1.5 mm. In *F. agassizii*, mean surface area was 320 $\pm$ 40 mm^2, with hair cells occupying 121.7 $\pm$ 22.9 mm^2, or 38% of the area of the sensory plate. The length of the kinocilium was 3.0 $\pm$ 1.5 mm. Each organ was raised above the skin on a fleshy papilla approximately 0.5 mm high. All cupulae were removed during processing.

Both species of cavefishes examined (*Typhlichthys subterraneus* and *Amblyopsis spelaea*) had more stiches than the two surface fishes (surface fishes = 18 $\pm$ 3 vs. cavefish = 25 $\pm$ 6; Figs. 4 and 5). The stitches were also longer in the dorsal-ventral dimension in *T. subterraneus*. All neuromasts in cavefishes had hair cells on papillae (height of papillla: *A. spelaea* = 0.55 $\pm$ 0.006 mm; *T. subterraneus* 0.73 $\pm$ 0.16 mm; Figs. 6 and 7). In *A. spelaea*, neuromasts had a surface area of 759.1 $\pm$ 133 mm^2. The sensory plate of the neuromast had a mean area of 210.8 $\pm$ 27.0 mm^2, or 27% of the surface area of the neuromast. The kinocilium was 7.0 $\pm$ 1.1 mm, and we were able to measure the cupula at 30.0 $\pm$ 6mm. In *T. subterraneus*, mean neuromast surface area resembled surface fishes at 224 $\pm$ 59.7 mm^2. The sensory plate area was 56.8 $\pm$ 18.0 mm^2, occupying 25% of the surface area of the neuromast. The length of the kinocilium was 5.4 $\pm$ 0.9 mm.
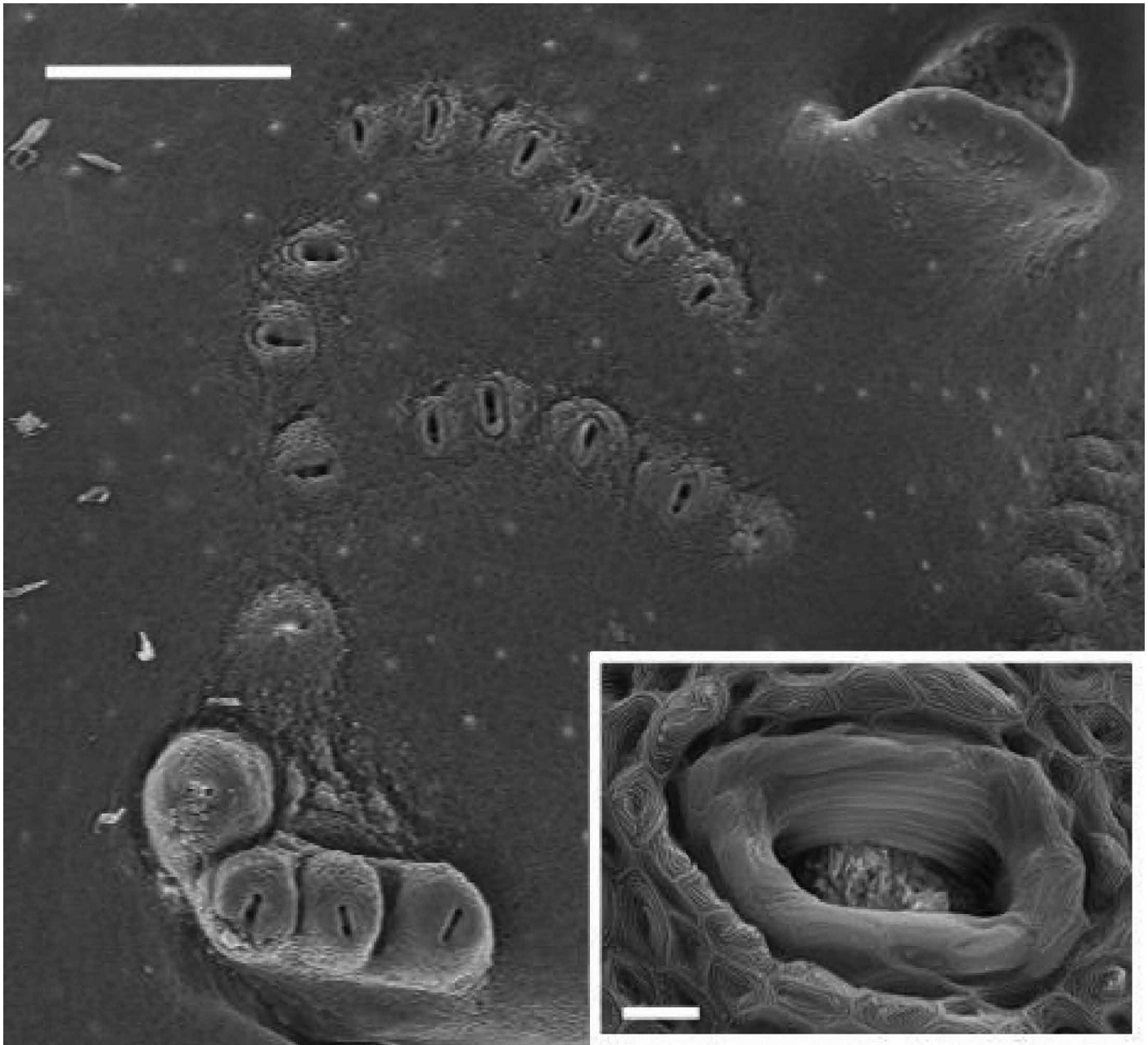
Figure 3. Receded neuromasts and neuromasts on papillae ("stitches") on the rostral end of the head of *C. cornuta*. Scale bar 250 µm. Insert: stereocilia after the cupula was removed. Scale bar 10 µm.

Amblyopsis spelaea had significantly larger neuromast areas than all other amblyopsids (HSD: $P < 0.01$; Fig. 8). There was no difference among *T. subterraneus, F. agassizii and C. cornuta* (ANOVA: $P < 0.0001$, $F = 70.34$, $df = 28$). Sensory plate areas were not significantly different between the two surface fishes but were both larger than *T. subterraneous* (HSD: $P < 0.01$), and smaller than *A. spelaea* (HSD: $P < 0.01$). Accordingly, *A. spelaea* had a larger sensory plate area than *T. subterraneus* (HSD: $P < 0.01$: ANOVA: $P < 0.0001$, $F = 62.53$, $df = 28$). *A. spelaea* had longer kinocilium than all other fishes (HSD: $P < 0.01$). *Typhlichthys subterraneus* had longer kinocilium than both *F. agassizii and C. cornuta* (HSD: $P < 0.01$), which were similar in length (ANOVA: $P < 0.0001$, $F = 108.95$, $df = 131$). Hair cells in the sensory plate of cavefishes also appear thicker than surface fishes.

Discussion

The successful colonization of the subterranean environment often is accompanied by the loss of vision. As eyes become less useful for detecting the environment, other sensory modalities such as mechanosensation become more prominent and even hypertrophied (Marshall, 1965). All four amblyopsid fishes included in this study had extensive
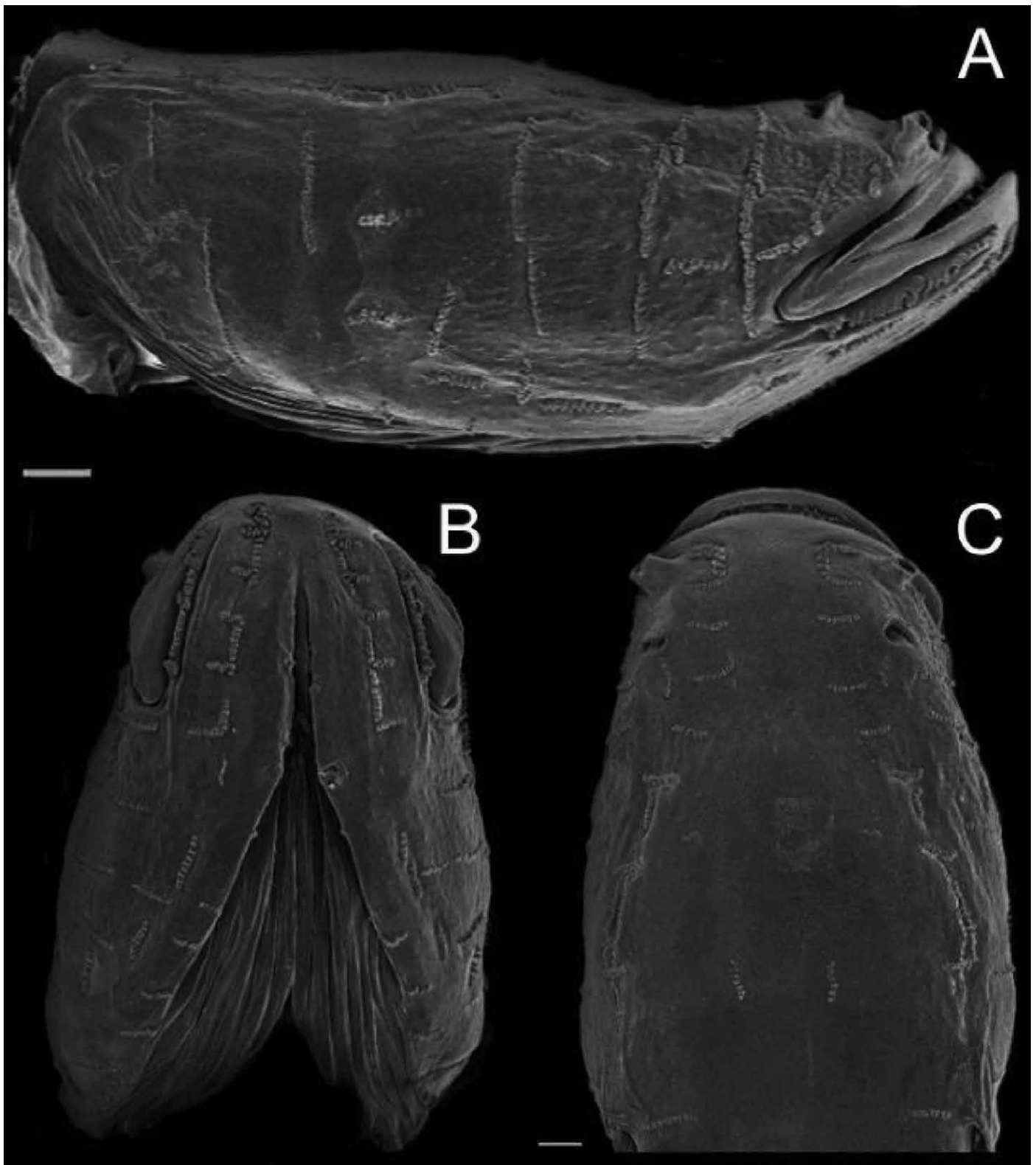
Figure 4. Lateral (A), ventral (B), and dorsal (C) SEM images of the head of *Typhlichthys subterraneus*. Scale bar 1 mm.

cephalic superficial lateral line systems. Two types of cephalic superficial neuromasts were present in amblyopsids: one receded into pits into the skin and one on top of papillae, which perhaps represents different biological strategies or the result of different environmental adaptations. Both types of superficial neuromasts are arranged in dorsal-ventral stitches on the head. As most of these sets of neuromasts are also arranged with best sensitivity perpendicular to the row, they give the whole lateral line a bias for detecting water movements in the rostral-caudal direction. There were
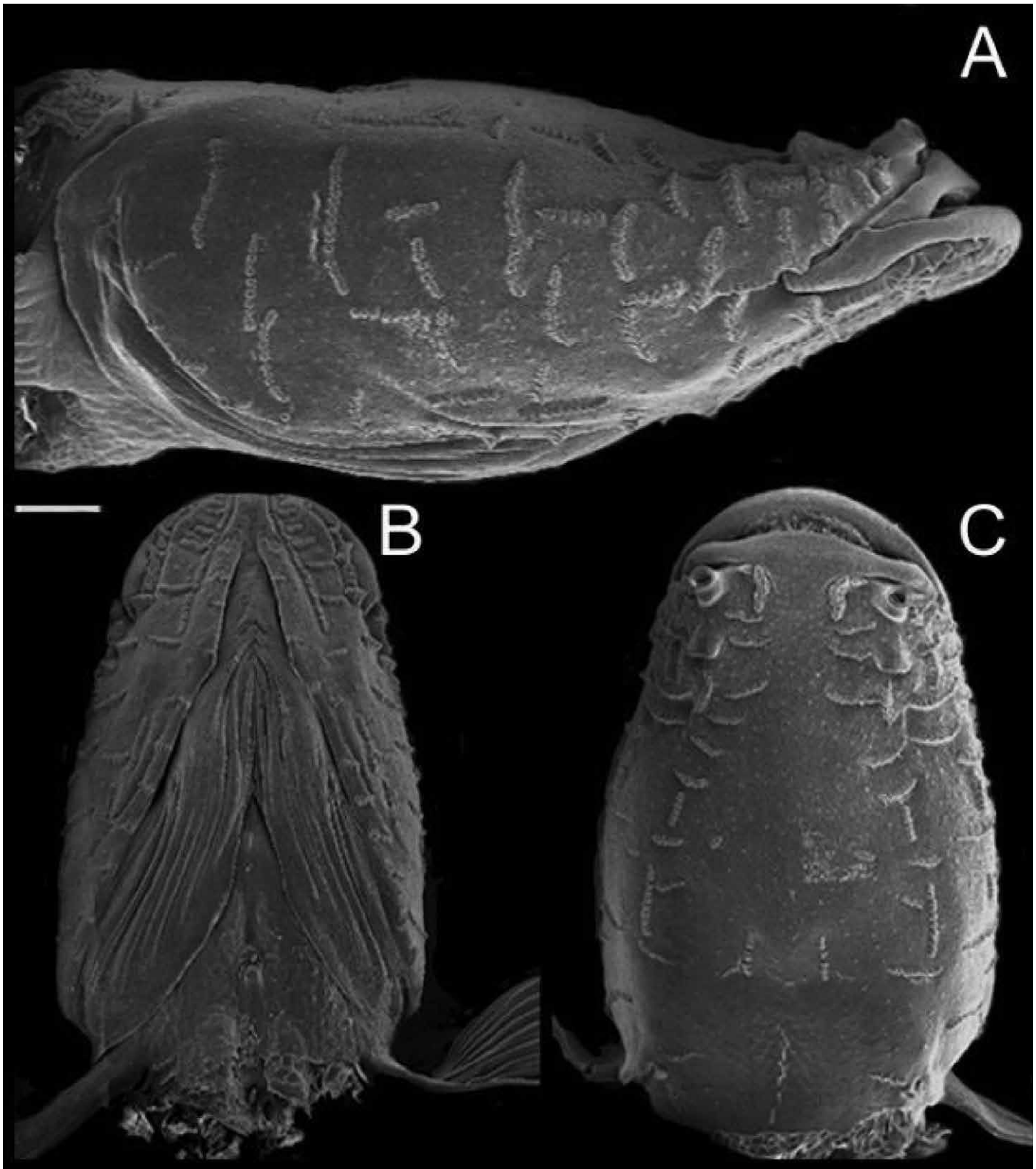
Figure 5. Lateral (A), ventral (B), and dorsal (C) SEM images of the head of *Amblyopsis spelaea*. Scale bar 1 mm.

no canal neuromasts seen on the heads of all amblyopsids. In general, proliferation of superficial neuromasts in surface-dwelling fishes is accompanied by the loss of canals (Moore and Burris, 1956; Webb, 1989a).

The difference in position of cephalic superficial neuromasts between primarily surface and cave-obligate amblyopsids, i.e., receded in pits versus positioned on top of papillae, may reflect differences in microhabitat use. Both *Chologaster* and *Forbesichthys* are nocturnal benthic predators that seek shelter during the daytime and exhibit strong thig-
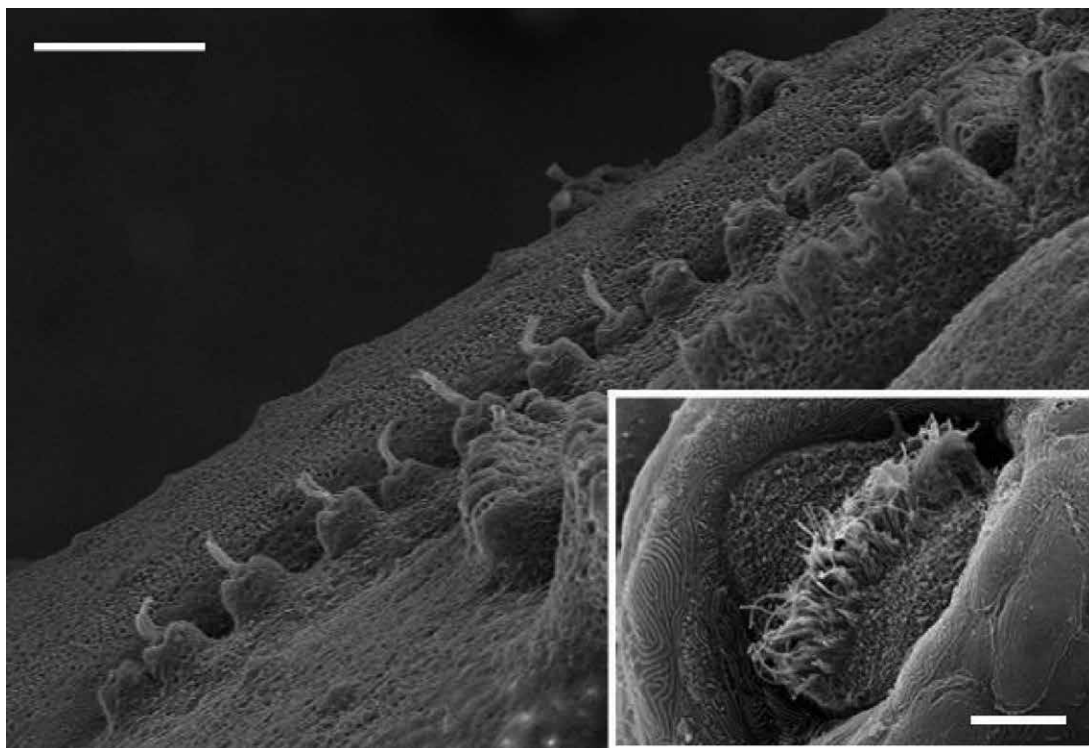
Figure 6. Neuromasts on papillae of Amblyopsis spelaea showing cupulae. Scale bar 250 µm. Insert: stereocilia after the cupula was removed. The kinocilium is the longest of the bundle. Scale bar 10 µm.

motaxis (Weise, 1957; Smith and Welch, 1978; Niemiller and Poulson, 2010). *Chologaster* typically occurs in heavily vegetated and shaded swamps and backwater habitats where they can be collected in dense vegetation, leaf litter, and other organic debris (Cooper and Rohde, 1980; Ross and Rohde, 2003) and are rarely found in flowing water (Poulson, 1960). Likewise, *Forbesichthys* typically are found in dense vegetation, under rocks, or seek shelter underground in springs and caves (Weise, 1957; Smith and Welch, 1978; Niemiller and Poulson,
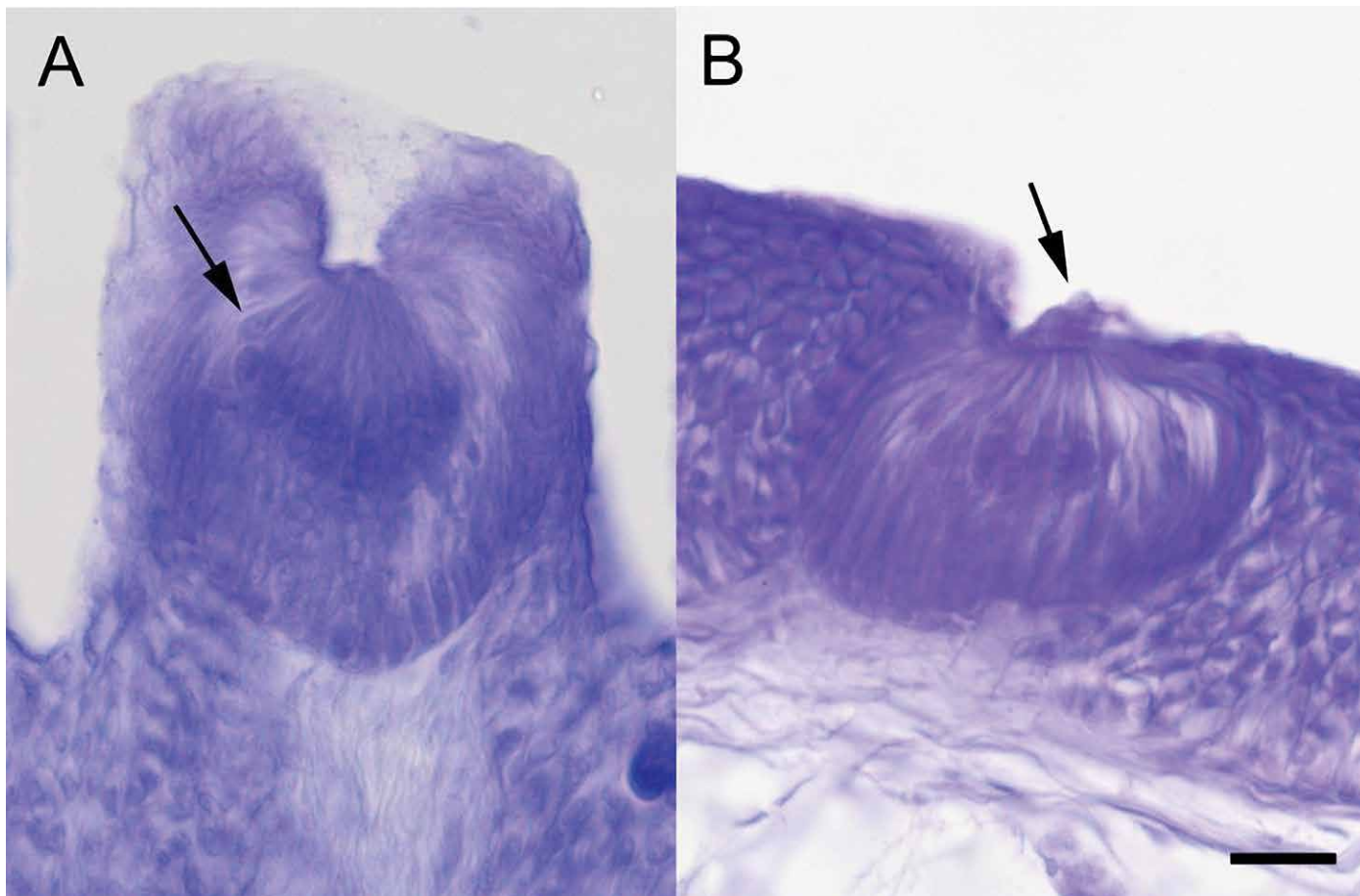

Figure 7. Cross-sections of both types of neuromasts. A) Papillate neuromast from *Amblyopsis spelaea*, arrow points at a single neuromast cell body. B) receded neuromast from *Chologaster cornuta,* arrow points at the collapsed cupula. Scale bar 100 µm.
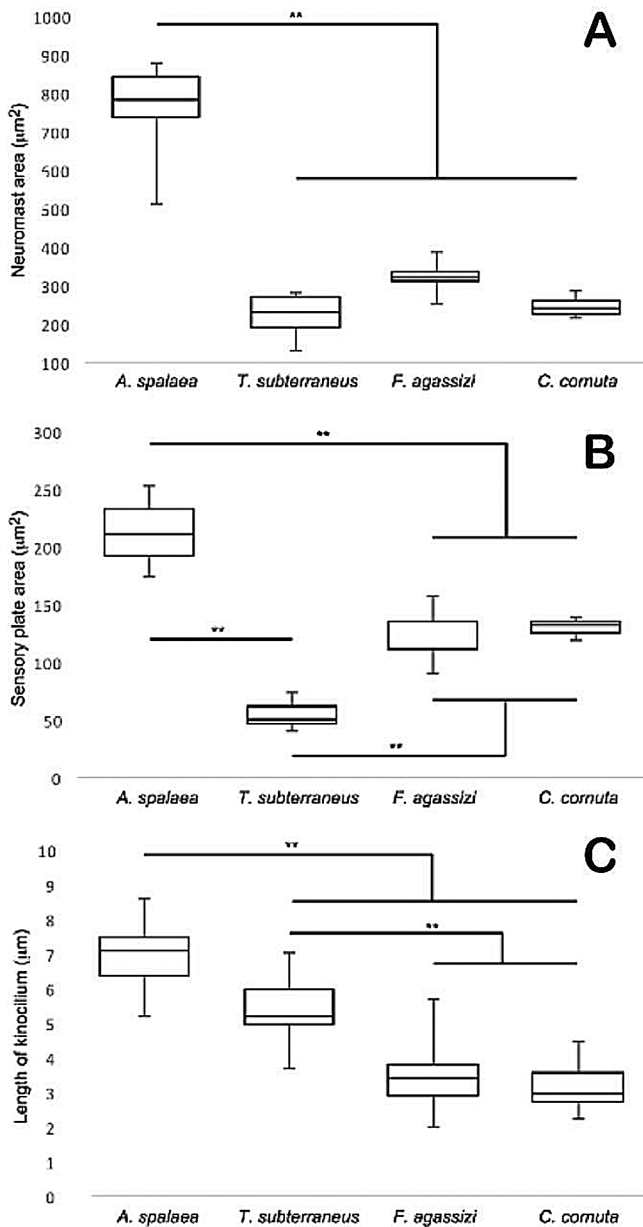
Figure 8. Comparisons of neuromast among fishes. *A. spelaea* has the largest superficial cephalic neuromasts of all fishes (A), with the largest sensory plate area (B) and the longest kinocilium (C). Both surface fishes sensory plate areas (B) and kinocelium lengths are similar to each other (C). Both cavefishes are not significantly different from each other but different from both surface fishes.

2010). The recession of superficial neuromasts, which could be damaged if exposed and extended from the body surface on papillae, into pits may be an adaptation for living among dense vegetation, organic debris, and other cover in these two species.

The difference in position of the neuromasts in the skin in relation to the water is likely to have a functional significance. The water flow that is detected by the superficial neuromasts is filtered by the hydrodynamics of the body surface of the fish (McHenry et al., 2008). The viscosity of water causes flow close to a surface to move slower, creating a spatial gradient known as the boundary layer (Lamb, 1945; Schlichting, 1979). The boundary layer over the surface of the body of the fish behaves as a high-pass filter that attenuates low-frequency stimuli (Kuiper, 1967; Hassan, 1985; Kalmijn, 1989; Teyke, 1988; McHenry et al., 2008). High frequency stimuli, such as that created by swimming prey or conspecifics, would become more salient to the fish. The boundary layer over the surface of the body of a fish plays a major role in determining the signals detected by superficial neuromasts (Batchelor, 1967; Schlichting, 1979; McHenry et al., 2008).

The boundary layer of swimming fish was studied in *Astyanax*, and it decreases with velocity so that it is 5 mm thick at 11 cm/s, and 1 mm at 150 cm/sec (Teyke, 1988). *Astyanax* is comparable in body size to amblyopsids, and although there are no measurements of swimming speed of amblyopsid cavefishes, the height of the papilla (*A. spelaea* = 0.55 ± 0.006 mm; *T. subterraneus* 0.73 ± 0.16 mm) suggests that the neuromasts likely do not escape the boundary layer. The attraction to live prey using the lateral line has been examined by Yoshizawa et al. (2010) also in *Astyanax*. In these fish, the vibration attraction behavior is tuned to 35 Hz, which is considered a high frequency and could denote a moving prey item. This behavior is abolished if the superficial neuromasts are ablated, specifically in the cephalic area.

The proliferation of superficial neuromasts is an adaptation for life not only in subterranean environments, but also in the deep sea and other low-flow habitats (Denton and Grey, 1989; Coombs et al., 1988; Northcutt, 1989; Marshall, 1996; Poulson, 2001). Deep-sea fishes are an interesting case because their visual world is very different than that of cavefishes. At depth, bioluminescence point sources dominate as visual stimuli, and eyes, although often referred to as "regressed" or "degenerate" are actually quite well-suited at this type of stimulus (Douglas et al., 1998; Warrant, 2000). Nonetheless, it appears that deep-sea fishes rely heavily on their lateral line to detect the environment and prey (Marshall, 1996; Johnson et al., 2009). Both cavefishes and deep-sea fishes do not display schooling behaviors, which require lateral line input (Cahn et al., 1968; Greenwood et al., 2013; Kowalko et al., 2013). Another group with significant cephalic surface neuromasts are gobies (Marshall, 1996; Webb, 1989a,b), and in these fishes, many of the stitches are also vertically-oriented (Moore and Burris, 1956), biasing the detection of environmental disturbances in the rostral-caudal dimension.

Although we were not able to measure the cupula of the surface species, both cavefishes had a relatively short cupulae, roughly 30 μm in length. The range of lengths of the cupula in surface fishes is variable dependent on the species and ranges between 20 μm and 500 μm, (Mukai and Kobayashi 1993). The cupulae of *Astyanax* are primarily 100 mm in length, but some are as long as 300 mm (Teyke 1990). The longer cupulae in *Astyanax,* therefore, can in-

crease lateral line sensitivity by protruding into the boundary layer. *Astyanax* and amblyopsid cavefishes appear to have different strategies to increase the height in which the cupula interacts with the water. *Chologaster* and *Forbesichthys* were not different from each other, but cavefishes (*A. spelaea* and *T. subterraneus*) appear to encode hydrodynamic information to a different extent. *Amblyopsis spelaea* has the most extreme cephalic superficial neuromast phenotype.

Our study supports the general rule that mechanosensation becomes hypertrophied during cave adaptation of fishes. However, our study also suggests that hypertrophy can be variable and possibly dependent on microhabitat, developmental constraints, and/or phylogeny.

References

Ahnelt, H., Göschl, J., Dawson, M.N., and Jacobs, D.K. 2004, Geographical variation in the cephalic lateral line canals of *Eucyclogobius newberryi*, Teleostei, Gobiidae, and its comparison with molecular phylogeography: Folia Zoologica, v. 53, p. 358–398.

Arai, R and Kato, K., 2003, Gross morphology and evolution of the lateral line system and infraorbital bone in bitterlings, Cyprinidae, Acheilognathinae, with an overview of the lateral line system in the family Cyprinidae: Bulletin of the Museum of Tokyo University, v. 40, p. 1–42.

Armbruster, J.W., Niemiller, M.L., and Hart, P.B., 2016, Morphological evolution of the cave-, spring-, and swampfishes of the Amblyopsidae, Percopsiformes: Copeia, v. 104, p. 763–777. doi:10.1643/CI-15-339

Baker, C.F., and Montgomery, J.C., 1999, The sensory basis of rheotaxis in the blind Mexican cave fish, *Astyanax fasciatus*: Journal of Comparative Physiology A, v. 184, pp. 519–527. doi:10.1007/s003590050351

Balco, G., Stone, J.O., and Mason, J.A., 2005, Numerical ages for Plio-Pleistocene glacial sediment sequences by 26Al/10Be dating of quartz in buried paleosols: Earth and Planetary Science Letters, v. 232, p. 179–191, doi:10.1016/j.epsl.2004.12.013.

Batchelor, G.K., 1967, An Introduction to Fluid Dynamics: Cambridge University Press, New York, 658 p.

Beckmann, M., Erős, T., Schmitz, A., and Bleckmann, H., 2010, Number and distribution of superficial neuromasts in twelve common European cypriniform fishes and their relationship to habitat occurrence: International Review of Hydrobiology, v. 95, p. 273–284. doi:10.1002/iroh.200911185

Bergman, L.M.R., 2004. The cephalic lateralis system of cardinalfishes, Perciformes: Apogonidae, and its application to the taxonomy and systematics of the family: [Ph.D. Thesis], University of Hawaii at Manoa, U.S, 373 p.

Blaxter, J.H.S., Gray, J.A.B., and Best, A.C.G., 1983, Structure and development of the free neuromasts and lateral line system of the herring: Journal of the Marine Biological Association U.K., v. 63, p. 247–260. doi:10.1017/S0025315400070648

Bleckmann, H., 1994, Reception of hydrodynamic stimuli: *In* Aquatic and Semiaquatic Animals: Rathmayer, W., ed., Progress in Zoology, v. 41, p. 1–115.

Cahn, P.H., Shaw, E., and Atz, E.H., 1968, Lateral-line histology as related to the development of schooling in the atherinid fish, Menidia: Bulletin of Marine Science, v. 18, p. 660–670.

Carton, A.G., and Montgomery, J.C., 2004, A comparison of lateral line morphology of blue cod and torrentfish: two sandperches of the family Pinguipedidae: Environmental Biology of Fishes, v. 70, p.123-131. doi:10.1023/B:EBFI.0000029340.57735.f8

Chakrabarty, P., Prejean, J.A., and Niemiller, M.L., 2014, The Hoosier cavefish, a new and endangered species (Amblyopsidae, Amblyopsis) from the caves of southern Indiana: ZooKeys, v. 412, p. 41. doi:10.3897/zookeys.412.7245

Coombs, S., Janssen, J., and Webb, J.F., 1988, Diversity of lateral line systems: evolutionary and functional considerations: *In* Sensory Biology of Aquatic Animals, Atama, J. Fay, R.R., Popper, A.N., and Travolga W.N., eds, p. 553–593. Springer, New York, NY.

Coombs, S., and Montgomery, J., 1994, Function and evolution of superficial neuromasts in an Antarctic notothenioid fish: Brain, Behavior and Evolution, v. 44, p. 287–298. doi:10.1159/000113590

Cooper, J.E., and Rohde F.C., 1980, *Chologaster cornuta* Agassiz: *In* Lee, D.S., Gilbert, C.R., Hocutt C.H., Jenkins, R.E., McAllister, D.E., and Stauffer, J.R., Jr., eds., Atlas of North American Freshwater Fishes, orth Carolina State Museum of Natural History, Raleigh, North Carolina, v. 1, 444 p.

Coughlin D.J., and Strickler J.R., 1990, Zooplankton capture by a coral reef fish: an adaptive response to evasive prey: Environmental Biology of Fishes v. 29, p. 5–42. doi:10.1007/BF00000566

Ćurčić-Blake, B., and van Netten, S.M., 2006, Source location encoding in the fish lateral line canal: Journal of Experimental Biology, v. 209, p.1548–1559. doi:10.1242/jeb.02140

de Perera, T.B., 2004, Fish can encode order in their spatial map: Proceedings of the Royal Society of London B: Biological Sciences, v. 271, p. 2131–2134. doi:10.1098/rspb.2004.2867

Denton, E.J., and Gray, J.A., 1989, Some observations on the forces acting on neuromasts in fish lateral line canals: *in* Coombs, S., Gorner P. and Munz, H. eds, The mechanosensory lateral line, Springer, New York, NY, p. 229–246. doi:10.1007/978-1-4612-3560-6_11

Dezfuli, B.S., Magosso, S., Simoni, E., Hills, K., and Berti, R., 2009, Ultrastructure and distribution of superficial neuromasts of blind cavefish, *Phreatichthys andruzzii*, juveniles: Microscopy research and technique, v. 72, p. 665−671. doi:10.1002/jemt.20714

Diaz, J.P., Prié-Granié, M., Kentouri, M., Varsamos, S., and Connes, R., 2003, Development of the lateral line system in the sea bass: Journal of Fish Biology v. 62, p. 24−40.

Douglas, R.H., Partridge, J.C., and Marshall, N.J., 1998, The eyes of deep-sea fish I: lens pigmentation, tapeta and visual pigments: Progress in retinal and eye research v. 17, p. 597–636. doi:10.1046/j.1095-8649.2003.00004.x

Faucher, K., Parmentier, E., Becco, C., Vandewalle, N., and Vandewalle, P., 2010, Fish lateral system is required for accurate control of shoaling behaviour: Animal Behaviour, v. 79, p. 679–687. doi:10.1016/j.anbehav.2009.12.020

Gosline, W.A., 1974, Certain lateral line canals of the head in cyprinid fishes, with particular reference to the derivation of North American forms: Japan Journal of Ichthyology, v. 21, p. 9–15.

Greenwood, A.K., Wark, A.R., Yoshida, K., and Peichel, C.L., 2013, Genetic and neural modularity underlie the evolution of schooling behavior in threespine sticklebacks: Current Biology, v. 23, p. 1884–1888. doi:10.1016/j.cub.2013.07.058

Hassan, E.S., 1985, Mathematical analysis of the stimulus of the lateral line organ: Biological Cybernetics, v. 52, p. 23–36.

Higgs, D.M., and Fuiman, L.A., 1998, Associations between sensory development and ecology in three species of clupeoid fish: Copeia, v. 1, p.133–144. doi:10.1007/BF00336932

Hoekstra, D., and Janssen, J., 1985, Non-visual feeding behavior of the mottled sculpin, *Cottus bairdi*, in Lake Michigan: Environmental Biology of Fishes v. 12, p. 111–117. doi:10.1007/BF00002763

Hoekstra, D., and Janssen J., 1986, Receptive field of the mottled sculpin lateral line for *Daphnia* and a vibrating inert stimulus: Copeia, v. 9, p.

1–96. doi:10.2307/1444893

Janssen, J., 1990, Localization of substrate vibrations by the mottled sculpin, *Cottus bairdi*: Copeia, v. 1, p. 349–355. doi:10.2307/1446340

Janssen, J., 1996, Use of the lateral line and tactile senses in feeding in four antarctic notothenioid fishes: Environmental Biology of Fishes, v. 47, p. 1–64. doi:10.1007/BF00002379

Janssen, J., 2004, Lateral line sensory ecology: *In* von der Emde, G., Mogdans, J. and Kappr, B.G., eds. The Senses of Fish, Springer, Dordrecht, p. 231–264. doi:10.1007/978-94-007-1060-3_11

Janssen, J., and Corcoran, J., 1998, Distance determination via the lateral line in the mottled sculpin: Copeia, v. 1, p. 657–661. doi:10.2307/1447795

Janssen, J., Jones, W.R., Whang, A., and Oshel, P.E., 1995, Use of the lateral line in particulate feeding in the dark by juvenile alewife, *Alosa pseudoharengus*: Canadian Journal of Fish Aquatic Sciences, v. 52, p. 358–363. doi:10.1139/f95-037

Janssen, J., Sideleva, V., and Biga, H., 1999, Use of the lateral line for feeding in two Lake Baikal sculpins: Journal of Fish Biology, v. 54, p. 404–416. doi:10.1111/j.1095-8649.1999.tb00839.x

Jiang, Y., Fu, J., Zhang, D., and Zhao, Y., 2016, Investigation on the lateral line systems of two cavefish: *Sinocyclocheilus macrophthalmus* and *S. microphthalmus* (Cypriniformes: Cyprinidae). Journal of Bionic Engineering, v. 13, p. 108–114. doi:10.1016/S1672-6529(14)60164-5

Johnson, G.D., Paxton, J.R., Sutton, T.T., Satoh, T.P., Sado, T., Nishida, M., and Miya, M., 2009, Deep-sea mystery solved: astonishing larval transformations and extreme sexual dimorphism unite three fish families: Biology Letters, v. 5, p. 235–239. doi:10.1098/rsbl.2008.0722

Kalmijn, A.J., 1989, Functional evolution of lateral line and inner ear sensory systems: *In* Coombs, S., Gorner P. and Munz, H. eds.,The Mechanosensory Lateral Line, Springer, New York, NY Springer, New York, NY., p. 187–215. doi:10.1007/978-1-4612-3560-6_9

Kowalko, J.E., Rohner, N., Rompani, S.B., Peterson, B.K., Linden, T.A., Yoshizawa, M., Kay, E.H., Weber, J., Hoekstra, H.E., Jeffery, W.R., and Borowsky, R., 2013, Loss of schooling behavior in cavefish through sight-dependent and sight-independent mechanisms: Current Biology, v.23, p. 1874–1883. doi:10.1016/j.cub.2013.07.056

Kuiper, J.W., 1967, Frequency characteristics and functional significance of the lateral line organ: *In* Cahn, P.H., ed., Lateral Line Detectors, Indiana University Press, Bloomington, p. 105–121.

Kurawaka, K., 1977, Cephalic lateral-line systems and geographical distribution in the genus *Tribolodon*, Cyprinidae: Japanese Journal of Ichthyology, v. 24, p. 167–175.

Lamb, H., 1945, Hydrodynamic: 6th Edition, Dover Publications, New York, 738 p.

Marshall, N.B., 1965, Systematic and biological studies of the macrourid fishes, Anacanthini-Teleostii: *In* Deep Sea Research and Oceanographic Abstracts, v. 123, p. 299–322. doi:10.1016/0011-7471(65)90004-5

Marshall, N.J., 1996, Vision and sensory physiology. The lateral line systems of three deep-sea fish: Journal of Fish Biology, v. 49, p. 239–258. doi:10.1111/j.1095-8649.1996.tb06079.x

McHenry, M.J., Feitl, K.E., Strother, J.A., and Van Trump, W.J., 2009, Larval zebrafish rapidly sense the water flow of a predator's strike: Biology Letters, v. 5, p. 477–479. doi:10.1098/rsbl.2009.0048

McHenry, M.J., Strother, J.A., and Van Netten, S.M., 2008, Mechanical filtering by the boundary layer and fluid–structure interaction in the superficial neuromast of the fish lateral line system: Journal of Comparative Physiology A, v. 194, p. 795–810. doi:10.1007/s00359-008-0350-2

Montgomery, J.C., Baker, C.F., and Carton, A.G., 1997, The lateral line can mediate rheotaxis in fish: Nature, v. 389, p. 960. doi:10.1038/40135

Montgomery, J.C., Coombs, S., and Baker, C.F., 2001, The mechanosensory lateral line system of the hypogean form of *Astyanax fasciatus*: Environmental Biology of Fishes, v. 62, p. 87–96. doi:10.1007/978-94-015-9795-1_5

Montgomery, J., Coombs, S., and Janssen, J., 1994, Form and function relationships in lateral line systems: comparative data from six species of Antarctic notothenioid fish: Brain, Behavior and Evolution, v. 44, p. 299–306. doi:10.1159/000113591

Moore, G.A., and Burris, W.E., 1956, Description of the lateral-line system of the pirate perch, *Aphredoderus sayanus*: Copeia, v. 1, p.18–20. doi:10.2307/1439238

Mukai, Y. and Kobayashi, H., 1993, Extremely long cupulae of embryonic neuromasts in cyprinid fish: Copeia, v. 4, p. 1157–1159. doi:10.2307/1447101

Müller, U. and Schwartz, E., 1982, Influence of single neuromasts on prey localizing behavior of the surface feeding fish, *Aplocheilus lineatus*: Journal of Comparative Physiology A: Neuroethology, Sensory, Neural, and Behavioral Physiology, v. 149, p. 399–408. doi:10.1007/BF00619155

Nelson, J.S., 1972, Cephalic sensory canals, pitlines, and the classification of esocoid fishes, with notes on galaxiids and other teleosts: American Museum Novitates v. 2492, p.1–49.

Northcutt, G. A. (1989). The phylogenetic distribution and innervation of craniate mechanoreceptive lateral lines. In The Mechunosensory Loferal Line (Coombs, S., Gomer, P. & Munz H., eds), pp. 17-78. New York: Springer-Verlag.

Niemiller, M.L., Fitzpatrick, B.M., Shah, P., Schmitz, L., and Near, T.J., 2013a, Evidence for repeated loss of selective constraint in rhodopsin of amblyopsid cavefishes, Teleostei: Amblyopsidae: Evolution, v. 67, p. 732–748. doi:10.1111/j.1558-5646.2012.01822.x

Niemiller, M.L., McCandless J.R., Reynolds R.G., Caddle J., Near T.J., Tillquist C.R., Pearson, W.D., and Fitzpatrick, B.M., 2013b, Effects of climatic and geological processes during the Pleistocene on the evolutionary history of the northern cavefish, *Amblyopsis spelaea*, Teleostei: Amblyopsidae: Evolution, v. 67, p. 41011–1025. doi:10.1111/evo.12017

Niemiller, M.L., and Poulson, T.L., 2010, Subterranean fishes of North America: Amblyopsidae: Biology of subterranean fishes, v. 169, p. 280. doi:10.1201/EBK1578086702-c7

Niemiller, M.L., and Soares, D., 2015, Cave environments: *In* Riesch, R., Tobler, M., Martin Plath, M., eds., Extremophile Fishes, p. 161–191, Springer, Cham. doi:10.1007/978-3-319-13362-1

Parin, N., Astakhov, D., 1982, Studies on the acoustico-lateralis system of beloniform fishes in connection with their systematics: Copeia, v. 1, p. 276–291. doi:10.2307/1444606

Partridge, B.L., Pitcher, T., Cullen, J.M., and Wilson, J., 1980, The three-dimensional structure of fish schools: Behavioral Ecology and Sociobiology, v. 6, p. 277–288. doi:10.1007/BF00292770

Pitcher, T.J., 2001, Fish schooling: implications for pattern in the oceans and impacts on human fisheries: *In:* Steele, J.H., Turekian, K.K., and Thorpe, S.A., eds., Encyclopedia of Ocean Sciences, London. Academic Press, p. 975–987. doi:10.1006/rwos.2001.0022

Poulson, T.L., 1960, Cave adaptation in Amblyopsidae fishes. [PhD thesis], Department of Zoology, University of Michigan, Ann Arbor. University Microfilms, 2787 p.

Poulson, T.L., 1963, Cave adaptation in amblyopsid fishes: American Midland Naturalist, p. 257–290. doi:10.2307/2423056

Poulson, T.L., 2001, Adaptations of cave fishes with some comparisons to deep-sea fishes: Environmental Biology of Fishes, v. 62, p. 345–364.

doi:10.1007/978-94-015-9795-1_28

Reno, N.W., 1966, The infraorbital canal, its lateral line ossicles and neuromasts, in the minnows *Notropis volucellus* and *N. buchanani*: Copeia, v. 1, p. 403–413. doi:10.2307/1441059

Ross, S.W. and Rohde, F.C., 2003. Life history of the swampfish from a North Carolina stream: Southeastern Naturalist, v. 2, p. 105–120. doi:10.1656/1528-7092(2003)002[0105:LHOTSF]2.0.CO;2

Schlichting, H., 1979, Boundary-Layer Theory. McGraw-Hill, New York., 815 p.

Schwarz, J.S., Reichenbach, T. and Hudspeth, A.J., 2011, A hydrodynamic sensory antenna used by killifish for nocturnal hunting: Journal of Experimental Biology, v. 214, p. 1857–1866. doi:10.1242/jeb.051714

Schmitz, A., Bleckmann, H. and Mogdans, J., 2014, The lateral line receptor array of cyprinids from different habitats: Journal of morphology, v. 275, p. 357–370. doi:10.1002/jmor.20219

Smith, P.W. and N.M. Welch. 1978, A summary of the life history and distribution of the spring cavefish, *Chologaster agassizi*, Putnam, with population estimates for the species in southern Illinois: Illinois Natural History Survey Biological Notes, v. 104, p. 1–8.

Soares, D. and Niemiller, M.L., 2013, Sensory adaptations of fishes to subterranean environments: BioScience, v. 63, p. 274–283. doi:10.1525/bio.2013.63.4.7

Stephens, R.R., 1985, The lateral line system of the gizzard shad, *Dorosoma cepedianum* Lesueur, Pisces: Clupeidae: Copeia, v. 1, p. 540–556. doi:10.2307/1444742

Sutterlin, A.M., and Waddy, S., 1975, Possible role of the posterior lateral line in obstacle entrainment by brook trout, *Salvelinus fontinalis*: Journal of the Fisheries Board of Canada, v. 32, p. 2441–2446. doi:10.1139/f75-281

Teyke, T., 1988, Flow field, swimming velocity and boundary layer: parameters which affect the stimulus for the lateral line organ in blind fish: Journal of Comparative Physiology A: Neuroethology, Sensory, Neural, and Behavioral Physiology, v. 163, p. 53–61. doi:10.1007/BF00611996

Teyke, T., 1990, Morphological differences in neuromasts of the blind cave fish *Astyanax hubbsi* and the sighted river fish *Astyanax mexicanus*: Brain Behavior and Evolution, v. 35, p. 23–30. doi:10.1159/000115853

Tittel, G., Müller, U. and Schwartz, E., 1984, Determination of stimulus direction by the topminnow *Aplocheilus lineatus*: *In* Varju, D., and Schnitzler, H.U., eds., Localization and Orientation in Biology and Engineering, Springer, Berlin, Heidelberg, p. 69–72. doi:10.1007/978-3-642-69308-3_14

van Netten, S.M., 2006, Hydrodynamic detection by cupulae in a lateral line canal: functional relations between physics and physiology: Biological Cybernetics, v. 94, p. 67–85. doi:10.1007/s00422-005-0032-x

van Netten, S.M., and Kroese, A.B., 1989, Hair cell mechanics controls the dynamic behaviour of the lateral line cupula: *In* Wilson, J ed., Cochlear Mechanisms: Structure, Function, and Models, Springer U.S., p. 47–55. doi:10.1007/978-1-4684-5640-0_6

Van Trump, W.J. and McHenry, M.J., 2013, The lateral line system is not necessary for rheotaxis in the Mexican blind cavefish, *Astyanax fasciatus:* Integrative and Comparative Biology, v. 53, p. 799–809. doi:10.1093/icb/ict064

Warrant, E., 2000, The eyes of deep–sea fishes and the changing nature of visual scenes with depth: Philosophical Transactions of the Royal Society of London B: Biological Sciences, v. 355, p. 1155–1159. doi:10.1098/rstb.2000.0658

Webb, J.F., 1989a, Developmental constraints and evolution of the lateral line system in teleost fishes: *In* Coombs, S., Gorner P., and Munz, H., eds, The Mechanosensory Lateral Line, Springer, New York, NY, p. 79–97. doi:10.1007/978-1-4612-3560-6_4

Webb, J.F., 1989b, Gross morphology and evolution of mechanoreceptive lateral line system in teleost fishes: Brain Behavior Evolution, v. 33, p. 34–53. doi:10.1159/000115896

Weise, J.G., 1957. The spring cave-fish, *Chologaster papilliferus*, in Illinois: Ecology, v. 38, p. 195–204. doi:10.2307/1931678

Yoshizawa, M., Gorički, Š., Soares, D., and Jeffery, W.R., 2010, Evolution of a behavioral shift mediated by superficial neuromasts helps cavefish find food in darkness: Current Biology, v. 20, p. 1631–1636. doi:10.1016/j.cub.2010.07.017

Yoshizawa, M., Jeffery, W.R., van Netten, S.M., and McHenry, M.J., 2014, The sensitivity of lateral line receptors and their role in the behavior of Mexican blind cavefish, *Astyanax mexicanus*: Journal of Experimental Biology, v. 217, p. 886–895. doi:10.1242/jeb.094599

SUNDATHELPHUSA PROSPERIDAD, SP. N. (DECAPODA: BRACHYURA: GECARCINUCIDAE), A NEW CAVE-OBLIGATE FRESHWATER CRAB FROM MINDANAO ISLAND, THE PHILIPPINES, WITH NOTES ON THE CONSERVATION STATUS OF PHILIPPINE CAVE SPECIES

Daniel Edison M. Husana

Abstract

A new species of cave-obligate freshwater crab of the genus *Sundathelphusa* Bott, 1969 (Gecarcinucidae) from Agusan del Sur, Philippines is described. The new species is morphologically close to *S. hades* Takeda and Ng, 2001 but distinctly differs in the shape of carapace and gonopods. Although the new species is found close to the type locality of *S. hades*, the morphological features are distinct and their habitats are separated by an extension of the Philippine fault-line and Oligocene-Miocene volcanic deposits. Six *Sundathelphusa* species having true troglobiomorphic characters are now recorded from caves in the Philippine archipelago.

Introduction

A significant number of cavernicolous crab species have been recorded from the Philippines. Eight species of freshwater crabs with various degrees of cave adaptations, all belonging to the genus *Sundathelphusa* Bott, 1969 of the family Gecarcinucidae Rathbun, 1904, have been described from different caves in the Philippine archipelago. Two of these species were described from Bantakay Cave in the northern island of Luzon, i.e. *S. holthuisi* Ng, 2010 and *S. danae* Husana, Yamamuro and Ng, 2014, while *S. niwangtiil* Husana, Kase and Mendoza, 2015, was described from Mabinay Cave in Negros Island. These three species exhibit partial cave adaptations, i.e. elongated slender ambulatory legs in proportion to their body size. Five species exhibit more advanced troglomorphism, with reduced eyes, elongated legs and loss of pigment. These are *S. cavernicola* Takeda, 1983 and *S. sottoae* Ng and Sket, 1996 from Bohol Island; *S. hades* Takeda and Ng, 2001 from Mindanao Island; *S. waray* Husana, Naruse and Kase, 2009 and *S. lobo* Husana, Naruse and Kase, 2009, from Samar Island.

The new species, *Sundathelphusa prosperidad*, described here is the ninth species in the genus and also exhibits advanced troglomorphism. It is the second cave-obligate crab recorded from the island of Mindanao.

Although other species of *Sundathelphusa* such as *S. philippina* (von Martens, 1868), *S. boex* Ng and Sket, 1996, *S. vedeniki* Ng and Sket, 1996, *S. urichi* Ng and Sket, 1996, *S. vienae* Husana, Yamamuro and Ng, 2014, and *S. quirino* Husana and Ng, 2019 were recorded from caves in various islands of the Philippines, these species do not exhibit any troglomorphic features. However, *S. vedeniki* and *S. urichi* have slightly reduced eyes and shortened eyestalks with noticeable reduction in the body pigmentation in the latter species (Ng and Sket, 1996). *Sundathelphusa spelaeophila* Stasolla, Abbarchi and Innocenti, 2015, was described from a cave but has no cave-adapted characters and is a junior synonym of *S. philippina* sensu stricto (Husana and Ng, 2019). All these species are just surface organisms that regularly enter and stay inside, near the entrance of the cave, for shelter during the day. It is important to note that *Sundathelphusa* species in the Philippines evolved rapidly as Klaus et al. (2013) demonstrated on the character change following the transition from surface to subterranean life of the five species of this freshwater crab in Bohol Island based on molecular genetic analyses.

Other species of cave crabs from the Philippines have been described and recorded from anchialine caves in various islands of the archipelago. These include species of Varunidae family, i.e. *Orcovita tabiacoud* Stasolla and Innocenti, 2014, from Pukaway Cave, Coron Island; *O. holthuisi* Ng and Ng, 2009, from Pukaway Cave, Coron Island; *O. angulata* Ng, Guinot and Iliffe, 1996 from Pukaway Cave, Coron Island; *O. fictilia* Ng, Guinot and Iliffe, 1996, Hinagdanan Cave, Panglao Island; Hymenosomatidae family, i.e. *Samarplax principe* Husana, Tan and Kase, 2011, Principe Cave, Guiuan Island; Sesarmidae family, i.e. *Karstarma philippinarum* Husana, Naruse and Kase, 2010, Bat Cave, Boracay Island and Tagbaobo Cave, Samal Island; *K. boholano* Ng, 2002, Tawala Cave, Panglao Island; *K. sulu* Ng, 2002, St. Paul N. P. Cave, Palawan Island; Gecarcinidae, i.e. *Discoplax gracilipes* Ng and Guinot, 2001, Virata Cave, Panglao Island, but my extensive field research shows that this latter species is widespread in many caves in karstic islands in the Philippines. Of these species, only *S. principe* has the complete troglomorphic features, while others have just elongated legs and/or slight eye reduction as the only cave adaptations.

Institute of Biological Sciences, College of Arts and Sciences, University of the Philippines Los Baños College, Laguna 4031, Philippines
E-mail: dmhusana@up.edu.ph

Materials and Methods

Materials were collected using opportunistic sampling methods from a cave on Mindanao Island. A minimal number of samples were hand-picked to avoid high impact that might cause population decline. They were treated with 10% formalin for a week after anesthetizing them in the freezer for about an hour. Specimens were transferred to 70% ethanol after rinsing in fresh flowing water for a few hours. Photographs of live individuals were taken in the field. Photographs of important parts for the description of the specimen were taken from the preserved holotype at the lab using a Canon 70D camera. Figures were made using a Nikon camera lucida.

Measurements provided are the maximum carapace width (CW) by carapace length (CL). The terminology follows that by Ng and Sket (1996) with modifications as recommended by Davie et al. (2015). Specimens were deposited at the National Museum of the Philippines, Manila (NMCR) and Zoological Reference Collection (ZRC) Lee Kong Chian Natural History Museum, National University of Singapore. The abbreviations G1 and G2 are used for male first and second gonopods, respectively.

Systematics

Family Gecarcinucidae Rathbun, 1904
Genus *Sundathelphusa* Bott, 1969
Sundathelphusa prosperidad, new species
Figs. 1–4

Material examined. **–** Holotype: Male (30.68 × 22.3 mm), NMCR 50776, Ognop Cave, Prosperidad, Agusan del Sur, Philippines, 345mASL. D.E. Husana and A. Pasilan, 14 May 2014. Paratypes: female (28.04 × 21.38 mm), NMCR 50777, same data as holotype; male (20.58 × 16.67 mm), female (25.77 × 20.19 mm), NMCR 50778, Lorenzo Cave, Prosperidad, Agusan del Sur, Philippines. A. Pasilan, January 2014; Male (25.74 × 19.33 mm), Females (26.16 × 19.91 mm; 22.69 × 18.02 mm) NMCR 57081, Ognop Cave, Prosperidad, Agusan del Sur, Philippines, 345mASL. D.E. Husana and A. Pasilan, 14 May 2014; male (25.33 × 20.2 mm), female (28.33 × 22.62 mm), NMCR 50779, Ognop cave, Prosperidad, Agusan del Sur, Philippines, 345mASL. D.E. Husana and A. Pasilan, 1 May 2012; male (25.29 × 19.79 mm), ZRC 2019.0876, Ognop cave, Prosperidad, Agusan del Sur, Philippines, 345mASL. D.E. Husana and A. Pasilan, 1 May 2012; female (24.68 × 19.61 mm), ZRC 2019.0877, males (25.92 × 21.1 mm; 24.4 × 20.62 mm; 26.54 × 20.89 mm), NMCR 50780, Ognop cave, Prosperidad, Agusan del Sur, Philippines, 345mASL. A. Pasilan, 20 Nov. 2011.

Comparative materials. **–** *Sundathelphusa cavernicola* Takeda 1983: holotype female (25.7 × 21.0 mm), NSMT-Cr 8937, Quinapon-an Cave, Antequera, Bohol, Philippines, 9º49'38"N, 123º54'10"E, coll. S. I. Ueno, 4 March 1983; 1 male (18 × 15.4 mm), 1 female (29.2 × 24 mm), NSMT-Cr 14130, Bongkawi Cave, Antequera, Villa Aurora, Bohol, Philippines, coll. P. K. L. Ng, 16 December 2000; 1 male (26.5 × 21.6 mm), 2 females (23.1 × 18.1, 26.5 × 21.8 mm), ZRC 2000.2079, Bongkawi Cave, Antequera, Villa Aurora, Bohol, Philippines, coll. B. Sket, 23 February 1999; 1 female (22.2 × 17.8 mm), ZRC 2001.0335, Bongkawi Cave, Antequera, Villa Aurora, Bohol, Philippines, coll. P. K. L. Ng, December 2000; 3 males (13.0 × 15.1−0.8 × 24.1 mm), Canantong Uno cave, Quinapon-an, Antequera, Villa Aurora, Bohol, Philippines, coll. B. Sket, 25 February 1999. *Sundathelphusa sottoae* Ng and Sket, 1996: 1 female (26.2 × 21.1 mm), ZRC 1996.1553, paratype, Bonugan, Batuan, Bohol, Philippines, coll. B. Sket, February 1995; 1 = (17.5 × 14.4 mm), ZRC 1996.1548, open well, Batuan, Bohol, Philippines, coll. B. Sket, February 1995; 1 male (18.0 × 14.9 mm), ZRC 2001.0343, Bongkawi Cave, Antequerra, Villa Aurora, Bohol, Philippines, coll. P. K. L. Ng, 16 December 2000. *Sundathelphusa hades* Takeda and Ng, 2001: holotype male (19.7 × 16.4 mm) NSMT-Cr 14274, Latay Cave, Agusan del Sur, Mindanao, Philippines 8º23'N, 126º05'E, Cave Research Group of Meiji University, 15 Nov. 1981; paratype female (24.9 × 20.8 mm) ZRC- 2001.1000, Sta. Rita Thinking Cave, Surigao del Sur, Mindanao, Cave Research Group of Meiji University, 27 Nov. 1998. *Sundathelphusa waray* Husana, Naruse and Kase 2009: holotype male (33.4 × 25.8 mm), NMCR 27059, Langun Cave, Calbiga, Western Samar, Philippines, 11º39.022'N, 125º02.991'E, coll. D. E. Husana, 28 October 2006. *Sundathelphusa lobo* Husana, Naruse and Kase 2009: holotype male (31.5 × 24.3 mm), NMCR 27061, Lobo Cave, Jiabong, Western Samar, Philippines 11º46.786'N, 124º55.732'E, coll. D. E. Husana, 1 August 2006.

Description. **–** Carapace quadrate to trapezoidal in shape, widest breadth at anterior quarter, dorsal surface convex longitudinally (Figs. 1A, 1M). Frontal region sloping antero-ventrally; branchial regions moderately inflated, with oblique rows of granules of various shapes and lengths; cervical grooves deep; H-shaped median groove deep; epigastric and postorbital with cristae, not confluent; epigastric cristae separated from each other by deep cleft. Frontal margin broadly protruded, two lobes clearly separated with deep broad median concavity; external orbital tooth low, outer margin slightly longer than inner margin, margins granulated; epibranchial tooth small, low, separated from external orbital tooth by deep notch, inner margin extended dorsally, lined with large granules; anterolateral margin gently convex, lined with large granules, not clearly demarcated from posterolateral margin; posterolateral margin gently concave, converg-
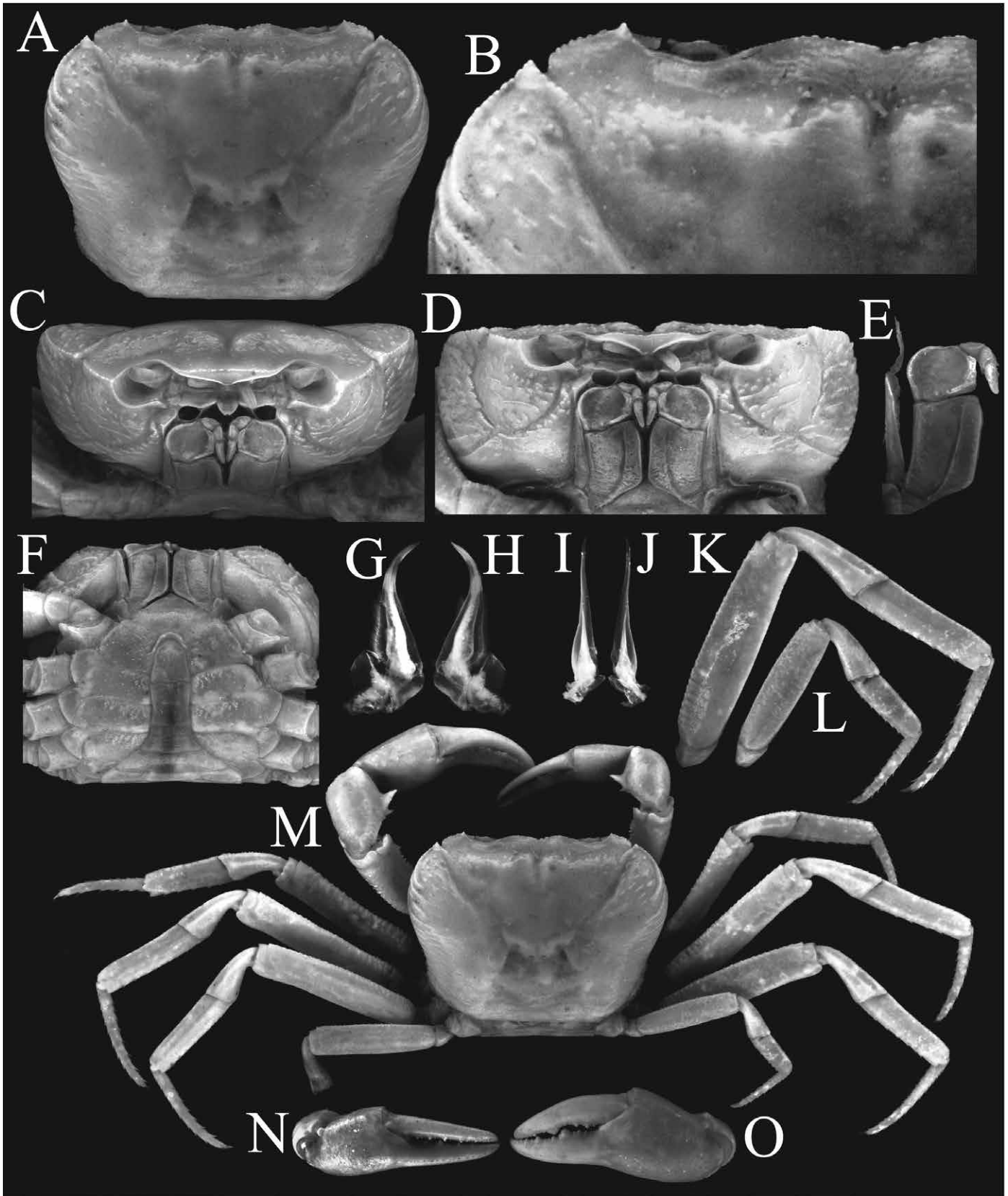
Figure 1. *Sundathelphusa prosperidad*, new species, holotype male (30.68 × 22.3 mm) (NMCR 50776). A) carapace; B) anterolateral margin; C-D) frontal; E) maxilliped; F) ventral view; G-H) left G1, ventral and dorsal views; I-J) left G2, ventral and dorsal views; K) right third ambulatory leg, dorsal view; L) right fourth ambulatory leg, dorsal view; M) habitus, dorsal view; N-O) right and left cheliped.
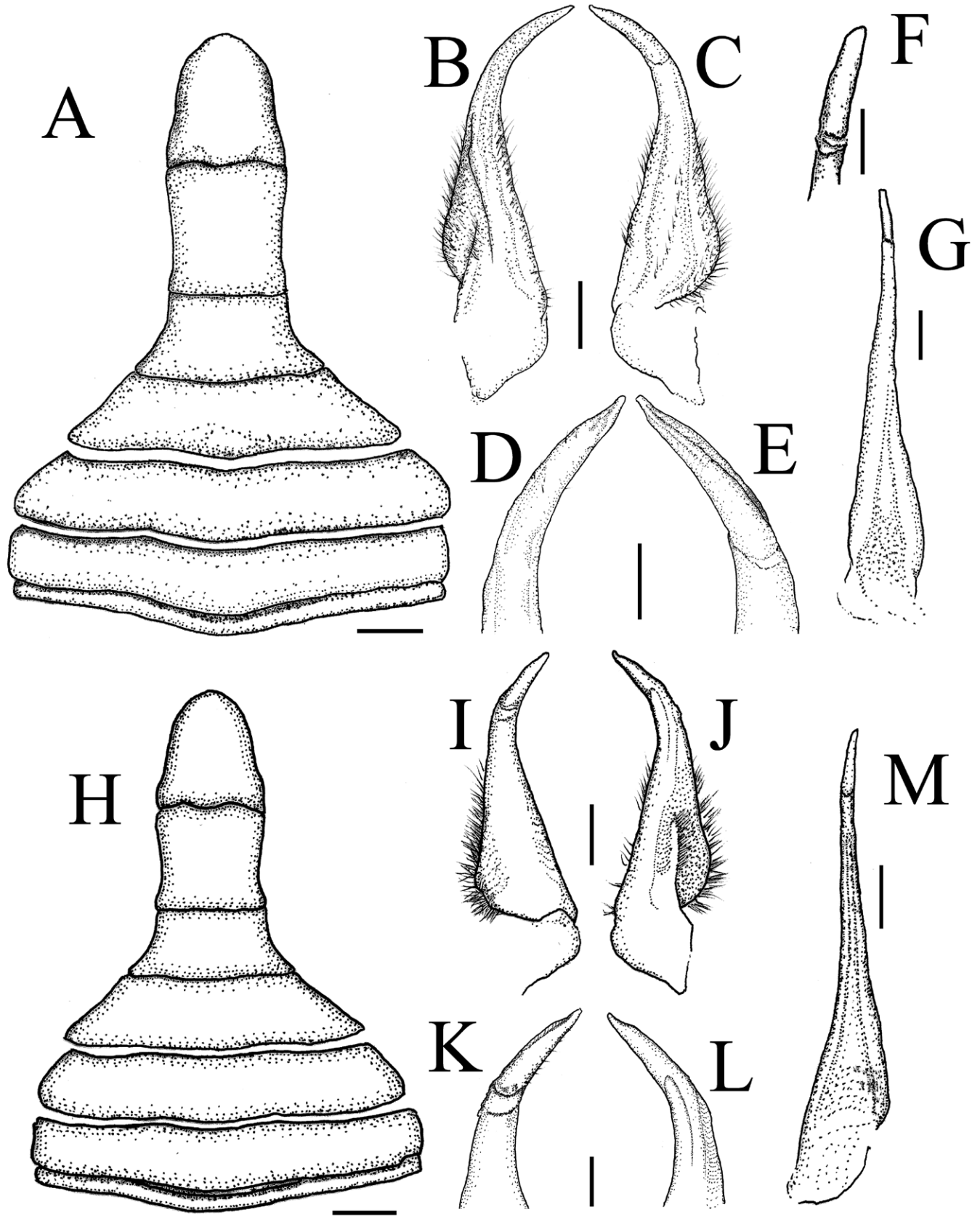
Figure 2. *Sundathelphusa prosperidad*, new species (A-G holotype male, 30.68 × 22.3 mm, NMCR 50776; H-M paratype male, 25.33 × 20.2 mm, NMCR 50779). A) abdomen; B-C) left G1, ventral and dorsal views; D-E) distal part of left G1, ventral and dorsal views; F) distal part of left G2, ventral view; G) left G2, dorsal view; H) abdomen; I-J) right G1, dorsal and ventral views; K-L) distal part of right G1, dorsal and ventral views; M) right G2, ventral view. Scale bars, in mm: A, H = 2; B-C, I-J = 1; D-E, G, K-M = 0.5; F = 0.25
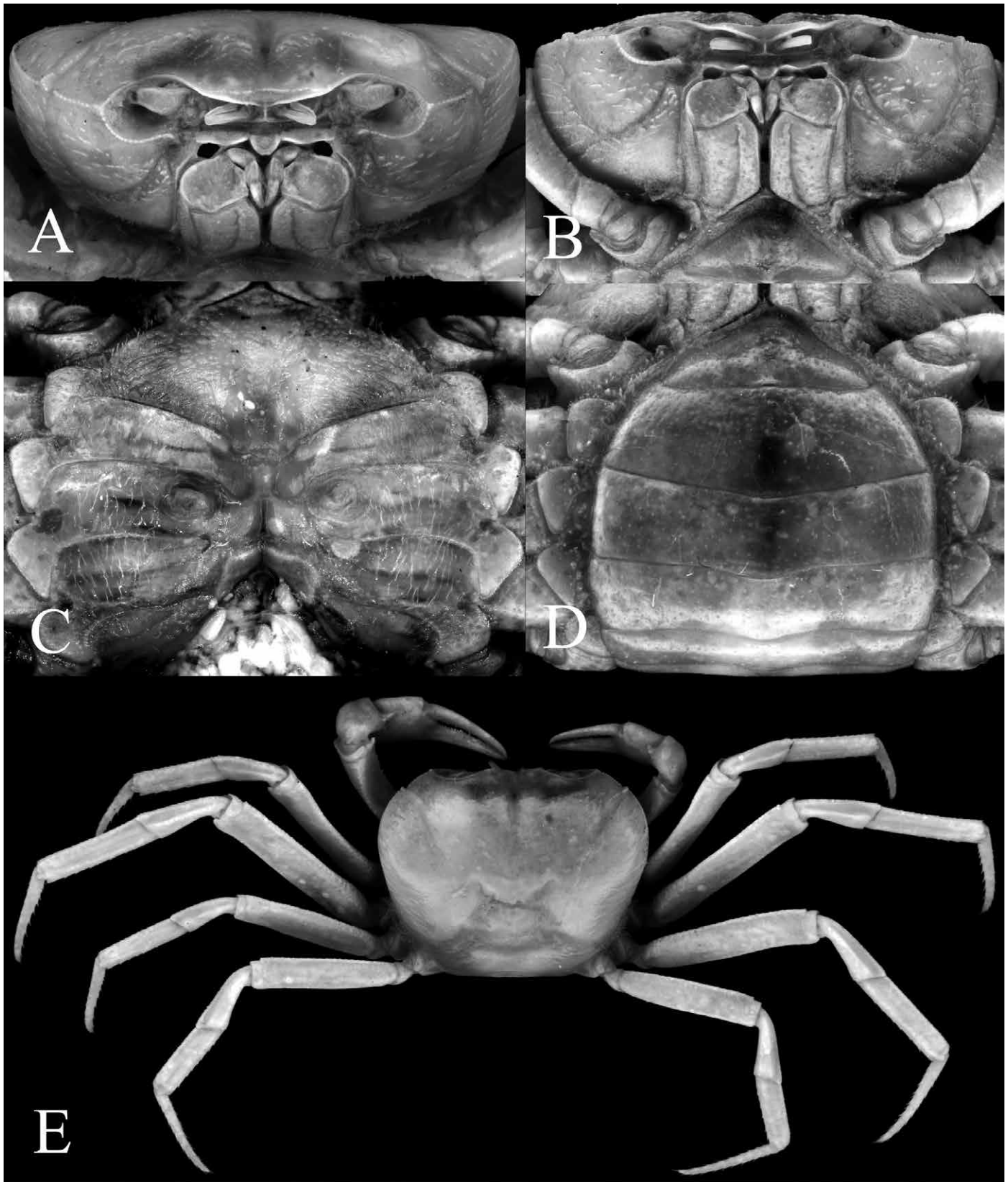
Figure 3. *Sundathelphusa prosperidad*, new species, paratype female, (28.04 × 21.38 mm) (NMCR 50777). A-B) frontal; C) thoracic sternum showing vulvae; D) abdomen; E) habitus, dorsal view.
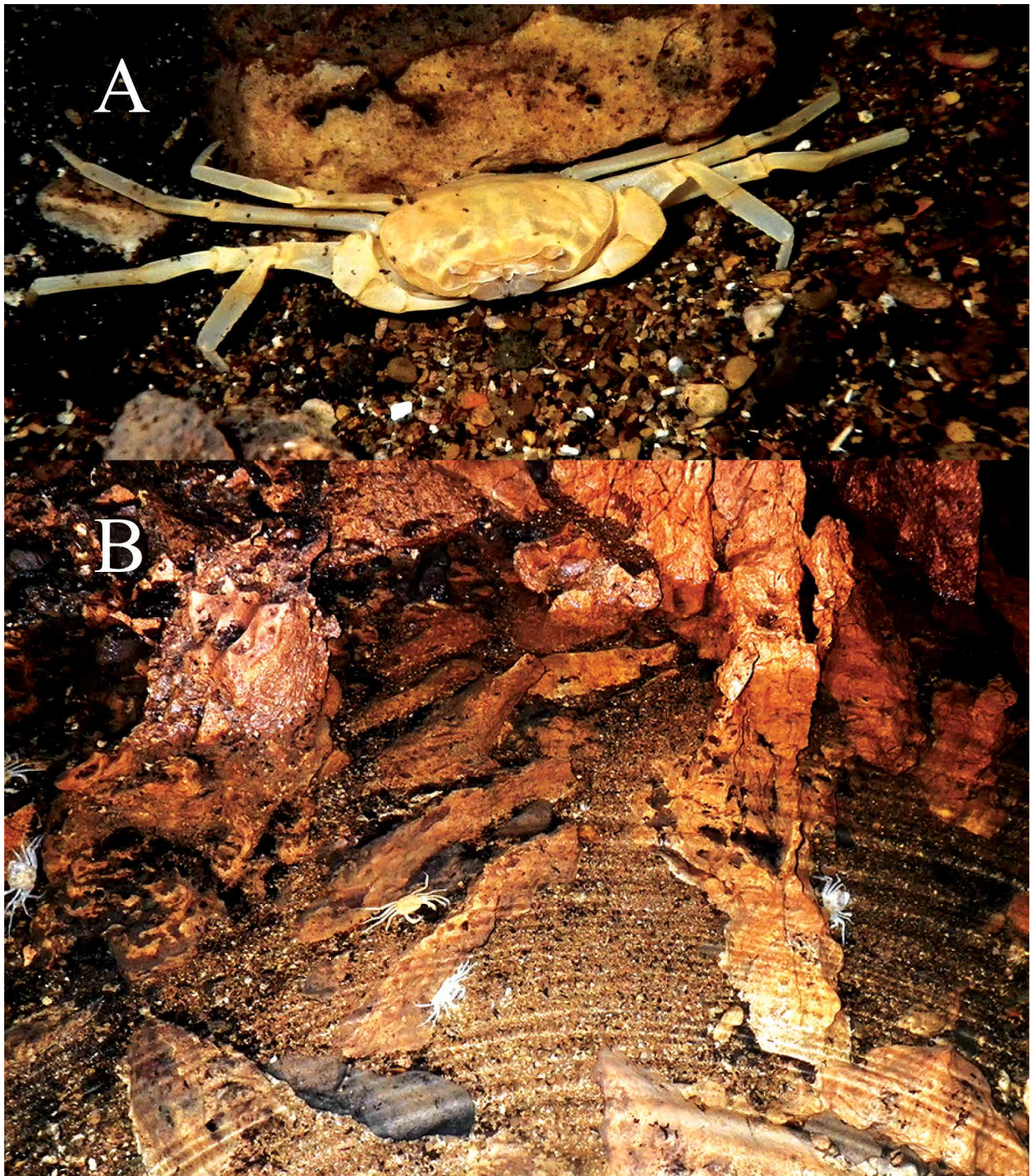
Figure 4. *Sundathelphusa prosperidad*, new species, in its natural habitat. A) live coloration; B) small colony of the new species in the clear subterranean water inside Ognop Cave.

ing gradually towards posterior margin of carapace (Figs. 1A, 1B, 1C, 1D, 1M). Frontal medial triangle complete; dorsal and lateral margins distinct, granulose, not fused; dorsal margin concave, lateral margins protruded distally over lateral ends of dorsal margin; orbit well developed; supraorbital margin granulated, sinuous; infraorbital margin beaded with distinct granules; outer edge reaching and fused with anterolateral margin; suborbital and subbranchial regions covered with scattered oblique long and short striae as well as small granules; pterygostomial region smooth with oblique ridges on upper outer region (Figs. 1C, 1D). Epistome divided into three lobes; median lobe large, circular, shallow notch present ventrally; lateral lobes wider and less protruded, sinuous, placed more anteriorly than median lobe (Figs. 1C, 1D).

Eyes reduced, tapering, cornea with traces of pigment, occupy two-thirds of orbit (Figs. 1C, 1D). Basal antennular segment large, subquadrate, flagellum long; antenna with long flagellum, distal end reaching beyond tip of eye when stretched laterally. Ischium of third maxilliped rectangular, bearing distinct oblique submedian sulcus; merus quadrate with shallow median depression; tip of exopod reaching to midpoint of outer margin of merus, with long flagellum (Fig. 1E).

Chelipeds noticeably elongated, subequal, stronger in males; all margins of merus serrated, ventral outer and inner margins more distinct, dorsal margin without distinct subdistal tooth, carpus armed with strong distal sharply-pointed inner angle, flattened dorso-ventrally, laterally fringed with proximal spines; palm minutely granulated on ventral surface, longer than finger; finger robust, cutting edges armed with many sharp teeth of various sizes (Figs. 1M, 1N, 1O).

Ambulatory legs long, slender, third leg longest, merus of third leg 0.89–0.95 times CL (n = 2); dorsal margins of meri indistinctly serrated, with subdistal tooth or spine, ventral margins serrated on first leg, second to fourth smooth; carpi short, with longitudinal submedian ridge on the dorsal surface except fourth leg, widened distally, dorsal margins indistinctly serrated; propodi armed with rows of spines on margins, longer on ventral than dorsal margins; dactyli armed with rows of spines on both margins, spines at ventral margins longer than on dorsal margins (Figs. 1K, 1L, 1M).

Male pleonal cavity reaching to level of proximal quarter of coxae of male chelipeds. Male pleon narrow, T-shaped; first somite very short, proximal and distal margins sinuous; second somite transversely subrectangular; third to fifth somites narrows abruptly; lateral margins of third somite convex, lateral margins of fourth somite straight, fifth somite strongly concave; sixth somite rectangular, longer than broad, lateral margins concave; telson subtriangular, longer than broad, lateral margins slightly concave, rounded distally (Figs. 1F, 2A, 2H).

G1 relatively slender; subterminal segment curved outward by distal half, outer margin distinctly concave; terminal segment, bended outward by almost 40-45º, straight, cylindrical, slightly setose, tapering towards distal end (Figs. G1, 1H, 2B, 2C, 2D, 2E, 2I, 2J, 2K, 2L). G2 straight, longer than G1, flagellum short (Figs. 1L, 1J, 2F, 2G, 2M).

Notes on the paratypes. All the paratypes agree well with almost all the major non-sexual characters of the holotype except for varied degree of pigmentation in the eyes (Figs. 1C, 1D, 3A, 3B, 4A). This new species exhibits sexual dimorphism. Oblique granules of striae in the branchial region of the carapace are stronger in males than females. The female possesses large semi-circular vulvae covered by the abdomen at the submedian level of fifth somite, abdomen is rounded with triangular telson (Figs. 3C, 3D). Right and left chelipeds (Fig. 3E) of the females are sub-equal in size but the larger one appeared weaker than that of the males. Granules on the ventral surface of the palm of the cheliped are more prominent in males, with the surface almost smooth in females.

Coloration. Pigmentless, dorsal surface white to pale yellow, ventral surface white (Fig. 4).

Etymology. Named after the Prosperidad town, the species type locality, also a Spanish/Filipino word that means prosperity or success, alluding to the species' successful colonization of the subterranean ecosystem. Used as a noun in apposition.

Habitat and Distribution. *Sundathelphusa prosperidad*, new species, is known only from Ognop Cave, the type locality of the new species, and Lorenzo Cave, both located within the karst system of Prosperidad, Agusan del Sur. The caves are part of an Oligocene-Miocene limestone formation (MGB, 2010) in Agusan del Sur, Mindanao Island, the Philippines.

This new species occurs in small numbers near the vertical entrance of Ognop Cave (Fig. 4). Two samples of *S. prosperidad*, new species, were collected from Lorenzo Cave (NMCR 50778, male 20.58 × 16.67mm; female 25.77 × 20.19mm). This distribution clearly suggests that Lorenzo Cave and Ognop Cave are interconnected and the possibility that other colonies could be present in other unexplored areas of the cave system.

Ognop Cave is a long cave system with fragments of sharp, brittle rock boulders along its shallow subterranean river and deep pools. Lorenzo Cave is just a few meters long with a subterranean stream that flows towards its entrance. The water originates from a sump that makes it impassable and cannot be explored further without the use of diving equipment. This cave is located southeast of the Ognop Cave entrance.

Co-inhabitants of the groundwater of Ognop Cave are species of cave goby *Caecogobius personatus* Larson and Husana, 2017, unidentified cyprinid fish (manuscript in preparation), and atyid shrimps. A colony of bats, a large population of crickets and other invertebrates are also present inside the cave.

The spring that comes out from the rubble of the collapsed portion of the entrance of Ognop Cave is the headwater of one of the major tributaries of the Bega River traversing Bega Falls.

Remarks. *Sundathelphusa prosperidad*, new species, closely resembles *Sundathelphusa hades* Takeda and Ng, 2001. However, *S. prosperidad* possesses the following characters that differentiate it from *S. hades*: 1) quadrate to trape-

zoidal carapace with proportionately wider breadth at about its one-third level (vs. squarish and narrower breadth in *S. hades*) (Figs. 1A, 1M, 3E vs. Takeda and Ng 2001, figs. 1a, 1b, 1e); 2) presence of a deep notch between the external orbital tooth and epibranchial tooth of the antero-lateral margin (vs. small or shallow in *S. hades*) (Figs. 1A, 1B, 1C, 1D, 1M, 3A, 3B, 3E vs. Takeda and Ng 2001, figs. 1a, 1b, 1c, 1e, 2a); 3) presence of a granulated crest formed as dorsal extension of the inner margin of the epibranchial tooth (vs. absent in *S. hades*) (Figs. 1A, 1B, 1C, 1D, 1M, 3A, 3B, 3E vs. Takeda and Ng 2001, figs. 1a, 1b, 1c, 1e, 2a); and 4) the distal part of the subterminal segment of the G1 is strongly curved outwards (vs. relatively straighter in *S. hades*) (Figs. 1G, 1H, 2B, 2C, 2D, 2E, 2I, 2J, 2K, 2L vs. Takeda and Ng 2001, figs. 3c,3d).

Both *S. prosperidad* and *S. hades* inhabit caves hence possessing strongly reduced eyes, with a small trace of pigmentation at the tip of the cornea (see Figs. 1C, 1D, 3A, 3B; Takeda and Ng 2001, figs. 1c, 2a, 2b). Such a degree of troglomorphism has also been observed in other freshwater crabs described from caves in the Philippines such as *S. cavernicola* Ng and Sket, 1996, *S. sottoae* Ng and Sket, 1996, *S. lobo* Husana, Naruse and Kase 2009, and *S. waray* Husana, Naruse and Kase 2009.

Sundathelphusa prosperidad, new species, and *S. hades* are both located in Agusan del Sur in the eastern part of Mindanao Island, and their type localities are close to each other. But unlike the overlapping habitat range of *S. sottoae* and *S. cavernicola* in Bohol Island, the habitats of these two cave species from Mindanao Island are separated by the extension of the Philippine fault-line and Oligocene-Miocene volcanic deposits (MGB, 2010). The type locality of *S. prosperidad*, new species, is a cave in an Oligocene-Miocene limestone formation, north of the type locality of *S. hades,* a cave in a younger Pliocene-Pliestocene limestone formation (MGB, 2010). Attempts to obtain fresh samples of *S. hades* from the type locality were in vain due to the security situation in the area.

About 98 percent of freshwater crabs in the Philippines are endemic to the archipelago and most of them are data deficient (Cumberlidge et al, 2009). Although there is a possibility that colonies of *S. prosperidad* are present in some unexplored areas of Ognop Cave, the population estimate of this new species may not go beyond 1,000 individuals, it has a small geographic range, and with a very small and restricted area of occupancy. Under IUCN Red List, this new species can be categorized between endangered to critically endangered species under Criterion B1 ($<$ 100 km^2 extent of occurrence), Criterion B2 ($<$ 10 km^2 area of occupancy), Criterion C ($<$ 2,500 mature individuals), and Criterion D ($<$ $\times$ 250 mature individuals per area inside the cave system).

Cave-obligate species in the Philippines are strictly endemic to the cave system they inhabit and cannot be found anywhere else. Similar to the *Sundathelphusa prosperidad*, new species, other cave crabs such as *S. cavernicola* Takeda, 1983, *S. sottoae* Ng and Sket, 1996, *S. hades* Takeda and Ng, 2001, *S. waray* Husana, Naruse and Kase, 2009, *S. lobo* Husana, Naruse and Kase, 2009, and *Samarplax principe* Husana, Tan and Kase, 2011; cave fishes such as *Caecogobius cryptophthalmus* Berti and Ercolini, 1991, and *C. personatus* Larson and Husana, 2019, and other cave-obligate species can fall into the same category. The limited distributional range, the restricted confinement in the cave habitat and small population size of cave-obligate species made them extremely vulnerable to human disturbance. Forest logging, slash and burn farming, and land conversion are common practice that will seriously threaten the cave and its inhabitants and should be strictly prohibited in the surrounding areas above the cave system. The increasing popularity of tourism in the country also poses a serious threat in this stenotopic species. Hence, it is strongly recommended that Ognop Cave and all other caves with cave-obligate species, as well as its surface vegetation, should be strictly protected to preserve the natural habitat of these species and other unique cave organisms.

Acknowledgements

References

Berti, R. and Ercolini, A., 1991, *Caecogobius cryptophthalmus* n. gen. n. sp. (Gobiidae Gobiinae), the first stygobic fish from Philippines: Tropical Zoology, v. 4, no. 1, p. 129–138. DOI: 10.1080/03946975.1991.10539482

Bott, R., 1969, Flußkrabben aus Asien und ihre Klassifikation (Crustacea, Decapoda): Senckenbergiana Biologica, v. 50, p. 359–366.

Cumberlidge, N., Ng, P.K.L., Yeo, D.C.J., Magalhães, C., Campos, M.R., Alvarez, F., Naruse, T., Daniels, S.R., Esser, L.J., Attipoe, F.Y.K., Clotilde-Ba, F.-L., Darwall, W., McIvor, A., Baillie, J.E.M., Collen, B., and Ram, M., 2009, Freshwater crabs and the biodiversity crisis: importance, threats, status, and conservation challenges: Biological Conservation, v. 142, p. 1665–1673. https://doi.org/10.1016/j.biocon.2009.02.038

Davie, P.J.F., Guinot, D. and Ng, P.K.L., 2015, Phylogeny of Brachyura: *in* Castro, P., Davie, P.J.F., Guinot, D., Schram, F., and Von Vaupel Klein, C., eds., Treatise on Zoology – Anatomy, Taxonomy, Biology: The Crustacea, complementary to the volumes translated from the French of the Traité de Zoologie, v. 9(C) (I), Decapoda: Brachyura (Part 2), p. 922–979.

Husana, D.E.M., Kase, T., and Mendoza, J.C.E., 2015, Two new species of the freshwater crab genus *Sundathelphusa* Bott, 1969 (Crustacea: Brachyura: Gecarcinucidae) from Negros Island, Philippines: Raffles Bulletin of Zoology, v. 63, p. 226–236. http://zoobank.org/urn:lsid:zoobank.org:pub:549829D6-65A9-4D97-B15E-361755F7577B

Husana, D.E.M., Naruse, T., and Kase, T., 2009, Two new cavernicolous species of the genus *Sundathelphusa* from Western Samar, Philippines (Decapoda: Brachyura: Parathelphusidae): Journal of Crustacean Biology, v. 29, no. 3, p. 419–427. https://doi.org/10.1651/08-3081.1

Husana, D.E.M., Naruse, T., and Kase, T., 2010, A new species of the genus *Karstarma* (Crustacea: Decapoda: Brachyura: Sesarmidae) from Anchialine Caves in the Philippines: Raffles Bulletin of Zoology, v.58, no. 1, p. 65–69.

Husana, D.E.M., and Ng, P.K.L., 2019, On the identity of *Sundathelphusa philippina* (von Martens, 1868) (Decapoda: Brachyura: Gecarcinucidae) from the Philippines, with descriptions of two new species: Zootaxa, v. 4585, no. 2, p. 315–331. https://doi.org/10.11646/zootaxa.4585.2.5

Husana, D.E.M., Tan, S.H., and Kase, T., 2011, A new genus and species of anchialine Hymeosomatidae (Crustacea: Decapoda: Brachyura) from Samar, Philippines: Zootaxa, v. 3109, p. 49–59. https://doi.org/10.11646/zootaxa.3109.1.3

Husana, D.E.M., Yamamuro, M., and Ng, P.K.L., 2014, Two new species of freshwater crabs of the genus *Sundathelphusa* Bott, 1969 (Decapoda: Brachyura: Gecarcinucidae) from caves in Luzon, Philippines: Zootaxa, v. 3815, no. 4., p. 565–574. https://doi.org/10.11646/zootaxa.3815.4.6

Klaus, S., Mendoza, J.C.E., Liew, J.H., Plath, M., Meier, R., and Yeo, D.C.J., 2013, Rapid evolution of troglomorphic characters suggests selection rather than neutral mutation as a driver of eye reduction in cave crabs: Biology Letters, v. 9, 20121098. https://doi.org/10.1098/rsbl.2012.1098

Larson, H.K., and Husana, D.E.M., 2019, A new species of the blind goby *Caecogobius* (Govioidei, Gobiidae, Gobinellinae) from a cave system in Mindanao, Philippines: Ichthyological Research, v. 66, no. 1, p. 97–103. Published online: 6 October 2018. https://doi.org/10.1007/s10228-018-0659-y

Martens, E. von, 1868, Ueber einige neue crustacean: Monatsberichte der Königlichen Preussische Akademie der Akademie der Wissenschaften zu Berlin: Sitzung der Physikalisch-mathematische Klasse, 1868:.*in* Mines and Geosciences Bureau, 2010, Geology of the Philippines, 2nd edition: p. 608–615, Department of Environment and Natural Resources, 532 pages.

Ng, N.K., and Ng, P.K.L., 2009, *Orcovita holthuisi*, a new species of anchialine crab (Brachyura, Varunidae) from Coron Island, Palawan, Philippines: Crustaceana, v. 82, no. 9, p. 1097–1108. https://doi.org/10.1163/156854009X407678

Ng, P.K.L., 2002, New species of cavernicolous crabs of the genus *Sesarmoides* from the western Pacific, with a key to the genus (Crustacea: Decapoda: Brachyura: Sesarmidae): Raffles Bulletin of Zoology, v. 50, no. 2, p. 419–435.

Ng, P.K.L., 2010, On the identity of *Para-Bary-Thelphusa grapsoides longipes* Balss, 1937, with description of a new species from the Philippines (Brachyura, Gecarcinucidae): *in* Fransen, C.H.J.M., De Grave S., and Ng, P.K.L., eds., Studies on Malacostraca: Lipke Bijdeley Holthuis Memorial Volume: Crustaceana Monographs, v. 14, p. 561–571.

Ng, P.K.L., and Guinot, D., 2001, On the land crabs of the genus *Discoplax* A. Milne Edwards, 1867 (Crustacea: Decapoda: Brachyura: Gecarcinidae), with description of a new cavernicolous species from the Philippines: Raffles Bulletin of Zoology, v. 49, no. 2, p. 331–338.

Ng, P.K.L., and Sket, B., 1996, The freshwater crab fauna (Crustacea: Decapoda: Brachyura) of the Philippines. IV. On the collection of Parathelphusidae from Bohol: Proceeding of the Biological Society of Washington, v. 109, p. 695–706.

Ng, P.K.L., Guinot, D., and Iliffe, T.M., 1996, Revision of the anchialine varunine crabs of the genus *Orcovita* Ng and Tomascik, 1994 (Crustacea: Decapoda: Brachyura: Grapsidae), with descriptions of four new species: Raffles Bulletin of Zoology, v. 44, no. 1, p. 109–134.

Rathbun, M.J., 1904, Les crabes d'eau douce (Potamonidae): Nouvelles Archives du Muséum d'Histoire Naturelle, 4e ser., v. 6, p. 225–311, pls. 9–18.

Stasolla, G., Abbarchi, A., and Innocenti, G., 2015, *Sundathelphusa spelaeophila*, a new species of cavernicolous crab from Samar, Philippines (Decapoda: Brachyura: Gecarcinucidae): Raffles Bulletin of Zoology, v. 63, p. 448–453.

Stasolla, G. and Innocenti, G., 2014, A new species of cavernicolous crab from Coron Island, Palawan, the Philippines (Decapoda: Brachyura: Varunidae): Raffles Bulletin of Zoology, v. 62, p. 591–599.

Takeda, M., 1983, A new cavernicolous crab from Bohol, the Philippines: Bulletin of the National Science Museum, Tokyo, Series A, v. 9, p.169–173.

Takeda, M., and Ng, P.K.L., 2001, The freshwater crab fauna (Crustacea, Brachyura) of the Philippines: VI. A new cavernicolous crab from Mindanao: Zoological Science, v. 18, p. 1123–1127. https://doi.org/10.2108/zsj.18.1123

GUIDE TO AUTHORS

The *Journal of Cave and Karst Studies* is a multidisciplinary journal devoted to cave and karst research. The *Journal* is seeking original, unpublished manuscripts concerning the scientific study of caves or other karst features. Authors do not need to be members of the National Speleological Society, but preference is given to manuscripts of importance to North American speleology.

LANGUAGES: The *Journal of Cave and Karst Studies* uses American-style English as its standard language and spelling style, with the exception of allowing a second abstract in another language when room allows. In the case of proper names, the *Journal* tries to accommodate other spellings and punctuation styles. In cases where the Editor-in-Chief finds it appropriate to use non-English words outside of proper names (generally where no equivalent English word exist), the *Journal* italicizes them. However, the common abbreviations i.e., e.g., et al., and etc. should appear in roman text. Authors are encouraged to write for our combined professional and amateur readerships

CONTENT: Each paper will contain a title with the authors' names and addresses, an abstract, and the text of the paper, including a summary or conclusions section. Acknowledgments and references follow the text. Manuscripts should be limited to 6,000 words and no more than 10 figures and 5 tables. Larger manuscripts may be considered, but the *Journal* reserves the right to charge processing fees for larger submissions.

ABSTRACTS: An abstract stating the essential points and results must accompany all articles. An abstract is a summary, not a promise of what topics are covered in the paper.

STYLE: The *Journal* consults The Chicago Manual of Style on most general style issues.

REFERENCES: In the text, references to previously published work should be followed by the relevant author's name and date (and page number, when appropriate) in brackets. All cited references are alphabetical at the end of the manuscript with senior author's last name first, followed by date of publication, title, publisher, volume, and page numbers. Geological Society of America format should be used (see http://www.geosociety.org/documents/gsa/pubs/GSA_RefGuide_Examples.pdf). Please do not abbreviate periodical titles. Web references are acceptable when deemed appropriate. The references should follow the style of: Author (or publisher), year, Webpage title: Publisher (if a specific author is available), full URL (e.g., http://www.usgs.gov/citguide.html), and the date the website was accessed in brackets. If there are specific authors given, use their name and list the responsible organization as publisher. Because of the ephemeral nature of websites, please provide the specific date. Citations within the text should read: (Author, Year).

SUBMISSION: Manuscripts are to be submitted via the PeerTrack submission system at http://www.edmgr.com/jcks/. Instructions are provided at that address. At your first visit, you will be prompted to establish a login and password, after which you will enter information about your manuscript and upload your manuscript, tables, and figure files. Manuscript files can be uploaded as DOC, WPD, RTF, TXT, or LaTeX. Note: LaTeX files should not use any unusual style files; a LaTeX template and BiBTeX file may be obtained from the Editor-in-Chief. Table files can be uploaded as DOC, WPD, RTF, TXT, or LaTeX files and figure files can be uploaded as TIFF, AI, EPS, or CDR files. Extensive supporting data may be placed on the Journal's website as supplemental material at the discretion of the Editor-in-Chief. The data that are used within a paper must be made available upon request. Authors may be required to provide supporting data in a fundamental format, such as ASCII for text data or comma-delimited ASCII for tabular data.

DISCUSSIONS: Critical discussions of papers previously published in the *Journal* are welcome. Authors will be given an opportunity to reply. Discussions and replies must be limited to a maximum of 1000 words and discussions will be subject to review before publication. Discussions must be within 6 months after the original article appears.

MEASUREMENTS: All measurements will be in Systeme Internationale (metric) except when quoting historical references. Other units will be allowed where necessary if placed in parentheses and following the SI units.

FIGURES: Figures and lettering must be neat and legible. Figure captions should be on a separate sheet of paper and not within the figure. Figures should be numbered in sequence and referred to in the text by inserting (Fig. x). Most figures will be reduced, hence the lettering should be large. Photographs must be sharp and high contrast. Figures must have a minimum resolution of 300 dpi for acceptance. Please do not submit JPEG images.

TABLES: See http://caves.org/pub/journal/PDF/Tables.pdf to get guidelines for table layout.

COPYRIGHT AND AUTHOR'S RESPONSIBILITIES: It is the author's responsibility to clear any copyright or acknowledgement matters concerning text, tables, or figures used. Authors should also ensure adequate attention to sensitive or legal issues such as land owner and land manager concerns or policies and cave location disclosures.

PROCESS: All submitted manuscripts are sent out to at least two experts in the field. Reviewed manuscripts are then returned to the author for consideration of the referees' remarks and revision, where appropriate. Revised manuscripts are returned to the appropriate Associate Editor who then recommends acceptance or rejection. The Editor-in-Chief makes final decisions regarding publication. Upon acceptance, the senior author will be sent one set of PDF proofs for review. Examine the current issue for more information about the format used.

Journal of Cave and Karst Studies

CONTENTS

Visit us at www.caves.org/pub/journal